UNIVERSITÀ DELLA CALABRIA

CAMPUS DI ARCAVACATA

DEPARTMENT OF MECHANICAL ENGINEERING

Doctoral of Philosophy Course
- XX CYCLE -

Thermomechanical characterization of
Nickel-Titanium Shape Memory Alloys

(SSD ING-IND/14)

Thesis submitted in fulfillment of the degree of
Doctor of Philosophy in Mechanical Engineering
by:

Andrea FALVO

Co-ordinator
Prof. Maria Laura LUCHI

Tutor
Prof. Franco FURGIUELE

…..Niente è impossibile,
al massimo è poco probabile…

AKNOWLEDGEMENTS

Three years ago, pushed by my curiosity about a so strange material I have start an experience that I never forget for its professional and human teachings; my dissertation is the result of this. Since that day in which I have met Prof. Franco Furgiuele and Eng. Carmine Maletta, I knew that I am going to work not only with two talented researches but also with two good and generous men. They have permit me to go in for the passion for the research in a very stimulant and cultured set and to have satisfaction by my work. For their availability and affection I will be always grateful to them.

Very thanks to my girlfriend Beatrice that have accepted faithfully and gladly the challenges and uncertainties associated with the life of a doctoral student; her love and patience are for me essential.

Finally, a special thanks to my father and my mother, always present with their love and support; all this could not be possible without them.

TABLE OF CONTENTS

CHAPTER 3 - LASER WELDING OF NITI ALLOYS: MECHANICAL AND SHAPE MEMORY BEHAVIOUR

CHAPTER 5 – NUMERICAL MODELLING OF TWSME IN NITI ALLOYS

CHAPTER 4 - BIOMIMETIC COATING OF NITI ALLOYS

INTRODUCTION AND SCOPE OF RESEARCH

In this dissertation, the results of the research activities carried out during the Doctoral Course at the University of Calabria are presented. The aim of these activities regarded the interesting field of Smart Materials and, in particular, some aspects related to the thermomechanical characterization of Nickel-Titanium (NiTi) Shape Memory Alloys (SMAs).

Smart Materials are able to note an external stimulus responding in a predetermined and repeatable manner; this capacity permits to interact with the material using it as an actuator able to modify shape and elastic properties, electric resistivity and damping capacities.

Shape Memory Alloys, and in particular the NiTi alloys, are the most promising Smart Materials. Due to their special functional properties, namely one way or two way shape memory effect (OWSME, TWSME) and superelastic effect (SE), NiTi alloys have seen growing use in recent years in a number of industrial fields as biomedical, automotive, aeronautic and many others. Generally, the use of the NiTi alloys seems to be very useful in applications were it is necessary to use smart components with low dimensions; many conventional actuators and sensors can be substituted with NiTi components obtaining high advantages in terms of reduction of weight and dimensions, reliability and costs. Furthermore, in the last years, their use for the realization of smart composites, as an example for vibration and shape control, is becoming very interesting. Unfortunately, there are still some difficulties with shape memory alloys that must be overcome before they can live up to their full potential. For example, these alloys are still relatively expensive to manufacture compared to other materials such as steel and aluminium. This difficulties regard the high sensibility to the production parameters, to the low workability with conventional machining processes as well as to the high non linearity in the mechanical and functional behaviour.

For this reason, in the last decades, many research activities have been addressed to the investigation of many aspect related to the influence of different working processes on the behaviour of the NiTi alloys and to develop simple numerical model able to simulate the non linearity associated to the NiTi functional properties.

In this dissertation, the results related to the experimental characterization and numerical modelling of different NiTi alloys are presented.

The experimental characterization are carried out on NiTi sheets in order to study the mechanical and functional behaviour of different NiTi alloys. Using proper experimental procedure, the thermomechanical behaviour of the materials are investigated under static and cyclic conditions to better understand the deformation mechanisms involved in the shape memory and superelastic effect.

Furthermore, the characterization of Nd:YAG laser butt welded NiTi sheets, in terms of mechanical, microstructural and shape memory behaviour, was executed in order to investigate the influence of this working process on the alloy behaviour. As said before, in fact, due to the low workability of these materials with conventional machining processes (milling, turning and drilling), suitable joining and cutting techniques must be used to obtain devices and components with complex geometries. In this field, laser welding is probably a good solution because, due to its high precision, permits to reduce the influence of the machining process on the material properties.

Then, starting from some experimental results and evidences, a phenomenological approach, based on the Prandtl-Ishlinskii hysteresis operators, was used to model the TWSME in NiTi alloys. Modelling the hysteretic behaviour of a smart material is not a simple task because the identification of many model parameters is required to adapt the model to the real behaviour of the material. For this reason, the developing of useful models based on a phenomenological approach could resolve many problems related to the simulation and control of this class of materials.

Finally, another important aspect related to the use of these alloys in biomedical field is investigated. Various approaches are currently under development to prevent undesirable Ni release and ensure implant safety in applications in which NiTi alloys are used at direct contact with the human tissues. Despite the satisfactory clinical use of NiTi, in some situations the high Ni content in the alloy is of great concern with regards to its biocompatibility; in fact, Ni has been reported to be responsible for the clinic toxic and allergic responses. It is theoretically possible that Ni may dissolve from NiTi due to corrosion phenomena, so that its necessary to modify the surface of NiTi alloys to improve their biocompatibility and restraining Ni release. Furthermore, coating NiTi

components with osteoconductive materials could improve their use in the realization of biomedical implants useful for the regeneration or substitution of bone in human body

In this research, a Calcium-Phosphates (CaPs) coating, was deposited by a biomimetic procedure on a NiTi alloy. The aim is to analyze the properties of the coatings, as function of different surface conditions of the material, in order to define a useful coating procedure.

CHAPTER 1

NICKEL - TITANIUM SHAPE MEMORY ALLOYS

1.1 HISTORY OF SHAPE MEMORY ALLOYS

The first reported steps towards the discovery of the shape memory effect were taken in the 1930s, when A. Ölander discovered the pseudoelastic behaviour of the Au-Cd alloy in 1932 (Otsuka, 1998). Greninger & Mooradian (1938) observed the formation and disappearance of a martensitic phase by decreasing and increasing the temperature of a Cu-Zn alloy. The basic phenomenon of the memory effect governed by the thermoelastic behaviour of the martensite phase was widely reported a decade later by Kurdjumov & Khandros (1949) and also by Chang & Read (1951).

In the early 1960s, Buehler and his co-workers at the U.S. Naval Ordnance Laboratory discovered the shape memory effect in an equiatomic alloy of nickel and titanium, which can be considered a break trough in the field of shape memory materials (Buehler et al. 1967). This alloy was named Nitinol (Nickel-Titanium Naval Ordnance Laboratory).

Since that time, intensive investigations have been made to elucidate the mechanics of its basic behaviour. The use of NiTi as is fascinating because of its special functional behaviour, which is completely new compared to the conventional metal alloys.

1.2 THERMOELASTIC MARTENSITIC TRANSFORMATION

NiTi shape memory alloys can exist in a two different temperature-dependent crystal structures (phases) called martensite (lower temperature) and austenite (higher temperature or parent phase). Several properties of austenitic NiTi and martensitic NiTi (such as Young modulus, electrical resistance, damping behaviour, etc..) are notably different (Otsuka et al. 2005, Duering et al. 1990).

The austenite is characterized by a Body Centered Cubic structure (BCC), where there is a nickel atom at the center of the crystallographic cube and a titanium atom at each of the cube's eight corners. Since the austenitic phase is microstructurally symmetric it is considered to be the parent phase. The martensite phase of NiTi is less symmetric and its lattice structure consists of a rhombus alignment with an atom at each of the rhombus corners. Fig.1 shows two NiTi crystals in the austenite and martensite phases.

The unique behaviour of NiTi is based on the temperature dependent austenite to martensite phase transformation on an atomic scale, which is called Thermoelastic Martensitic Transformation (TMT). TMT causing the functional properties as a result of the need of the crystal lattice structure to accommodate to the minimum energy state for a given temperature (Otsuka et al. 1998).

TMT, and its reversion, is a shear-dominant diffussionless solid-state phase transformation occurring by nucleation and growth of the martensitic phase from the parent austenitic phase. TMT could be activated, so that NiTi alloys could be transformed from austenite to martensite and vice versa, either by reducing the temperature (Thermally Induced Martensite, TIM) or applying a mechanical stress (Stress Induced Martensite, SIM). On the other hand the martensite transforms into austenite through either increasing the temperature or removing the applied stress. This shows that mechanical loading and thermal loading have opposite effects on NiTi alloys.
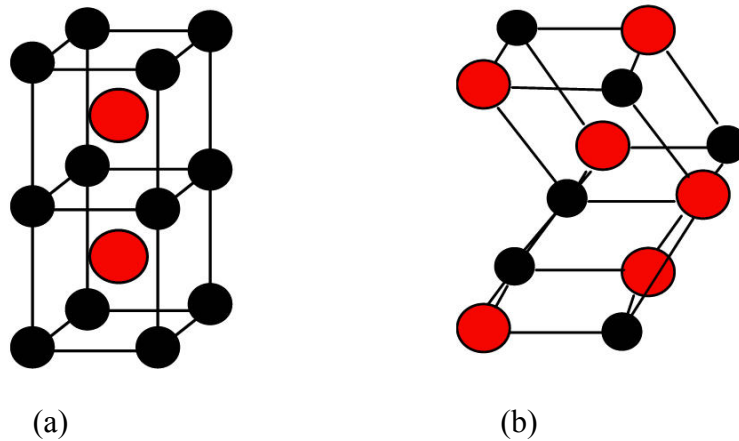
Fig. 1: (a) Austenite and (b) Martensite lattice structures

When austenite is cooled, it begins to change onto martensite; the temperature at which this phenomenon starts is called martensite start temperature (M_s), while the temperature at which martensite is again completely reverted is called martensite finish temperature (M_f). When martensite is heated, it begins to change into austenite; the temperature at which this phenomenon starts is called austenite start temperature (A_s), while the temperature at which this phenomenon is complete is called austenite finish temperature (A_f). (Buehler et al. 1967, Duering et al. 1990).

Due to the TMT characteristics, applied stress plays a very important role. During cooling of the NiTi material below temperature M_s in absence of applied stresses, the variants of the martensitic phase arrange themselves in a self-accommodating manner, with a total of 24 crystallographically equivalent habit planes, resulting in no observable macroscopic shape change. The mechanism by which single martensite variants form from austenite by cooling is called twinning and it can be described as a mirror symmetry displacement of atoms across a particular atom plane, the twinning plane (Buehler et al. 1967, Otsuka et al. 2005). Crystal twinning occurs when two separate crystals share some of the same crystal lattice points in a symmetrical manner. The result is an intergrowth of two crystals in a variety of specific configurations separated by a twin boundary surface. Twin boundaries occur when two crystals of the same type intergrowth, so that only a slight misorientation exists between them. Twin boundaries are partly responsible for shock hardening and for many of the changes that occur in cold work of metals with limited slip systems or at very low temperatures (Hurlbut et al. 1985).

By applying mechanical loading on the martensitic structure, martensitic variants reorient into a single variant; the reorientation mechanism is called detwinning (Liu 2005, Otsuka et al. 2005) and it is the cause of the shape memory behaviour in the SMAs as explained in the following sections.

The martensitic phase transformation can also be induced by pure mechanical loading while the material is in the austenitic phase, in which case detwinned martensite is directly produced from austenite by the applied stress at temperatures above M_s (SIM). This means that the energy necessary for the martensitic transformation can be provided, not only by a thermal input but also by a mechanical input (Otsuka et al. 2005, Duering et al. 1990). It is important to point out that the SIM transformation can be induced in the material at temperatures up to A_f but lower than a threshold value defined as M_d. Up to this temperature, an applied stress do not generate the SIM transformation but dislocation effects as consequence of the minor energy needs with respect to the SIM.

Fig. 2 shows the NiTi in austenitic and martensitic forms in a two dimensional view. As shown in the figure, the austenite is symmetric and thus has one layout for the atoms, while the martensite could be found in two different alignments based on the level of stress applied to the alloy. Based on the stress direction, the martensite could be detwinned either to the left or to the right direction. Thus from a two dimensional point of view there are two possible variants for martensite.

(a)   (b)   (c)

Fig. 2: Austenite and martensite microstructural view in a two-dimensional plan:
(a) austenite, (b) twinned martensite, (c) detwinned martensite

Fig. 3 summarizes the above considerations showing the relationship between the phase transformation temperatures, the applied stress and the crystalline structure of a NiTi alloy.

From the figure, it is possible to observe that an increase in the applied stress increases the four phase transformation temperatures in a linear manner. In particular, the effect of the applied stress can be computed according to the well known Clausius-Clapeyron rule, $d\sigma/dT = const$ (Otsuka et al. 2005).

Fig. 3: Relationship between phase transformation temperatures and applied stress

In Fig. 4, a Differential Scanning Calorimetry (DSC) thermogram related to a NiTi alloys is shown; this technique is the main used to identify the transformation temperatures of the NiTi alloys. As clearly shown in the figure, the temperature range for the martensite to austenite transformation, that takes place upon heating, is somewhat higher than that for the reverse transformation upon cooling. The difference between the transition temperatures upon heating and cooling is called hysteresis. Hysteresis is generally defined as the difference between the temperatures at which the material is 50 % transformed to austenite upon heating and 50 % transformed to martensite upon cooling. This difference can be up to 30-40 °C and it is associated with the energy dissipated during the transformation (Otsuka et al. 2005, Buehler et al. 1967). A hysteretic behaviour is also present in the stress induced martensitic transformation in terms of transformation stress as explained in the following; generally, the hysteretic behaviour characterizes all NiTi properties.
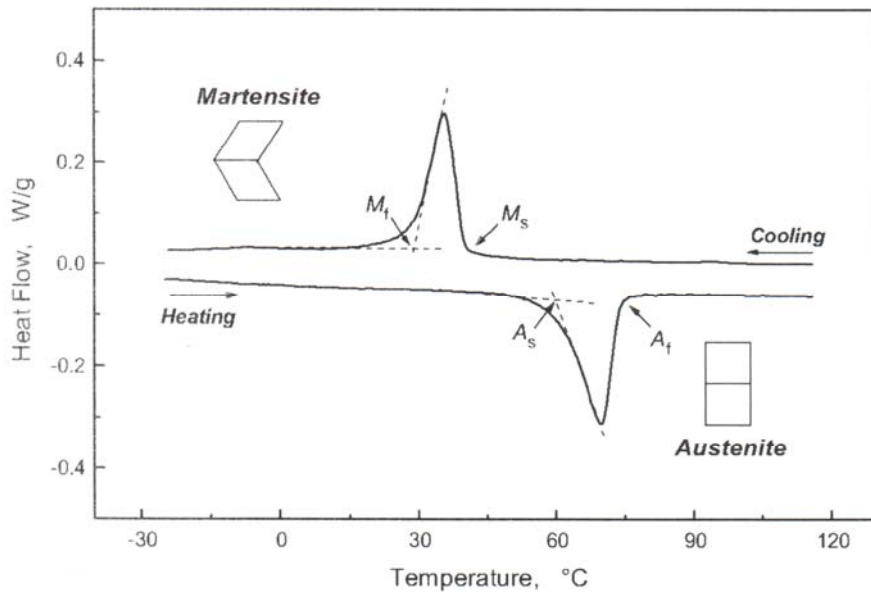
Fig. 4: DSC thermogram of a NiTi alloy

1.3 MECHANICAL AND FUNCTIONAL PROPERTIES OF NITI ALLOYS

A relatively large number of researchers have been interested in exploring the mechanical characteristics of NiTi in its two phases. Researchers are interested in studying and specifying the properties of NiTi materials under various types of thermomechanical loadings. Several experimental studies have been conducted to specify the mechanical properties of SMAs (Otsuka et al. 2005, Brinson et al. 2004, Liu et al. 1998, Lagoudas et al. 2000, Gall et al. 2001, Wada et al. 2005). The outcomes of experimental research in the past two decades assisted in developing a range for the mechanical parameters that would be expected from NiTi in its austenite and martensite phases. Table 1 presents a summary of the mechanical properties for NiTi. As explained in the following, mechanical properties could be due to several factors such as alloys composition, manufacturing process, strain rate and cyclic loading.

Table 1: Summary of NiTi mechanical properties

	Austenite	**Martensite**
Young's modulus	*30-83 GPa*	*20-45 GPa*
Ultimate Tensile Strength	*800-1900 MPa*	*800-1900 MPa*
Elongation at Failure	*20-25%*	*20-25%*
Recoverable strain	*8-10 %*	*8-10%*
Poisson Ratio	*0.33*	*0.33*

Fig. 5 illustrates the mechanical behaviour of a NiTi alloy as a function of temperature. In order to relate the mechanical behaviour of the alloy which occurs on the macro level with the phase transformations that occur on the micro level, the microstructure of the alloy is shown in the figure at the various strain/temperature levels (Shaw 2002).

While most metals deform by slip or dislocation, NiTi responds to stress by simply changing the orientation of its crystal structure through the movement of twin boundaries (detwinning). This orientation is evident in the stress-strain behaviour by the stress plateau that occurs both in martensitic than in austenitic NiTi, until the material consists only of the correspondence variant which produces maximum strain. However, deformation beyond this will result first in elastic deformation of the oriented structure and than in classical plastic deformation by slip and dislocation.

At low temperature, so that in martensitic condition, the mechanical behaviour of the material is characterized by large inelastic deformation after unloading that could be recovered by heating the alloy (Shape Memory Effect, SME). As the multivariant martensitic phase is deformed, a detwinning process takes place, as well as growth of certain favourably oriented martensitic variants at the expense of other variants. The mechanical loading in the martensitic phase induces reorientation of the variants and results in a large inelastic strain, which is not recovered upon unloading. At the end of the deformation, and after unloading, it is possible that only one martensitic variant remains if the end of the stress plateau is reached; otherwise, if the deformation is halted midway, the material will contain several different correspondence variants. This mode of deformation dominates at temperatures lower than M_f and results in the stress plateau (Otsuka et al. 2005, Liu 1998 and 2001).
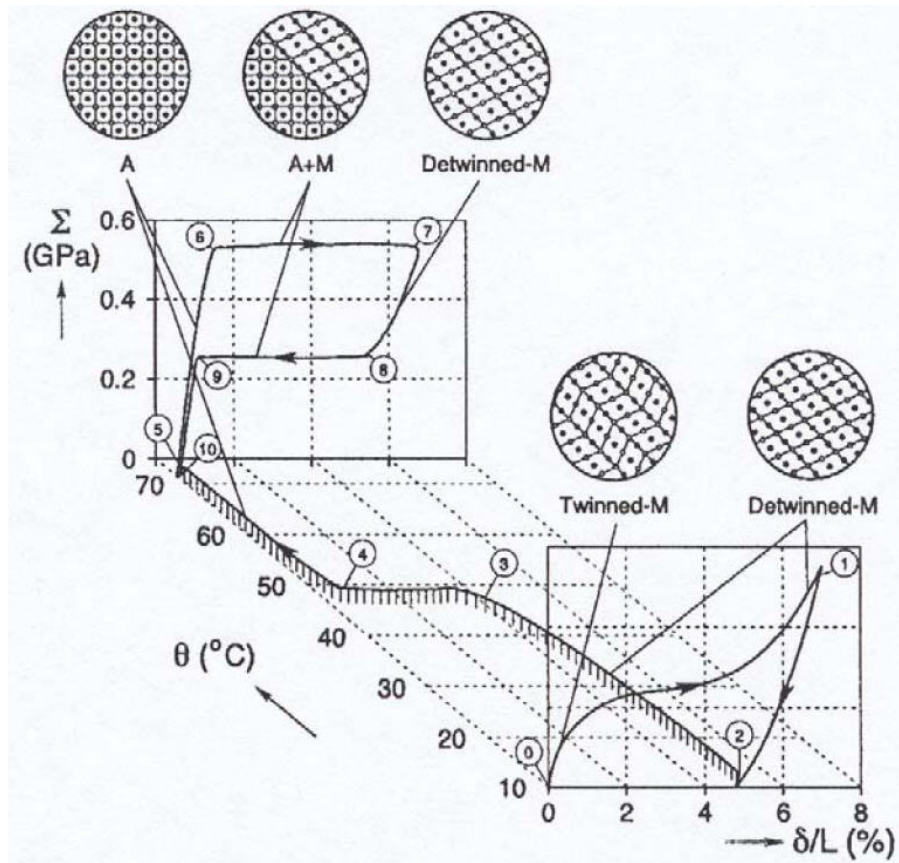
Fig. 5: Stress (Σ)-strain (δ/L)-temperature (θ) relationship in shape memory alloys (Shaw, 2002)

Instead, at high temperatures, the stress-strain relation exhibits a flag shape. The figure demonstrates that the stress plateau at high temperatures is developed due to the conversion of austenite to detwinned martensite. During unloading, the detwinned martensite transforms in austenite due to its instability at temperature up than A_f, so that, a lower stress plateau, related to the reverse transformation, appears in the stress-strain curve (Superelastic Effect, SE), generally, without inelastic strain (Otsuka et al. 2005, Duering et al. 1990).

The above descriptions are related to ideal deformation behaviour of the material; in the following chapter, starting from experimental results, a better description of the mechanical behaviour is reported.

1.3.1 SHAPE MEMORY EFFECT (SME)

NiTi alloys exhibits the Shape Memory Effect (SME) when it is deformed while in the martensitic phase and then unloaded while still at a temperature below M_f. If it is subsequently heated above A_f it will regain its original shape by transforming back into the parent austenitic phase as schematically shown in Fig. 6 and represented in Fig. 5 in terms of stress-strain-temperature curve.

The stress-free cooling of austenite produces a complex arrangement of several variants of martensite. Self-accommodating growth is obtained such that the average macroscopic transformation strain equals zero, but the multiple interfaces present in the material (boundaries between the martensite variants and twinning interfaces) are very mobile. This great mobility is the heart of the SME; movement of these interfaces accompanied by detwinning is obtained at stress levels far lower than the plastic yield limit of martensite but, as said before, after unloading, large inelastic strain can be observed.

The reverse transformation induced by heating recovers the inelastic strain; since martensite variants have been reoriented by stress, the reversion to austenite produces a large transformation strain having the same amplitude but the opposite direction with the inelastic strain and the SMA returns to its original shape of the austenitic phase. Note that subsequent cooling will result in multiple martensitic variants with no substantial shape change (self-accommodated martensite).

The above described phenomenon is called one-way shape memory effect (or simply, shape memory effect) because the shape recovery is achieved only during heating.
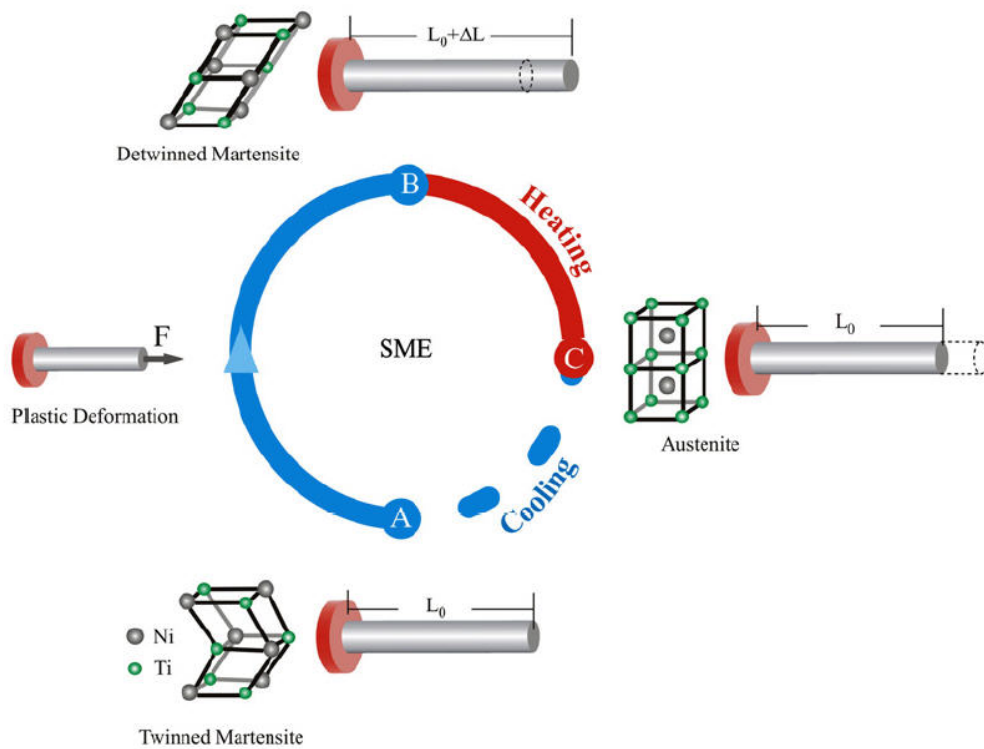
Fig. 6: Shape memory effect phenomenon in shape memory alloys

1.3.2 SUPERELASTIC EFFECT (SE)

The superelastic behaviour of NiTi alloys is associated with the recovery of the deformation upon unloading known as Superelastic Effect (SE). The superelastic behaviour is observed during loading and unloading above A_f and is associated with stress-induced martensitic transformation and reversal to austenite upon unloading.

As said before, if the alloy is externally stressed at a temperature above A_f , it deforms transforming into a detwinned martensite, which is unstable at high temperatures, thus when the load is removed the SMA transforms back into austenite and the original shape of the alloy is fully recovered. The loading and unloading paths during this loading cycle do not coincide, with the unloading path being a lower stress plateau compared to the loading plateau. As a result, there is an area enclosed under the stress-strain diagram which represents the energy dissipated during the transformation. A schematic representation of the superelastic phenomenon is illustrated graphically in Fig. 7 and represented in Fig. 5 in terms of stress-strain-temperature curve.
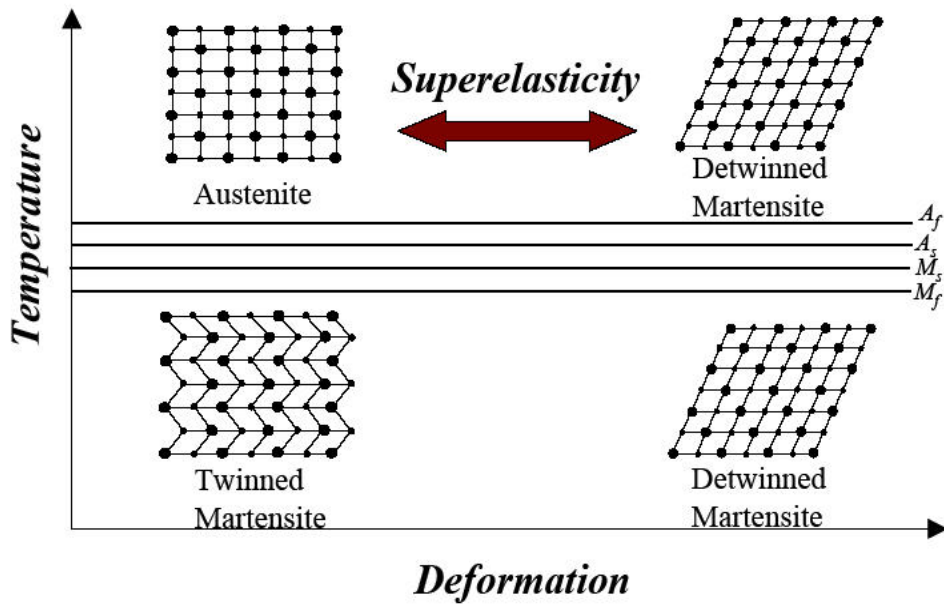
Fig. 7: Schematic representation of Superelastic Effect in shape memory alloys

1.3.3 TWO WAY SHAPE MEMORY EFFECT (TWSME)

In the shape memory effect discussed in the preceding section, what is remembered was the shape of the parent phase only; however, under certain conditions it is possible to remember the shape of the martensitic phase. This effect was first called ''the reversible shape memory effect'' (Nagasawa et al. 1974, Saburi et al. 1974), but now it is called two-way shape memory effect (TWSME), while the ordinary shape memory effect in the preceding section is sometimes called one-way shape memory effect (OWSME), in contrast to two-way. Whereas the SME and SE are intrinsic in the material, the TWSME can be observed only after proper thermomechanical procedure called training. Due to this property, it is possible to modify the shape of the material, in a reversible way between two different ones and without applied stress, only by changing of temperature across Af and Mf. As reported in the previous sections, due to the hysteresis in the transformation temperatures the TWSME is characterized by a strongly non linear hysteresis loops. Unfortunately the intrinsic two-way effect suffers a quite strong deterioration during the working cycles due to microstructural changes (Scherngell et al. 1998). Promising approach to improve the stability of the effect is reported in literature; the aim is to increase the intensity of internal stresses that it is possible by different microstructural features (Scherngell et al. 1998).

The first report of two-way shape memory effect is due to Wang and Buehler [260] for a Ti–Ni alloy; however, a more clearly description of the phenomena is reported by Nagasawa et al. that describe, for Ti–Ni, Cu–Zn and Ni–Al alloys, a reversible shape memory effect obtained when specimens are severely deformed below M_s temperature. A schematic representation of the observed behaviour is reported in Fig. 8.
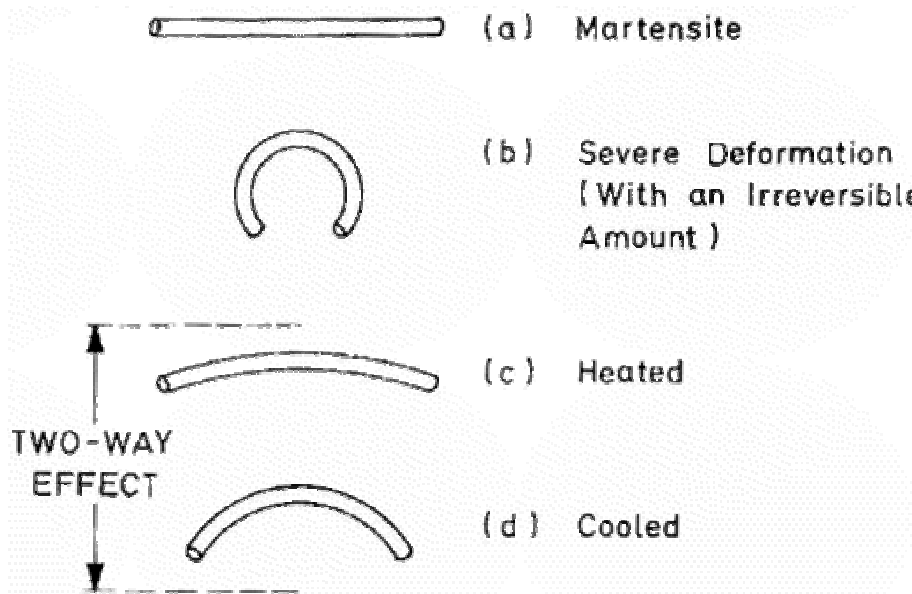
Fig. 8: Schematic representation of Two Way Shape Memory Effect

Thereafter many reports appeared how to realize two-way shape memory effect including the above: (1) introduction of plastic deformation, (2) constraint aging (Takezawa et al. 1976), (3) thermal cycling (Schroeder et al. 1977), (4) utilization of precipitates (Oshima et al 1975, Nishida et al, 1981) and others. Miyazaki et al. (1982) show that there are different possibilities to induce an intrinsic two-way effect
It will be easily expected that in order to realize the shape of martensitic phase, certain martensite variants need to be selected. Since the martensitic transformation strongly interacts with stress, the stress selects certain variants of martensite in the nucleation process in order to lower the energy of the system (Otsuka et al, 1977) and contributes to create the certain shape of martensite. In the above process (1)–(4), certain stress sources are created during the processes such as dislocation configurations, precipitates etc., which produce internal stress fields to choose specific martensite variants. It is clear from the above that two-way shape memory effect is a rather weak effect

compared to one-way shape memory effect, since the former is due to the selective nucleation of certain martensite variants, while the latter is due to the strong reversibility and unique lattice correspondence upon reverse transformation.

In the following chapter, an experimental investigation of the TWSME induced by martensite deformation in a NiTi alloy is reported.

1.4 CYCLIC LOADING AND MARTENSITE STABILIZATION

The cyclic loading effects on NiTi alloy mechanical behaviour has been studied by a large number of researchers; they are in agreement that the changes in the mechanical properties that are associated with the cyclic loading are mainly referred to the martensite stabilization effect, or better to the accumulation of residual martensite at each cycle. This residual martensite is permanent martensite and thus never participates in proceeding phase transformation cycles. The residual strain measured during cycling increase with increasing the number of cycles confirming that at each cycles more and more martensite is stabilized (Otsuka et al. 2005, Tanaka et al., 1995, Liu 1999, Liu et al. 1998, Tobushi et al. 1996; Friend et al. 1999; Gall et al. 1999).

The stabilization effect was observed as an increase in the critical temperatures for the reverse transformation of the deformed martensite; this effect vanishes once the deformed martensite is reverted back to austenite (Otsuka et al. 2005, Tanaka et al. 1995, Liu et al. 1998). In terms of stress-strain curves, this particular effect is evident in the decreasing of the stress for the onset of the plateau, in the increase of its slop and, for an austenitic alloy, in the reduction in the area of hysteresis loops (Otsuka et al. 2005, Liu et al. 1998, Brinson et al. 2004). However, these effects in a polycrystalline alloy are due to the interaction between martensite stabilization and plastic deformation that develop in the material during cycling (Otsuka et al. 2005, Tanaka et al. 1995, Liu et al. 1998 and 1999).

Experimental evidences of martensite stabilization for a martensitic NiTi alloy are reported in the following chapters.

1.5 EFFECT OF STRAIN RATE

The effects due to the strain rate on the NiTi behaviour is an important aspect to be considered above all for understanding its applicability in damping control applications. In these types of applications, the intrinsic damping properties of the martensitic phase and the energy dissipation capability of the material in its austenitic condition (Otsuka et al. 2005) could be successfully used. In particular, in the last decades, NiTi alloys seems to be useful for realizing smart composites for the damping and vibration control (Basavaraj et al 2006, Hurlebaus et al. 2006, Yuse et al. 2005, Nagai et al. 2006, Ogisu et al. 2006). Their use as seismic dampers is also investigated by some researchers (Grasser et al. 1991, De Roche et al. 2002, Dolce et al. 2000).

Many researchers (Dolce and Cardone 2001; Delemont 2002; and Tobushi et al. 1998) have focused their interest on studying the behaviour of NiTi when subjected to dynamic loading with various strain rates. Most of these researchers agree that loading rate affects the mechanical behaviour of the alloy (Graesser et al. 1991, Dolce et al. 2001).

In 2001 Dolce and Cardone conducted a series of experimental tests using NiTi wires under tensile loads with a strain rate that varied between 0.01 and 4 Hz; Figs 9 is related to 0.02 Hz, 0.2 Hz and 2 Hz as strain rates for the cyclic load; the results show as the rate of loading is increased the loading and unloading plateau are shifted upwards. This shift is associated with a reduction in the hysteresis area. The authors found that the change in behaviour tends to stabilize after a strain rate equal to 0.2 Hz, and no more significant changes in the stress-strain curve were noticed. On the other hand, Tobushi and his colleagues in 1998 conducted a series of experimental tests using strain rates that were smaller compared to Dolce and Cardone. Tobushi et al. found that at very small rates of loading, the stress-strain curves of the alloys are stable while at higher strain rates the martensitic phase transformation is increased.

Most of the researchers agreed that the reason for such change in the material mechanical behaviour at higher strain rates is the fact the material releases heat during the martensitic transformation and absorbs heat in the reverse transformation. If the strain rate is high, there will not be enough time for the material to transfer or absorb heat from the surrounding environment and this might lead to self-heating of the

material, which results in changing the mechanical characteristics of the alloy (Wu 1996, and Dolce et al. 2001).
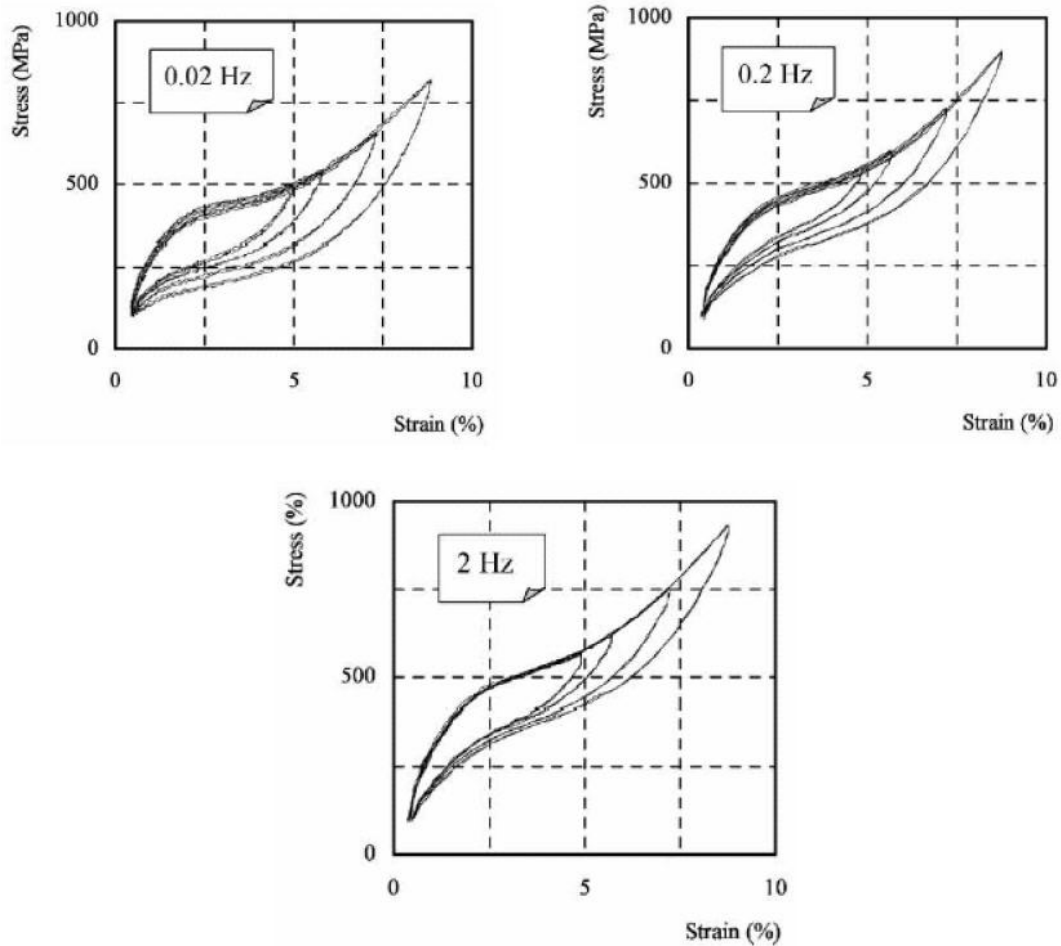
Fig. 9: Stress-strain curves for austenite NiTi alloy at 0.02 Hz, 0.2 Hz, and 2.0 Hz strain rates (Dolce and Cardone, 2001)

1.6 ASPECTS RELATED TO THE PRODUCTION OF NiTi ALLOYS

1.6.1 ALLOY COMPOSITION

General requirements on Nitinol chemistry and trace elements are defined in an ASTM standard, F2063-00. The chemical composition of the alloy affects directly the phase transformation temperatures (Birman, 1997 and Serneels 1999, Otsuka et al 2005), which plays an important role in defining the alloys mechanical properties as explained in the previous sections. The sensitivity increases with Ni content in the alloy; a one

24

weight percent deviation in Ni (or Ti) concentration would result in approximately a 100°C shift in transformation temperatures. This extreme sensitivity puts a strict requirement on any melting practice to tightly control the Ni and Ti ratio in order to meet the required tolerance in transformation temperatures.

Generally, a significant decrease of the Af temperature is observed increasing Ni content in the alloy. A reduction of the hysteresis width in the characteristic transformation temperature and stresses is also clearly explained (Serneels, 1999). There has been much effort to modify Ti–Ni shape memory alloys by adding various alloying elements to the binary system. It was found alloying elements often alters transformation temperature greatly. The effect of third element on transformation temperature are clearly reported in the literature (Homa et al. 1987, Angst et al. 1995)

1.6.2 MANUFACTURING PROCESS

After melting, the Nitinol ingot is usually forged and rolled into a bar or a slab at elevated temperatures. Optimal hot working temperatures appear to be around 800°C where the alloy is easily workable and the surface oxidation in air is not too severe (Suzuki, 1998). Following hot working, NiTi alloys are cold worked and heat-treated to obtain final dimensions with desired physical and mechanical properties. Generally, cold work percentage between 15% and 40% and thermal treatment at temperatures between 350 °C and 700 °C are used.

The mechanical behaviour of NiTi is determined by the method used to process the alloy (Otsuka et al. 1998 and 2005). The combination of the effects due to cold work and heat treatment defines the material behaviour in terms of both mechanical and functional properties.

As example, in Figs 9 and 10, the effects of different thermal treatments and cold working on the material transformation temperatures are reported.

In particular, Fig. 9 shows as both martensite and austenite temperatures increase with increasing heat treatment temperature; they reach a plateau once they are fully annealed and all cold work effects are removed.

Instead, as shown in Fig. 10, high cold work percentage stabilizes the austenitic structures in the material decreasing the transformation temperatures. The higher the

heat treatment temperature, the more the dislocations introduced during cold working are rearranged and annihilated and the curves are coming closer to each other.

According to these considerations, for a defined chemical composition, the percentage of cold working and the temperature of heat treatment must be chosen accurately in order to set a desired mechanical and functional behaviour of the material.
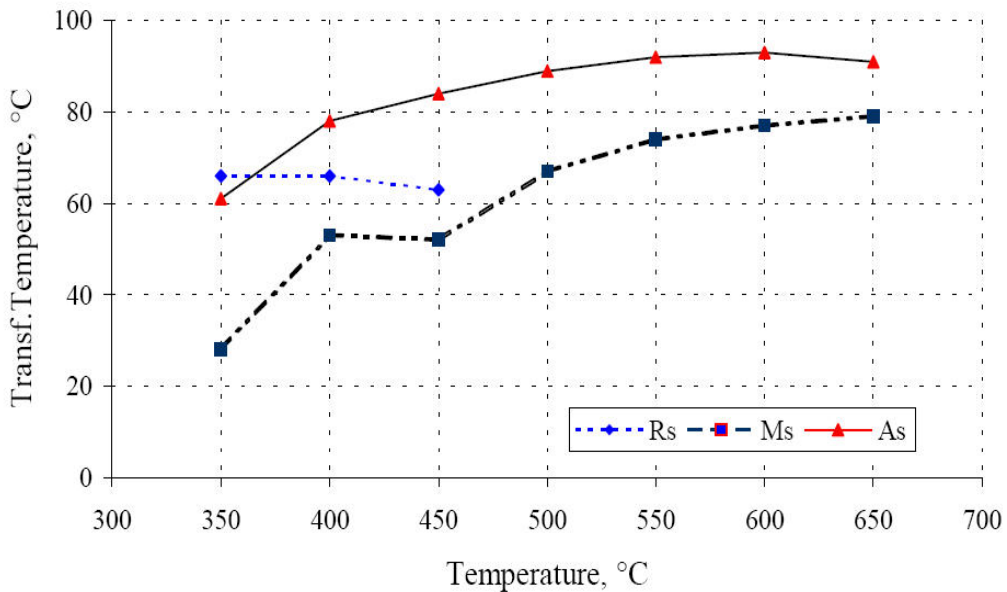
Fig. 9: Transformation temperatures for a Ni-50.5 at% Ti alloy 18% cold worked followed by a heat treatment at a temperature specified in the x-axis followed by water quenching (Serneel, 1999)
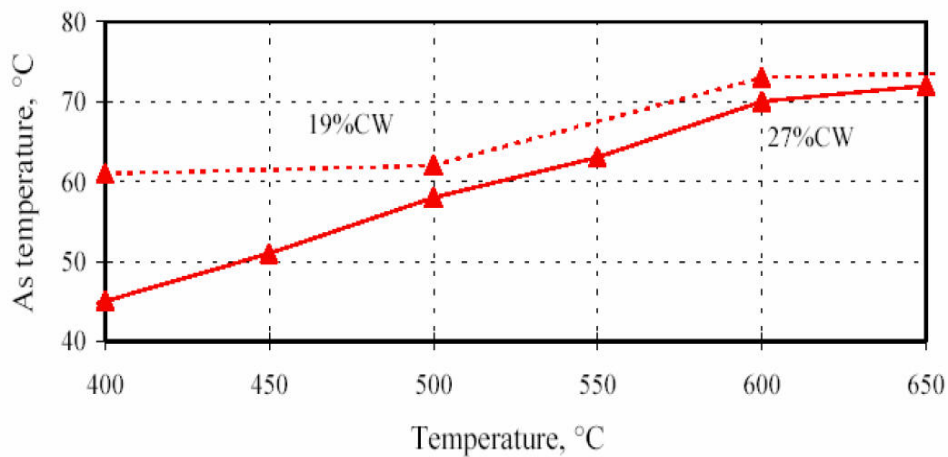
Fig. 10: Effect of cold work on the phase transformation temperatures (Serneel, 1999)

1.6.3 MACHINING OF NITI ALLOYS

One of the problems related to the industrial applicability of NiTi alloys is the difficulties related to their machining using conventional techniques such as milling, turning and drilling; the significant tool wear and the need of high experienced operators increase the costs with respect to conventional materials. Furthermore, the convectional technique have a strong influence on the material behaviour because of their high thermal and mechanical effects; so that, especially for components with low dimensions, their use could cause an excessive degradation in the material performance. For these reason, laser machining, electro-discharge machining (EDM) and photochemical etching processes are often used to fabricate NiTi components. In particular, laser machining has become the preferred process for the manufacture of NiTi alloys because offers high speed, high accuracy and the capability for rapid prototyping (Meijer 2004). The drawbacks of this technique are linked to the extension of heat-affected zone (HAZ) and the presence of microcracks.

EDM works well with most Nitinol compositions. In this case, very low influence on the material properties are assured by the intrinsic characteristics of the technique (Ho et al. 2003); however, in some applications, the drawbacks could be the contaminations due to Cu electrode and dielectric; the recast surface layer formed on the material in the machining zone may need to be removed in some application like biomedical components (Lin et al. 2001).

CHAPTER 2

CHARACTERIZATION OF SHAPE MEMORY BEHAVIOUR IN NITI ALLOYS

2.1 INTRODUCTION

In the previous chapter, a general description of the NiTi properties are carried out in terms of mechanical and functional behaviour. In order to better understand and describe the material properties, in this chapter the results related to the experimental investigations carried out on a NiTi alloys are reported. In particular, a martensitic alloy is characterized in terms of uniaxial tensile behaviour and shape memory (OWSME and TWSME), in order to investigate the deformation mechanisms involved in the material performance.

2.2 CHARACTERIZATION OF A NI-51 AT.% TI ALLOY

In this section, the results of the characterization of a Ni-51 at. % Ti alloy, that is in martensitic conditions at room temperature, are presented. The thermomechanical characterization was executed in terms of mechanical behaviour and shape memory effect (OWSME and TWSME); furthermore, the effects on the stress-strain uniaxial behaviour of the material due to a thermal treatment are evaluated.

The shape memory behaviour was analyzed under training cycles executed by induce plastic deformations in the martensitic structure. This training procedure permits to develop the TWSME in the material and to evaluate the material deformation behaviour during repeated thermomechanical cycles executed at fixed training deformation and temperatures. The hysteresis loops, strain versus temperature, describing the two way shape memory behaviour of the material were measured and the influence of the training deformation and the number of training cycles were investigated. Furthermore, the stability of the TWSME was evaluated at increasing number of thermal cycles, under several values of constant applied stress.

The experimental investigations were carried out using Ni-51 at.% Ti sheets, 1.15mm in thickness and 25.5 mm in width, that are supplied by CNR-IENI of Lecco (Italy) and which were produced by cold-rolling with a thickness reduction of about 22%. The as received material is cold worked without any successive thermal treatment, so that, in order to reduce the effects of cold working and to obtain a complete martensitic structures at room temperature, a proper thermal treatment was executed on the NiTi sheets (Otsuka et al. 2005, Serneels 1999). The material was thermally treated, at 700 °C for 20 min, and the effect of the treatment on the stress–strain behaviour are investigated by a comparison between treated and untreated material.

Dog bone shaped specimens were cut from the sheets and used for the thermomechanical tests. As explained in the previous chapter, NiTi properties are strongly influenced by the thermal effects related to the production processes, furthermore, NiTi alloys are characterized by a poor workability with conventional machining processes such as milling, turning and drilling; so that the specimens was realized by electro-discharge machining (EDM) (Theisen et al. 2004). In Fig. 1 the mould used for the EDM process and the dimensions of the specimens is shown.
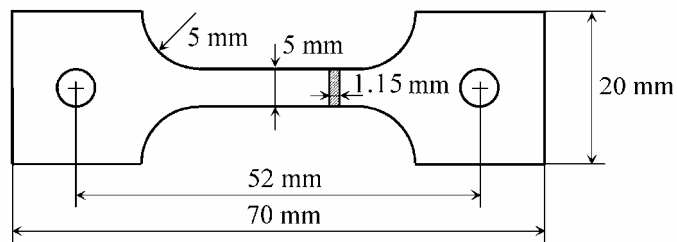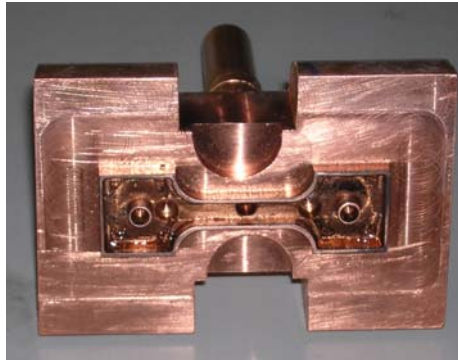
Fig. 1: Copper mould and specimen for thermomechanical tests

The thermo-mechanical tests were carried out by using a universal testing machine (Instron 8500), equipped with a furnace (MTS 653). The local deformation of the specimen were measured by a resistance extensometer with a gauge length of 10 mm, while the temperature was acquired, in the middle of the gauge length, by a thermocouple type J. Load, deformation and temperature outputs were acquired by means of a data acquisition system, represented by a personal computer equipped with a National Instruments acquisition card (DAQ PCI-MIO16-E-1) controlled by the Labview® 6.0 software package.

2.3 RESULTS

2.3.1 EFFECT OF THERMAL TREATMENT AND MECHANICAL BEHAVIOUR

Thermal treatment was carried out at 700 ∘C for 20 min in air and its effect on the stress–strain behaviour are investigated by a comparison between treated and untreated material as reported in Fig.2. The isothermal stress–strain curves are measured at room temperature for two different values of the total deformation (ε_{tot} = 3.5% and 5.5%).
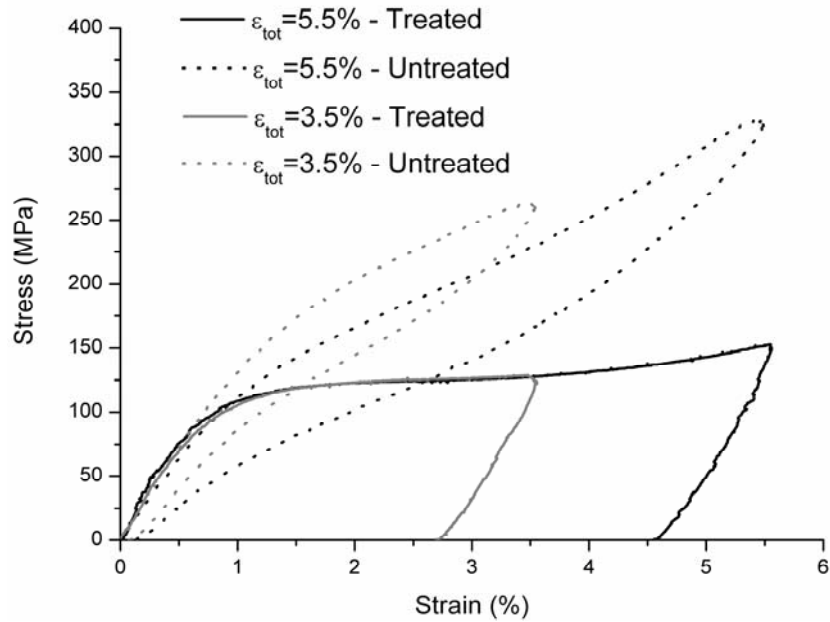
Fig. 2: Stress-Strain curves of treated and untreated materials

The dashed curves show the superelastic behaviour of the untreated material that reveal its highly hardening at room temperature. As said in the previous chapter, the cold working processes stabilize the austenitic structure decreasing the transformation temperatures. In fact, the A_f temperature of the investigated alloy, measured by Differential Scanning Calorimetry (DSC) tests, is about -12 °C. Furthermore, the high slope of the characteristic stress plateau is a consequence of the hardening due to the cold-rolling process carried out during the production of the material.

The stress–strain response of the thermally treated material is represented by the continuous curves in Fig. 2; the results show that the adopted thermal treatment permits to obtain a martensitic structure of the material. The DSC thermogram of the thermal treated material is reported in Fig. 3; the measured phase transition temperatures were: M_f=42 °C, M_s=63 °C, A_s=76 °C and A_f=94 °C.
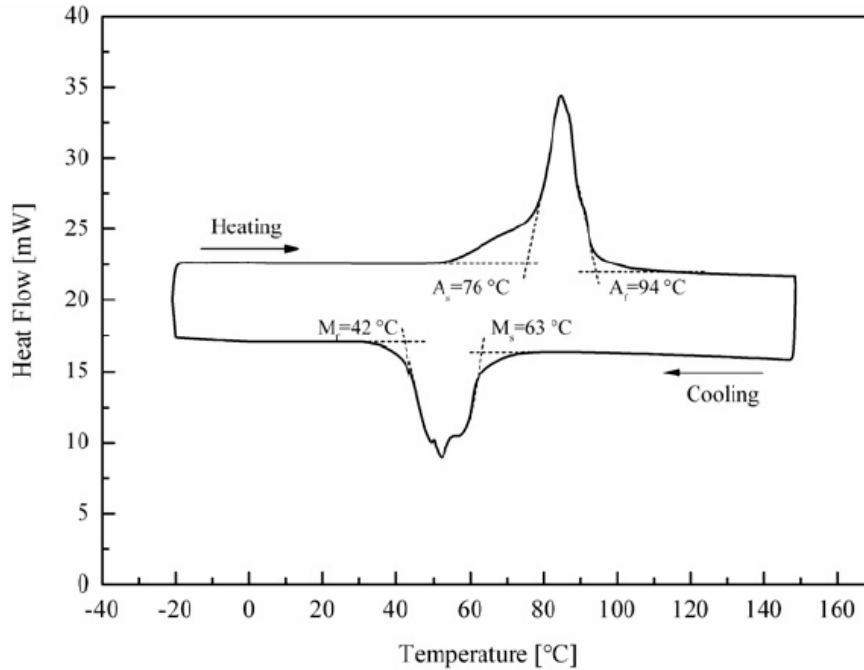
Fig. 3: DSC thermogram of treated material

The characteristic stress-strain behaviour associated to the martensitic detwinning mechanisms is clearly evident in Fig.2 for the treated material; in particular, the first branch of the curve represents its elastic behaviour while the following one, starting from an apparent yield point, denotes the detwinning deformation process that evolves in a Löuders manner (Otsuka et al. 2005, Liu et al. 1998). The plateau occurs at a stress level of about 120 MPa and seems to be quite flat until 5.5% confirming that the thermal treatment is able to significantly reduce the effects of cold working.

In order to not damage the specimens, no tests are performed at deformation higher than 5.5% for this material. However, as reported in Fig. 4 as example, after the stress plateau the curve of a martensitic NiTi alloy shows a rapid increase of the stress mainly due to the elastic deformation of the detwinned structure (Otsuka et al. 1998, Liu et al. 1998); finally, a second apparent yield, characterized by high plastic strain, occurs at higher stress level before fracture. Practically, after the stress plateau, the deformation behaviour of the alloy becomes similar to that of traditional structural materials; most of the special properties of the NiTi alloys lies in the stress plateau.

As reported in reference (Otsuka et al. 2005, Liu et al. 1998), for a polycrystalline matrix, an exact definition of the different zones is difficult due to the coexistence of the several mechanisms associated to the deformation process. In particular, due to the

32

mismatch in the martensite variants, it is impossible to achieve a full reorientation of the material structures without plastic deformation. The plastic deformation is required to co-ordinate the mismatch in orientation in order to maintain the integrity of the matrix. For the tested material, until a deformation of 5.5%, the main deformation mechanism involved is the orientation of the martensite variants that assures the shape memory behaviour of the material. However, as explained before, and experimentally evidenced in the following, the development of plastic strain and elastic strain occurs during each stage of the stress-strain curve.
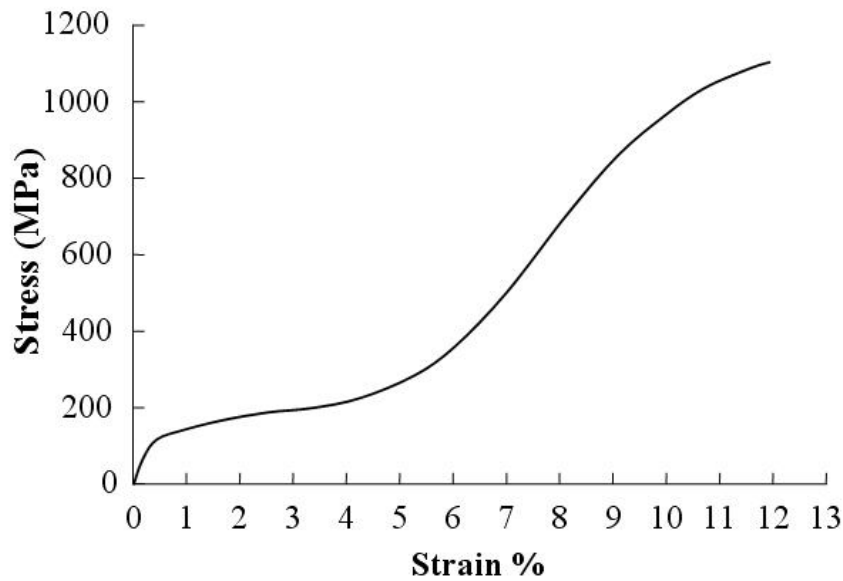
Fig. 4: Stress-Strain curves of a NiTi in martensitic conditions

2.3.2 TRAINING AND TWSME

In order to study the shape memory behaviour of the material, and to induce in it the two way shape memory effect by martensite deformation (Liu et al. 1998), a training procedure was carried out through the repetition of several thermo-mechanical cycles, which consist in a mechanical load, a complete unloading and a subsequent thermal cycle, between the temperatures M_f and A_f. In Fig. 5 an example of the generic i-th thermo-mechanical cycle is shown, which is composed of four subsequent steps: (1) strain controlled uniaxial tensile loading at a strain rate of 0.06 min-1 up to a total deformation $\varepsilon_{tot}(i)$; (2) complete unloading at the same rate and recording the residual strain $\varepsilon_{res}(i)$ and the strain recovered upon unloading, termed the mechanical recovery,

$\varepsilon_{mech}(i)=\varepsilon_{tot}(i)-\varepsilon_{res}(i)$; (3) heating up to A_f to activate SME and measuring the deformation in austenitic condition $\varepsilon_A(i)$, which can also be regarded as plastic strain $\varepsilon_{pl}(i)$, and the strain recovered upon heating, termed the thermal recovery $\varepsilon_{th}(i)=\varepsilon_{res}(i)-\varepsilon_A(i)$; (4) cooling down to M_f and recording the deformation in martensitic condition $\varepsilon_M(i)$, the two way strain $\varepsilon_{tw}(i)=\varepsilon_M(i)-\varepsilon_A(i)$ and the one way strain $\varepsilon_{ow}(i)=\varepsilon_{res}(i)-\varepsilon_M(i)$. In each thermo-mechanical cycle a training deformation, ε_{tr}, of 3.5 or 5.5% was applied, starting from the end of the previous one, so that the total martensite deformation, ε_{tot}, increases with increasing the number of cycles, $\varepsilon_{tot}(i)=\varepsilon_M(i-1)+\varepsilon_{tr}$, due to the formation plastic strain at the end of the cycle.
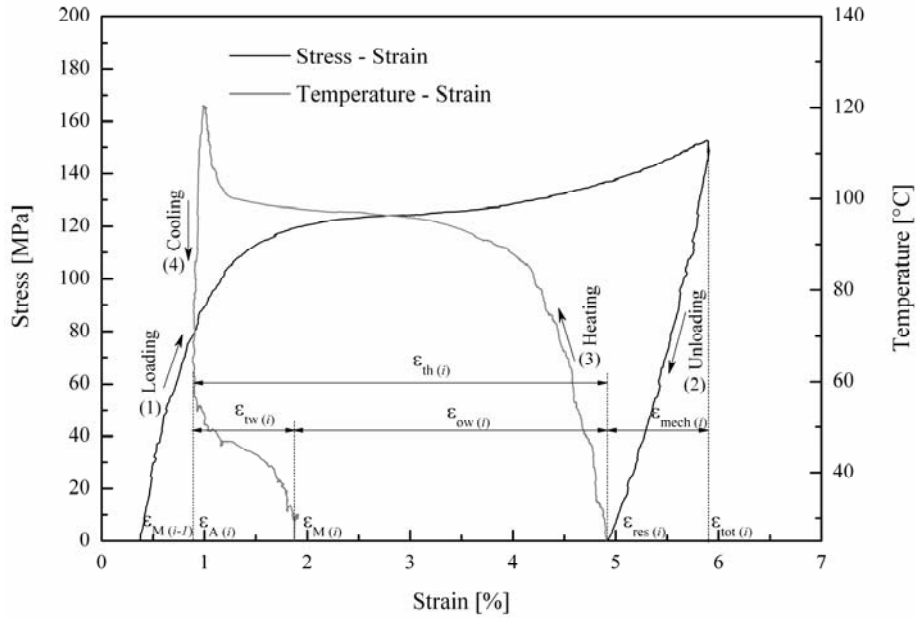
Fig. 5: Example of the *i*-th training cycle.

The modifications in the stress-strain response, during thermo-mechanical training, for the two training deformation $\varepsilon_{tr}=3.5\%$ and $\varepsilon_{tr}=5.5\%$ are shown in Figures 6(a) and 6(b), respectively. Eight subsequent training cycles were carried out with $\varepsilon_{tr}=3.5\%$, while six cycles were executed with $\varepsilon_{tr}=5.5\%$ in order to avoid fracture, due to the formation of high stresses and strain. Both figures illustrate the stress-strain curves for the first, an intermediate and last thermo-mechanical cycle, and the following observations can be drawn: when increasing the number of training cycles an hardening of the material is observed, resulting in large stress level, together with a decrease in the stress for the

onset of the detwinning. These evidences are an indication of the stabilization of the martensite variants as consequence of the cycling.

The stabilization effect is a particular effect generally attributed to the modifications in the variant structures of martensite caused by the deformation (Otsuka et al. 2005, Liu et al. 1998, Liu 1999, Wada et al. 2005). In particular, the internal elastic strain energy, stored in the twinned martensite, as consequence of the constraint to the lattice distortion of the transformation in a polycrystalline matrix, serves as a driving force for the reverse transformation for a thermal martensite. This elastic energy, or better this internal elastic stress field, is sensitive to martensite variant accommodation structures. Deformation by martensite reorientation, or by detwinning, releases this internal elastic energy and further deformation creates an opposite internal elastic stress field in the direction of the oriented martensite. This new internal elastic stress field acts as a resistance to the reverse transformation; the loss of the internal elastic energy stored in the self-accommodating martensite and the creation of an opposite internal elastic energy in the oriented martensite contribute together to the stabilization effect (Liu 1999, Wada et al. 2005). The experimental evidence of the TWSME, developed after the deformation, is indicative of the establishment of an internal stress field in the direction of the deformed martensite. The reverse transformation of the deformed martensite, which involves a shape change in the opposite direction to the original deformation, is resisted by this internal stress field, that, instead, guides the formation of a oriented-accommodating variant structures during the martensitic transformation, generating the TWSME of the material. The stabilization effect is also observable, as reported in the following, in the increase of the temperatures for the M→A transformation; this increase happens because the energy required for the M→A transformation in a stabilized martensitic structure is higher as consequence of the mechanical effect due to the internal stress field (Liu 1999, Wada et al. 2005).

As shown in Fig. 6(b) the stabilization effect is more evident when the material is subjected to a training deformation of 5.5%, because of the high values of deformation and, consequently, of the internal elastic stress field created.
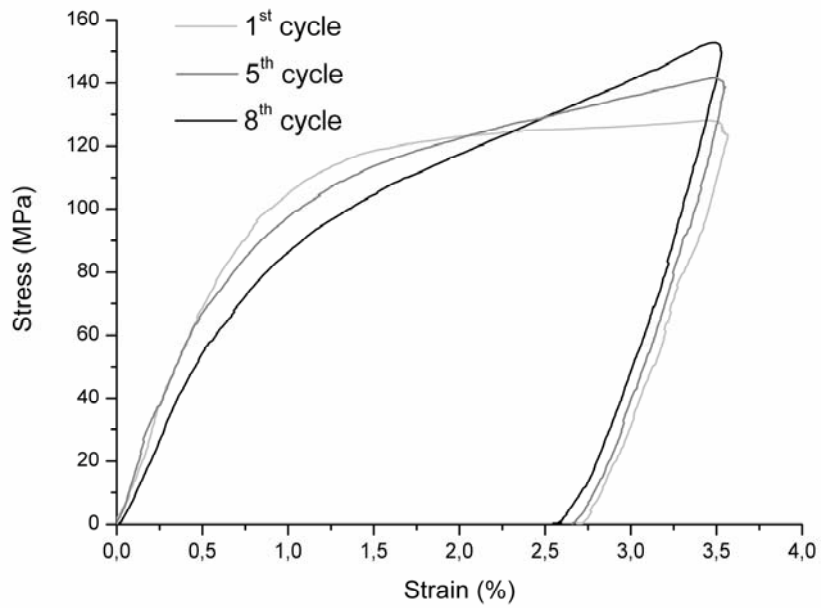
(a)
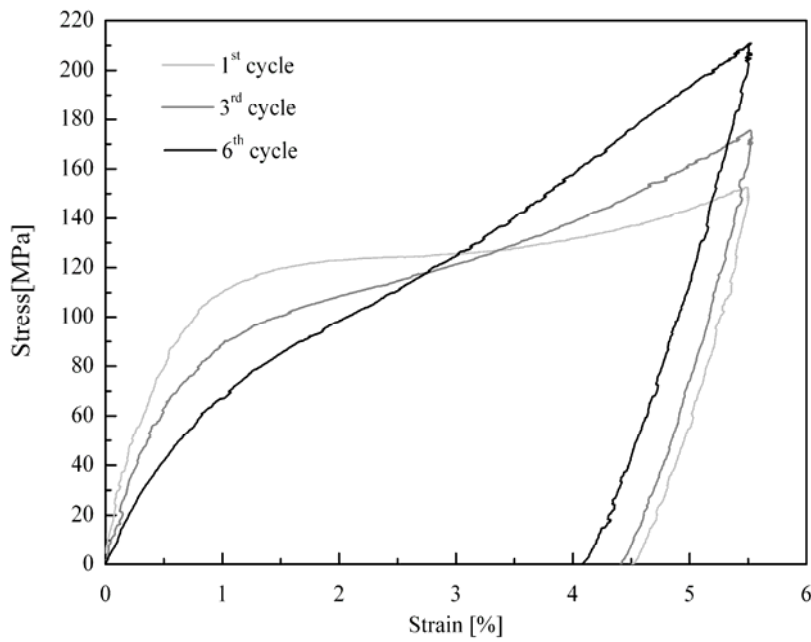
(b)

Fig. 6: Stress-strain curves during thermo-mechanical training:

a) Training deformation ε_{tr}=3.5 %; b) Training deformation ε_{tr}=5.5 %

Fig. 7 report the measured values of ε_{tot}, ε_{res}, ε_A and ε_M versus the number of training cycles, for the two values of training deformation; in particular, Fig.s 7(a) and 7(b) illustrate the results for ε_{tr}=3.5% and ε_{tr}=5.5%, respectively.

(a)

(b)
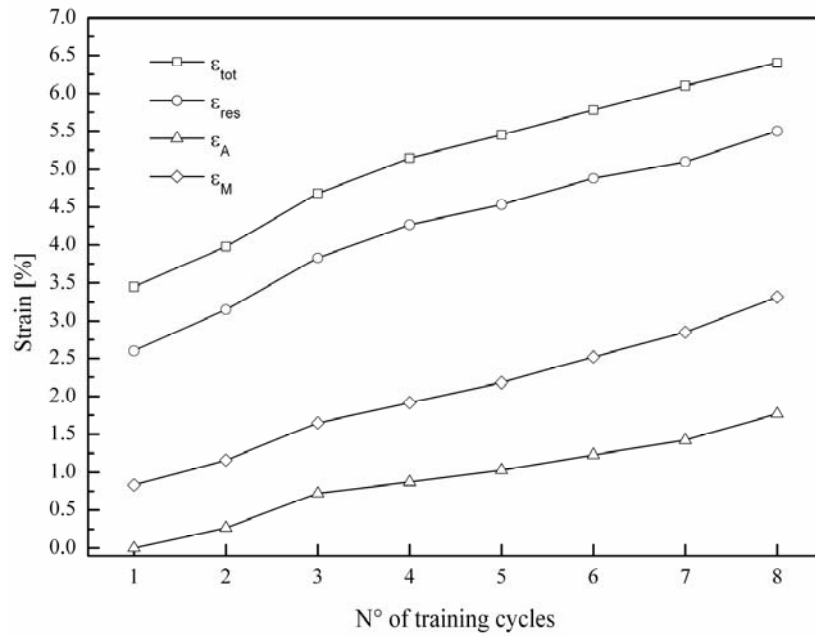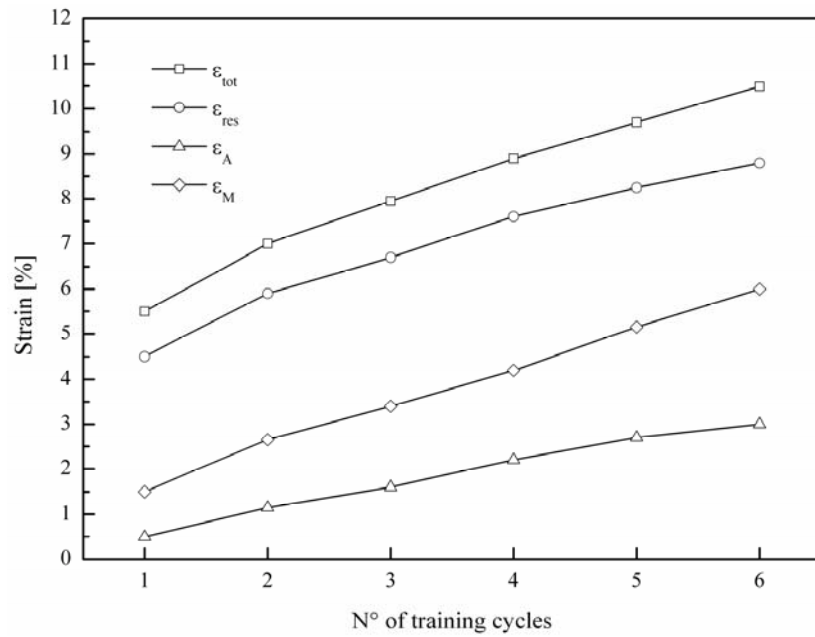
Fig. 7: ε_{tot}, ε_{res}, ε_A and ε_M versus the number of training cycles:
a) Training deformation ε_{tr}=3.5 %; b) Training deformation ε_{tr}=5.5 %

(a)

(b)

Fig. 8: ε_{th}, ε_{tw}, ε_{ow} and ε_{mech} versus the total strain ε_{tot}:

a) Training deformation $\varepsilon_{tr}=3.5$ %; b) Training deformation $\varepsilon_{tr}=5.5$ %

As expected, both figures clearly show that all the deformations increases with increasing the number of training cycles as a consequence of the formation of a dislocation structure, which is confirmed by the increase in the plastic strain ε_{pl}, i.e. the deformation in austenitic condition ε_A. In particular, Figure 7(a) shows that ε_{tot} increases from 3.5 %, at the first training cycle, to 6.4% after eight cycles, whereas ε_{pl} raises from 0 to 1.8%. As expected Figure 7(b), which is relative to a training deformation of 5.5%, shows higher values of both ε_{tot} and ε_{pl}, which increase from 5.5% to 10.5% and from 0.5% to 3.0 %, respectively. As said before, the development of the plastic strain benefits the two way shape memory behaviour of the material. It is important to point out that in the measured ε_{pl} also the deformation due to the martensite stabilization is computed.

Figs 7 show the measured values of the two-way strain, ε_{tw}, one-way strain, ε_{ow}, thermal recovery strain, ε_{th}, and mechanical recovery strain, ε_{mech}, versus the total strain ε_{tot}, during the thermo-mechanical training; in particular, Fig. 8(a) and 8(b) are relative to a training deformation of 3.5% and 5.5%, respectively. Both figures show that the thermal recovery, ε_{th}, increases with increasing the total strain, with maximum values of 3.8% and 5.8% for ε_{tr}=3.5% and ε_{tr}=5.5%, respectively; as the thermal recovery ε_{th} can be regarded as $\varepsilon_{tw}+\varepsilon_{ow}$ (see Fig. 5), this result indicates that, in the investigated range, an overall increase in the shape memory performances of the material when increasing the total strain in the investigated ranges as consequence of the developing of detwinned martensite and plastic strain. In fact, the graphs show that the two way strain increases with increasing the total deformation, for both training conditions, whereas an increase in the one way strain is observed in the first cycles.

The subsequent decrease of the one way strain with further increasing the total deformation can be attributed to the formation of a dislocation structure and stabilized martensite, which in turn benefit the two way shape memory performance of the material, as consequence of the establishment of a directional internal residual stress field and, consequently, cause a reduction of the one way recovery capability of the material, due to the smaller fraction of M→A transformation during thermal cycles (Liu et al. 1998, Liu 1999, Wada et al. 2005, Otsuka et al. 2005).

 In particular, the curves in Fig. 8(a), which are relative to a training deformation ε_{tr}=3.5%, show an increase in ε_{tw} from 0.8% to 1.6%, and an increase in ε_{ow} from 1.8%

to 2.4%, when ε_{tot} raises from 3.5 % to 5.8%, and a subsequent small decrease to 2.3% with further increasing the total deformation. As shown in Fig. 8(b), the aforementioned effect is more evident for a training deformation of 5.5%, where ε_{tw} raises from 1.0% to 3.0%, whereas ε_{ow} reaches a maximum value of 3.4%, when ε_{tot} is about 9%, and a subsequent marked decrease to 2.8% is observed when ε_{tot}=10.5%. The graphs also show a very small increase in the mechanical recovery ε_{mech} when ε_{tr}=3.5%, whereas a marked increase is observed when ε_{tr}=5.5%. At each cycles more and more stabilized martensite are not detwinned but deformed elastically; this causes the increase of the slope of the plateau during loading and the increase in the ε_{mech} upon unloading. This effect is also qualitatively shown in Fig. 6(b) where a strong hardening of the material is observed when the thermo-mechanical cycles are carried out with a training deformation of 5.5%; because of the higher value of reached deformation, a more rapid stabilization effect, with respect to a training deformation of 3.5%, is observed, resulting also in higher value of ε_{mech}.

The two way shape memory strain of the material, obtained by a training deformation of 5.5%, was also measured under a fixed applied stress, as illustrated in Fig. 9. This investigation permits to understand the capability of the material to produce work during the TWSME cycle and to evaluate the modifications induced in the material behaviour by the applied stress. In fact, The production of work, in applications where the material is used as actuators, is obtained applying a resistance force that oppose itself to the shape recovery of the material.

The figure shows the measured hysteresis loops, two way strain versus temperature, in the case of stress free condition, together with those obtained by two fixed values of tensile stress, 50 and 100 MPa. As clearly shown ε_{tw} increases when increasing the applied stress, from 3.1% to 3.6% and 4.2% under 50 MPa and 100 MPa, respectively. As can be seen, the external stress, applied in the same direction of the previous deformation, benefits the formation of further stabilised preferentially oriented martensite variants and, consequently, an increase in the ε_{tw} (Wada et al. 2005, Otsuka et al. 2005).

The figure also shows, as expected, a systematic increase of the transformation temperatures as consequence of the applied stress, or rather the volume fraction of the

stabilised martensitic variants (Liu et al. 1998, Liu 1999, Wada et al. 2005, Otsuka et al. 2005).

In Fig. 10 the transformation temperatures, which were identified by using the slope line extension method, as function of the applied stress are shown. The linear increase in the transformation temperatures is an accordance with the well known Clausius-Clapeyron rule. In particular, as reported in the following, the $d\sigma/dT$ is a characteristic constant of the material. In the investigated range, an increase of about 10 °C is observed for all transformation temperatures when the specimen is subjected to a tensile stress of 50 MPa, and an increase of about 15 °C is measured in the specimen under 100 MPa.
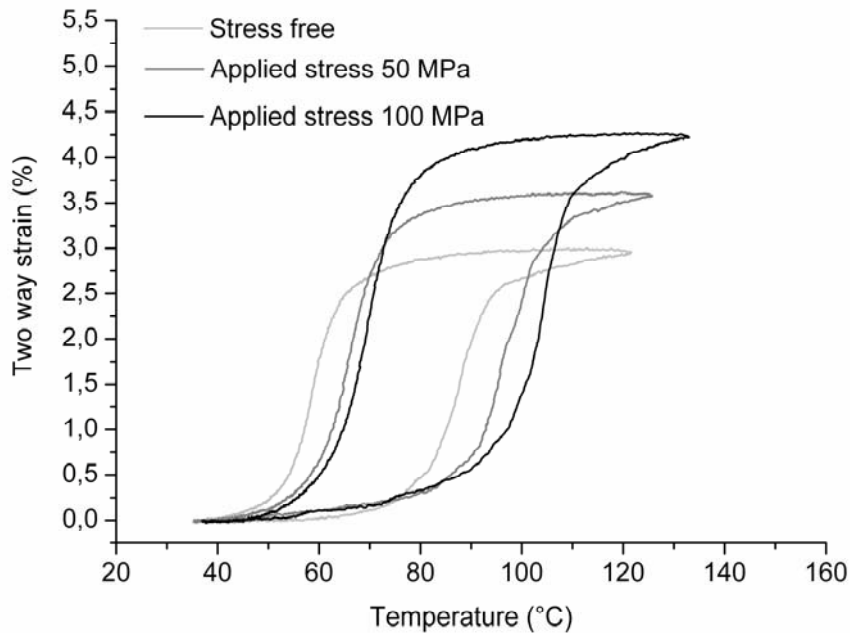
Fig. 9: Hysteresis loops at different applied stress
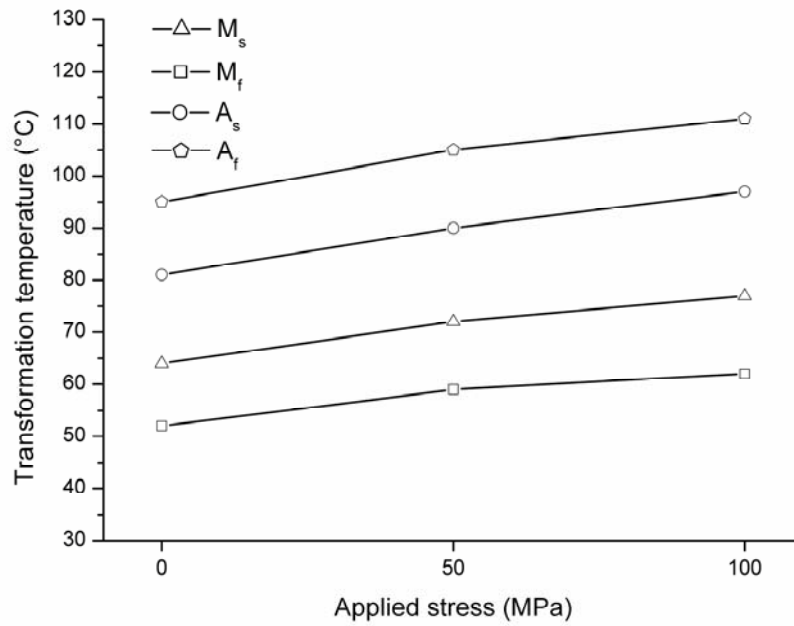
Fig. 10: Transformation temperatures as function of the applied stress

In many practical application the NiTi alloys are subjected to cycling by repeated heating and cooling; therefore the thermal stability of two way shape memory effect is an important issue to design and control smart sensors and actuators. In Fig. 11 the stability of two way shape memory effect, for the specimen obtained by a training deformation of 5.5%, is shown versus the number of thermal cycles.

The material shows a degradation of ε_{tw} from about 3.1% to 2.1 % after 35 thermal cycles; it seems that degradation occurs in two stages, in fact, ε_{tw} decreases rapidly in the first 25 thermal cycles and then becomes stable with further increasing their number. In the first stage a rearrangement of the internal stress field seems to come until a new saturated state is reached at higher number of cycle. This behaviour is due to a partially relaxation of the stress field formed by the training process, leading to the difficulty to form the preferentially oriented martensite variants (Perkins 1973, Miyazaki et al. 1986).
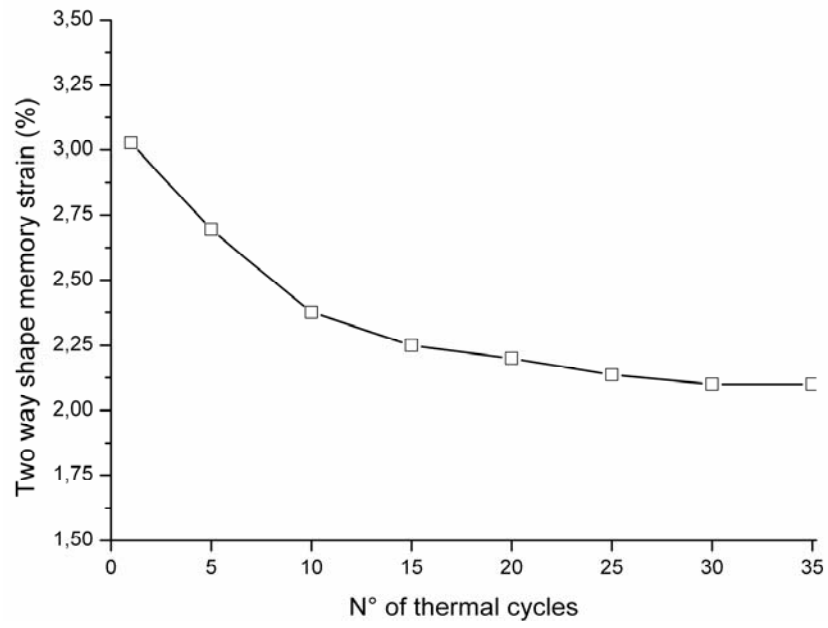
Fig. 11: Two way shape memory strain versus n° of thermal cycles

CHAPTER 3

LASER WELDING OF NITI ALLOYS: MECHANICAL AND SHAPE MEMORY BEHAVIOUR

3.1 OVERVIEW

Because of reduced manufacturing costs and improvements in product quality, the demand for NiTi alloys is expected to rise considerably in the near future. Unfortunately, due to the low workability of these materials with conventional machining processes (milling, turning and drilling), suitable joining and cutting techniques must be used to obtain devices and components with complex geometries. Furthermore, as described in the previous chapters, NiTi properties strongly depend on the production parameters; the modifications induced by the working processes, in terms of thermo-mechanical effects and chemical contaminations, have a strong influence on the functional behaviour of the material (Otsuka et al, 2005; Serneels, 1999). A deeper understanding of the modifications due to various working processes on the properties of these alloys, could be useful for developing new industrial applications. In this field, obtaining welded joints with similar mechanical and functional properties of the unwelded ones, could create new possibilities for the realization of complex shaped components. Welding NiTi to itself can be more easily

44

performed with respect to the welding with dissimilar metals (H. Wu Ming, 2001). A degradation in SE and SME is generally observed in the homologous weld joints together with a degradation in tensile strength and in the resistance to permanent deformation, due to the microstructural modifications induced in the welding zone (Beyer et al, 1986 and 1989; Schlossmacher et al, 1995 and 1997; Haas et al, 1999; Falvo et al, 2005). Joining NiTi alloys with dissimilar metals, and in particular with stainless steel (Wang, 1997), is very difficult due to the formation of brittle intermetallic compounds. Generally, these types of weld joints are made using a interlayer material (H. Wu Ming, 2001).

One of the main problems involved in the welding of NiTi alloys is the oxidation of the weld bead due to the high reactivity of the titanium; for this reason, the protection of the welding zone using inert gas (Tuissi et al, 1999, Falvo et al, 2005 and 2007; Schlossmacher et al, 1995 and 1997), such as helium or argon, is necessary together with an accurate cleaning of the weld zone to avoid chemical contaminations.

Another important aspect to be considered is the formation of cracks in the heat affected zone and molten zone in terms of hot and cold cracking (H. Wu Ming, 2001; Beyer et al, 1986; Falvo et al, 2005); this problem is more evident in the welding of Ti rich NiTi alloys.

The hot, or solidification, cracks sensibility of NiTi welded joints are mainly due to the presence of impurities with lower melting temperatures than the NiTi material. Solidification cracking occurs during the terminal stage of solidification, when grains are separated from one another by a small amount of liquid in the form of grain-boundary films (Weman, 2003). At this time, the weld metal can be rather weak and thus susceptible to cracking in the presence of tensile stresses/strains. The weld metal tends to contract during cooling because of solidification shrinkage and thermal contraction, so that tensile stresses/strains can be induced in the weld metal if it cannot contract freely during cooling, for instance in a highly restrained workpiece.

The cold cracking, instead, is caused by the residual stresses that are in the welding components as consequence of the thermal effects due to the welding and it occurs at temperatures close to the ambient temperature (Weman, 2003). In particular, if the material is embrittled by the welding, these residual stresses can cause the fracture of the joint. The embrittlement of the welded material can be attributed to the formation of

some chemical compounds that decrease the ductility of the joints, such as oxides, or to particular microstructures of the material formed during the cooling of the weld bead. These types of cracks are generally observed in the HAZ and in material characterized by a microstructure transformations that occur at low temperatures (Weman, 2003). Obviously, in a highly restrained workpiece, cold cracking appears more easily because the residual stresses are higher than in a free one.

The effects introduced by the welds on the martensitic transformation depend both on the microstructural state of the reference material and on the welding process parameters (Tuissi et al, 1999). Although significant efforts have been devoted to these aspects, not many studies concerning welding techniques for joining NiTi alloys are reported in literature (Beyer et al, 1986 and 1989; Ikai et al, 1996; Schlossmacher et al, 1995 and 1997; Haas et al, 1999; Tuissi et al, 1999; Falvo et al, 2005 and 2007; Shinoda et al, 1991; Nishikawa et al, 1982; Jackson et al, 1972; H. Wu Ming, 2001; Hirose et al, 1990).

In friction welding and resistance butt-welding (Beyer et al, 1986 and 1989; H. Wu Ming, 2001), the joint is under a great compression force during the welding process. This closes any possible grain boundary crack and leads to an outward extrusion of the fusion zone, so that oxidation is largely prevented. Using consumable filler metal could be helpful to reduce cracks formation and to increase the joint strength (H. Wu Ming, 2001; Weman, 2003). The major disadvantage of these methods are that the welding zones have to be trimmed due to the strong extrusion of matter, and that they are executed in ambient atmosphere.

Tungsten inert gas (TIG) welding (Ikai et al, 1996) generally causes a great degradation in the mechanical and functional properties of the joint due to an extended heat affected zone (HAZ) that reduces the applicability of this welding technique.

In the last few decades, laser technologies have reached a great importance in the field of mechanical processes due to the possibility to focus the energy of working in very small spots (Cary Howard et al, 2005). This processes minimizes the HAZ and permits to reduce the influence on the material properties. However, very few studies concerning laser welding of NiTi alloys are reported in literature (Schlossmacher et al, 1995 and 1997; Haas et al, 1999; Tuissi et al, 1999; Falvo et al, 2005 and 2007) in these

works, the properties of the welded joints was investigated in terms of mechanical and functional behaviour.

Generally, laser welding of NiTi alloys can be well performed using Nd:YAG and CO_2 sources. A significant reduction of mechanical and functional properties are always observed in CO_2 laser welded joints (Hirose et al, 1990; Tuissi et al, 1999) while Nd:YAG source seems to be more useful for welding NiTi alloys preserving a good tensile strength and functional behaviour (Schlossmacher et al, 1995 and 1997; Haas et al, 1999; Falvo et al, 2005 and 2007). Furthermore, Nd:YAG source is suitable for welding low thickness components, due to its high precision and reduced HAZ moreover, an appropriate control of the process parameters ensures a good repeatability of the results (Geusic, 1964).

Most of the works concerning laser welding of NiTi alloys have investigated the effects of the process on the mechanical and functional properties in terms of SME and SE, while the TWSME of laser-welded joints was not investigated.

Finally, in the last years, some researches are investigating the possibility to obtain functionally graded NiTi alloys by different procedure. Laser welding could be a suitable method for obtaining this type of components welding together different NiTi alloys; this aspect is not investigated but can open new possibilities for innovative applications.

In this chapter, the results related to different investigations executed on laser welded NiTi sheets, realized in the Laser Laboratory of the ENEA Research Centre of Trisaia (Rotondella, MT), are reported.

In the first investigation, the joints are studied in terms of microstructure and uniaxial stress-strain curves; a measurement of the transformation temperature of base and welded material by Differential Scanning Calorimetry (DSC) tests is also executed. In the successive investigation, carried out after an optimization of the welding process, a proper thermal treatment was executed on both welded and base (reference) NiTi sheets and their shape memory behaviour is investigated by training procedure. In particular, the deformation mechanism involved in the material behaviour during repeated thermomechanical cycles was evaluated together with the incoming of the Two Way Shape Memory Effect (TWME) in the material. The effects of the number of training cycles and plastic strain on the hysteretic behaviour, strain versus temperature,

characteristic of the TWSME were also investigated. Finally, a systematic comparison of the results was carried out in order to evaluate the influence of the welding process on the material behaviour.

3.2 WELDING PROCESS

3.2.1 WELDING EQUIPMENT AND SPECIMENS PREPARATION

As said before, the major aspects involved in the welding of NiTi alloys, are the oxidation of the weld bead and the formation of hot cracks that drastically reduce the mechanical and functional properties of the welded joints. To avoid these failure events, a special experimental set-up was realized; in particular, a shielding chamber was built to protect the welding zone by oxidation, while a particular positioning system was utilized to reduce the formation of cracks, by applying a constant compression force on the welded zone.

The shielding system permits to create an inert atmosphere around the component to be welded by introducing in it Argon. The chamber is characterized, in the upper zone, by a polymeric (PMMA) glass through which laser beam was focalized on the sheets. The type of glass chosen is transparent to the Nd:YAG wavelength and so the power leak, due to refraction phenomena and glass heating, is minimized.

In Fig. 1, a model of the shielding chamber is reported. As can be seen, the argon input was executed in proximity of the glass to shielding it from damages due to molten bath squirts; instead, through a pipe realized in the base of the chamber, the protection of the lower welded zone was realized. From another pipe, the aspiration of the smokes was executed during welding in order to reduce the temperature in the chamber and, consequently, the soften of the glass and the overheating of the components. The chamber utilized in these experiments is shown in Fig. 2; even though a good result was obtained, an optimization of the system must be one of the future topics.
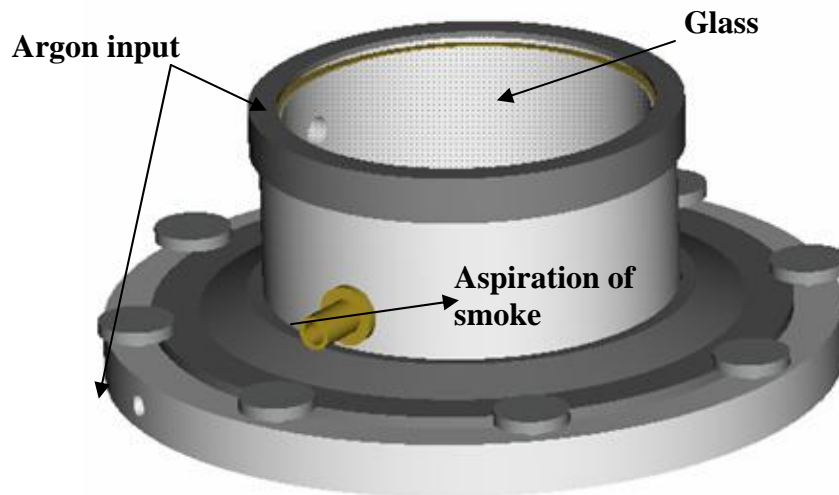
Fig. 1: CAD model of the shielding chamber

Fig. 2: Shielding chamber

As said before, the crack sensibility of the NiTi alloys is an important aspect to be considered. In order to reduce the formation of cracks and, consequently, to obtain good performance of the welded joints, a special sledge, moved by a screw, was built; the system, showed in Fig. 3, permits the alignment of the components, with respect to the beam and to apply a constant compression force between them.
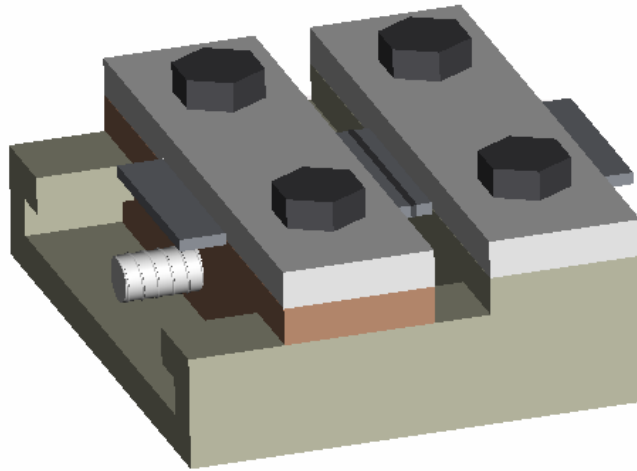
Fig. 3: Sledge used for alignment and compression of NiTi sheets

The system was characterized by two components coupled by a prismatic guide; the NiTi sheets are moved and compressed together by the screw, while a cup spring, mounted equiaxially, is used to maintain constant the force during the fusion of the material. This force closes any possible grain boundary cracks and leads to an outward extrusion of the fusion zone, so that oxidation is also better prevented. Furthermore, the spring permits the contraction of the sheets during welding reducing the cold cracking problem.

A preliminary optimization of the welding parameters, in terms of welding speed and laser beam power, was executed in order to define their better values; however, a more accurate study on the influence of the different parameters with respect to the quality of the joints is necessary.

In Fig. 4, some examples of weld cracks due to incorrect restraining of the sheets are reported.

Early experiments have showed the difficulties to weld NiTi alloys without take in account the important aspects related to the oxidation of the joints, the crack sensibility and the weld parameters.
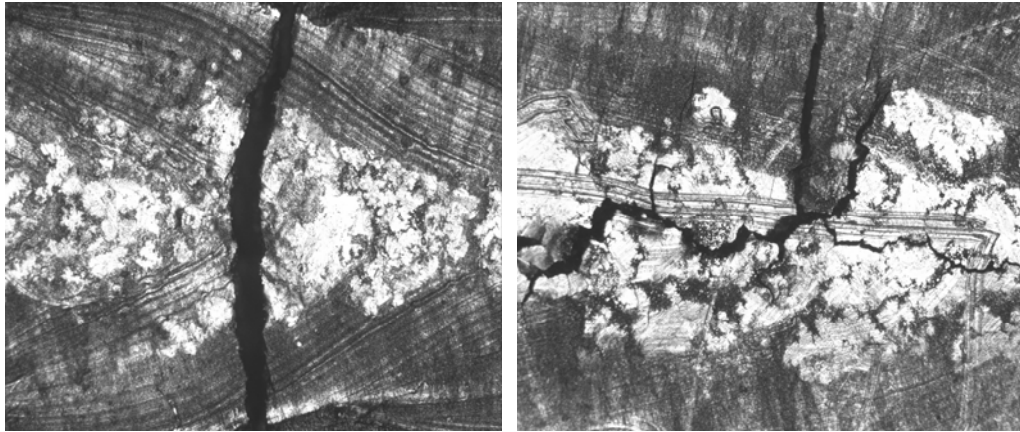
Fig. 4: Cracks observed in some NiTi welded joints

In Fig. 5, instead , an example of gas pore observed in some joints is shown; this is probably due to a prolonged heating time that permits the intrusion of harmful elements (O, H or N) in the weld bead (Chen, 2005). The presence of these elements is very dangerous because they can form chemical compounds that make the joint very brittle with a consequent significant increasing of the cold cracking in the welded material.

The welding process was carried out using a Nd:YAG laser source (HAASHL2006D, 2 kW), operating in continuous mode; the welding parameters and the path of the laser beam can be set by a personal computer. Different welding experiments were carried out using values of the beam power in the range of 600-1000 W and of welding speed in the range of 1000 and 1600 mm/min; the focusing of the laser been was always executed on the surface of the component.
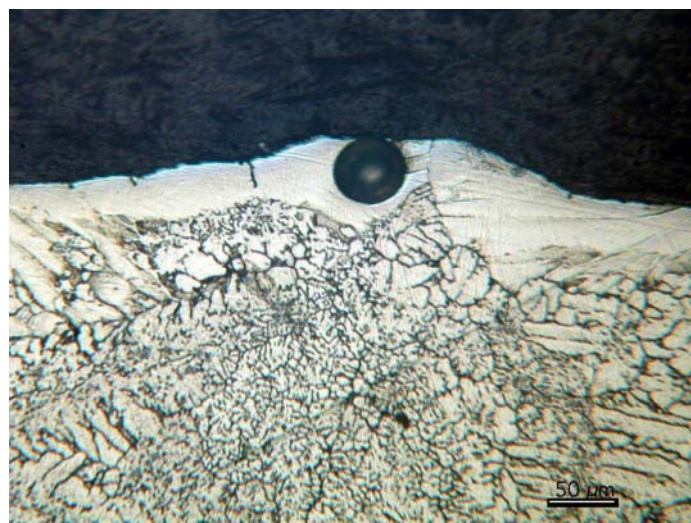
Fig. 5: Pore observed in the molten zone
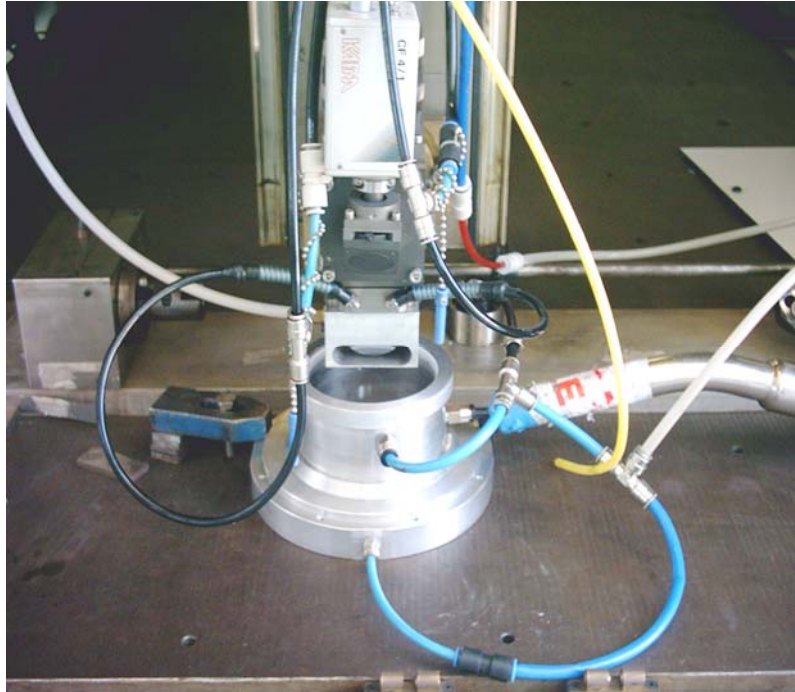
Fig. 6: Laser welding set-up

Fig. 7: Butt welded sheets

3.3 MICROSTRUCTURE AND MECHANICAL BEHAVIOUR OF WELDED JOINTS

Ni–51 at.% Ti was obtained by melting in a plasma arc furnace and successive hot pressing at 900°C and rolling to tapes (Tuissi et al. 1999). Finally, sheets, of about 1.15mm in thickness, were produced by cold rolling with a thickness reduction of about 22%; a successive ageing by heat treatment at 400 °C for 45 min in pure Argon atmosphere was executed. The material have a martensitic structure at ambient temperature. The modifications in the microstructure induced by the welding process have been analysed by micro hardness measurements and light microscopy (LM)

observations while Differential Scanning Calorimeter (DSC) investigations were carried out to determine the phase transformation temperatures. The uniaxial stress-strain behaviour of the welded joints is investigated under static condition by isothermal tensile tests and he fracture surfaces of the specimens has been evaluated by Scanning Electron Microscopy (SEM).

In this investigation, butt welded sheets was realized using the following parameters: spot diameter = 0.6 mm; welding rate = 1.6 m/min; average power = 850 W.

3.3.1 DSC TESTS

DSC measurements, carried out under a controlled cooling/heating rate of 5 °C/min, at temperatures ranging from −25 °C to 150 °C, reveal the phase transformation temperatures for both reference and welded materials in terms of M_s (Martensite start), M_f (Martensite finish), A_s (Austenite start) and A_f (Austenite finish). Cylindrical specimens with diameter of 4.5 mm and height 1.15mm were made to carry out the DSC tests. The welded specimens were cut across the welding region in order to include the HAZ as shown in Fig. 8.

Fig. 9 shows the DSC thermograms of reference and welded materials respectively; no energetic considerations were carried out. The onset temperatures of the phase transformations are determined as the intersection of tangents to the slopes of a peak with the base line.
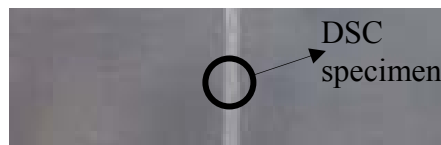
Fig. 8: DSC specimen

The DSC curve in Fig. 9(a) shows an R-phase (Rhombohedral phase) transformation during cooling prior to the martensitic transformation, while a reverse martensitic transformation appears during heating. The presence of R-phase is due to the low temperature of the heat treatment executed on the material after the cold working (Otsuka et al. 2005, Serneels 1999).In the present work, the presence of the R-phase

was neglected and the martensite start temperature was assumed to be the same as the R-phase start temperature (R_s).

The curve in Fig. 9(b) clearly shows that there is no R-phase transformation and that the weld has the typical behaviour of a fully annealed NiTi alloy. The significant modification in the transformation behaviour occurs because welding resets the effects of the cold-working and heat treatments carried out on the material during the production process; so that the transformation temperatures of laser welded specimen appear significantly different from those of the reference material as shown in Fig. 9.

3.3.2 MICRO-HARDNEES TESTS AND MICROSCOPIC INVESTIGATIONS

Microscopic observations and hardness measurements were carried out to analyse the modifications in the microstructure induced by laser welding. In particular, to evaluate the width of the Melting Zone (MZ) and the Heat Affected Zone (HAZ), microhardness measurements, using a load of 200 g, and microscopic investigations were carried out on a cross section of the welded joint. Fig. 10 shows the Vickers hardness, $HV_{0.2}$, as a function of the distance from the centre of the weld.
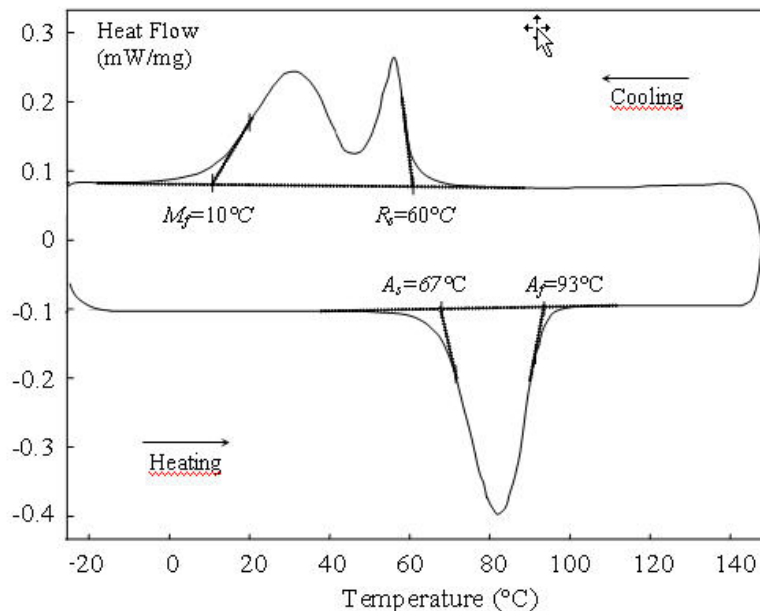
(a)
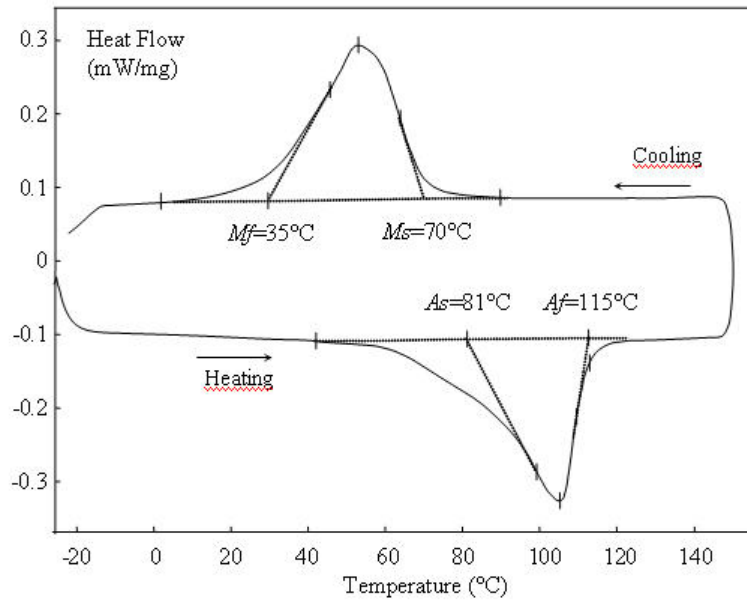
(b)

Fig. 9: DSC thermograms: (a) reference material; (b) welded material

The results show that there is no significant modification of the hardness values in the welding zone compared with those of the reference material. The observed mean values for the welded and reference materials are, respectively, 262 and 278 $HV_{0.2}$.
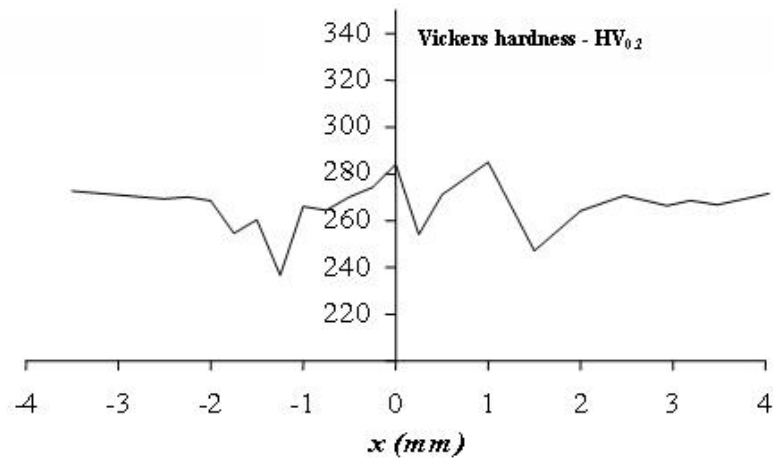
Fig. 10: $HV_{0.2}$ as a function of the distance from the centre of the weld (x)

The small variation in hardness is probably due to the production process of the reference material, characterized by a low reduction in thickness (22%) and by a successive ageing heat treatment, so that the hardening effect of the cold work in the

reference material is partially reduced. Because of the small variation in hardness, an accurate definition of the width of the MZ and the HAZ is difficult.

Therefore, microscopic investigations of the welded joint were performed; Fig. 11 shows a micrograph of a cross-section of the welded joint, which shows that towards the centre of the welded zone (melting zone) a region of recrystallization is followed by a columnar structure.
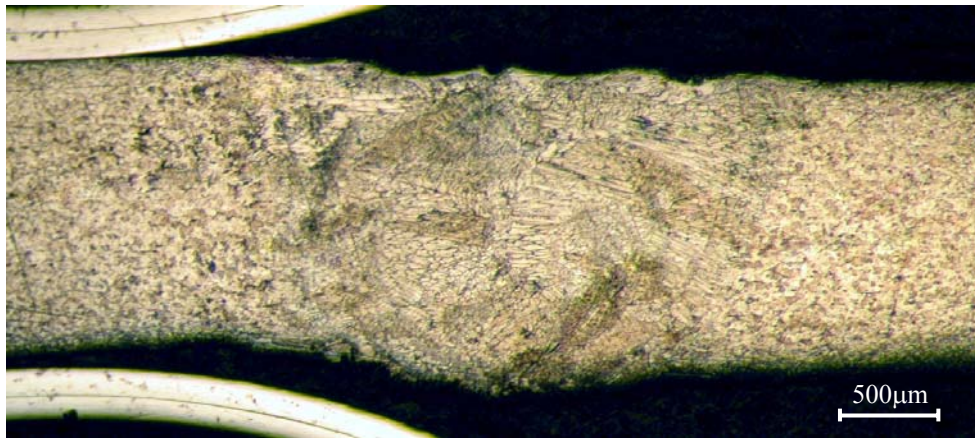
Fig. 11: Micrograph of a cross section of the welded joint

By combining the micro hardness results with the microscopic observations of the welded zone an extension of about 1.5 mm and 1 mm, for the MZ and the HAZ, respectively, is found.

Fig. 12 shows a light micrograph of the reference material, those relative to the HAZ and MZ are reported in Fig. 13 e Fig. 14 respectively; figures show as the welding process causes an enlargement of the grain size in the HAZ with respect to the reference material. Furthermore, the reference material also shows a number of precipitates which appears to be partially dissolved in the HAZ probably as consequence of solubilization phenomena induced by the laser welding.

These precipitates are probably TiC compounds formed during the production of the NiTi ingot; in particular, it is known that NiTi melts react with graphite crucibles and the associated carbon pick up will affect the alloy properties (Zhang et al, 2005). However, the nature and the influence of these precipitates could be investigated in detail in the near future.

The melting zone, in Fig. 14, shows a dendritic structure (Falvo et al, 2005; Schlossmacher et al, 1995 and 1997), with large grains in the centre and small grains in the upper and lower zones as consequence of the gradient in the cooling velocity; many segregations at the grain boundaries, are also evident.
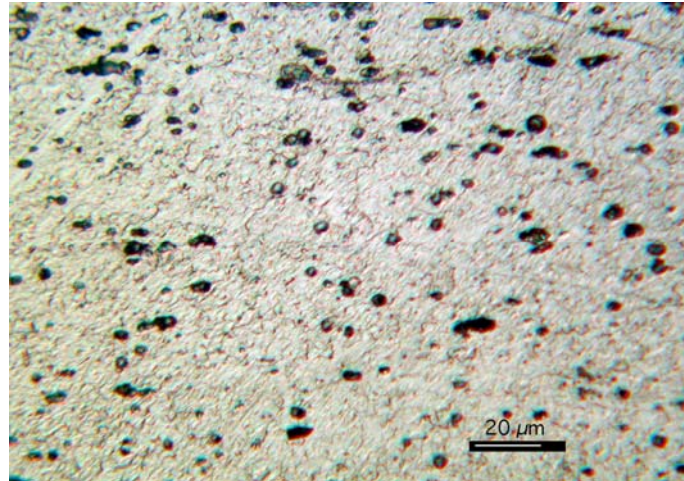
Fig. 12: Micrograph of the reference material
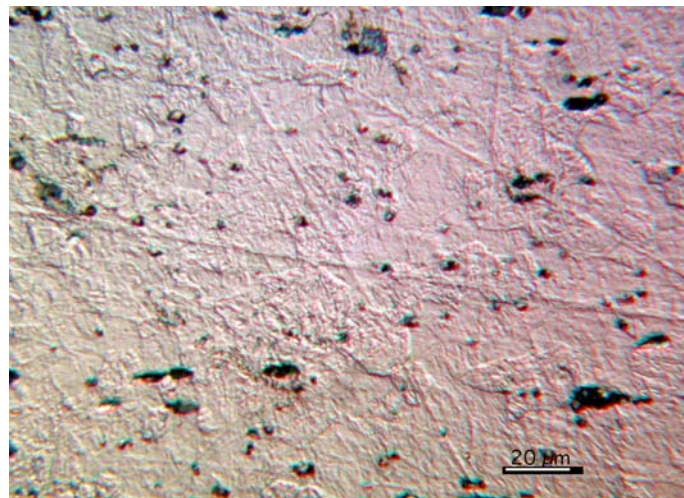
Fig. 13: Micrographs: (a) HAZ; (b) MZ
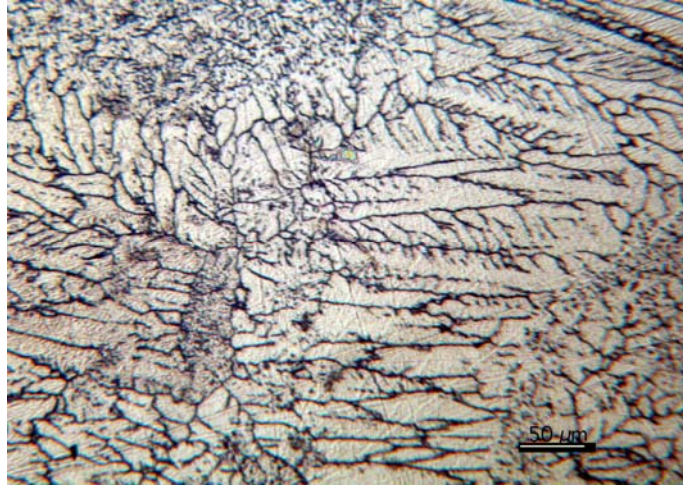
Fig. 14: Micrographs: (a) HAZ; (b) MZ

3.3.3 MECHANICAL BEHAVIOUR

In this section, the mechanical behaviour of the welded joints are evaluated in terms of stress-strain curve.

For the stress–strain tests, a universal testing machine (Instron 8500) was used while the local deformation was measured by a resistance extensometer with a gauge length of 25 mm. Load and deformation outputs were acquired by means of a data acquisition system represented by a personal computer equipped with a National Instruments acquisition card (DAQ PCI-MIO16-E-1) controlled by the Labview® 6.0 software package.

The specimens for stress–strain measurement were cut by Electro Discharge Machining (EDM) (Theisen et al, 2004) according to the geometry and dimensions showed in Fig. 15, from the as received sheets and butt welded ones. All the welded specimens present the weld bead in the middle of the gauge length as shown in figure.
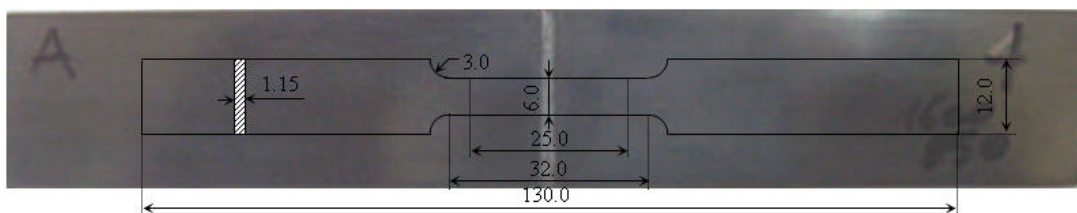
Fig. 15: Specimen for thermo-mechanical cycle

58

In order to evaluate the modification in the stress-strain behaviour of the material produced by the welding process, standard tensile tests were carried out at a temperature less than M_f.

The stress-strain curves of the welded and reference material are shown in Fig. 16.

The graphs clearly show a significant decrease in the mechanical strength of the welded specimen compared with that of the unwelded one. An ultimate strength of about 1100 MPa with an elongation to fracture of about 12% is observed for the reference; the welded specimen exhibits an ultimate strength of 520 MPa while the fracture always occurs in the welding zone with an elongation of about 7%.

The curves in Fig. 16 also show that laser welding strongly reduces the martensitic plateau, or rather the detwinning deformation is reduced probably as a consequence of the slips in the HAZ; in particular, in the welded zone, the stress necessary to produce detwinned martensite is higher than the stress for slips. The lower resistance of the welded material and the reduce of the detwinning deformation mechanism could be due to the microstructure modifications in the welded zone in terms of segregations, enlargement of grains and dendrites.
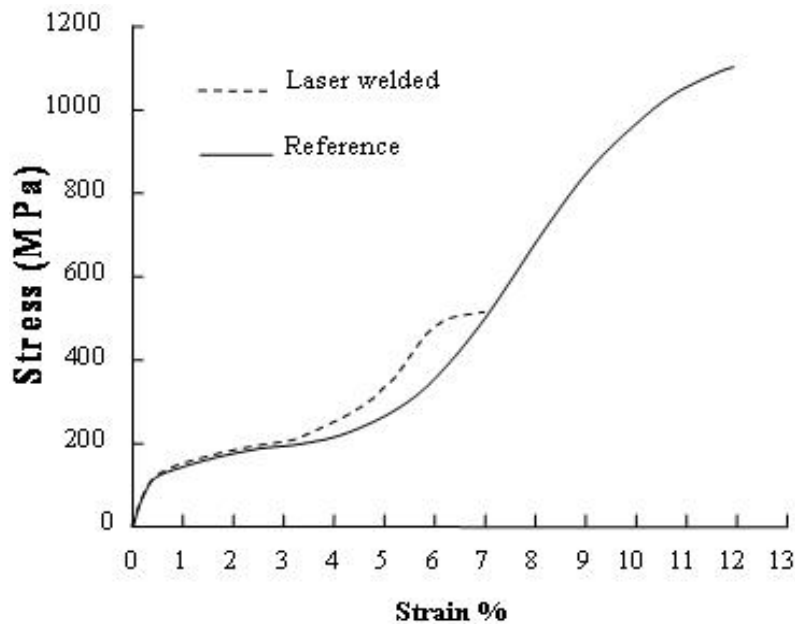
Fig. 16: Stress-Strain curve of reference and welded materials
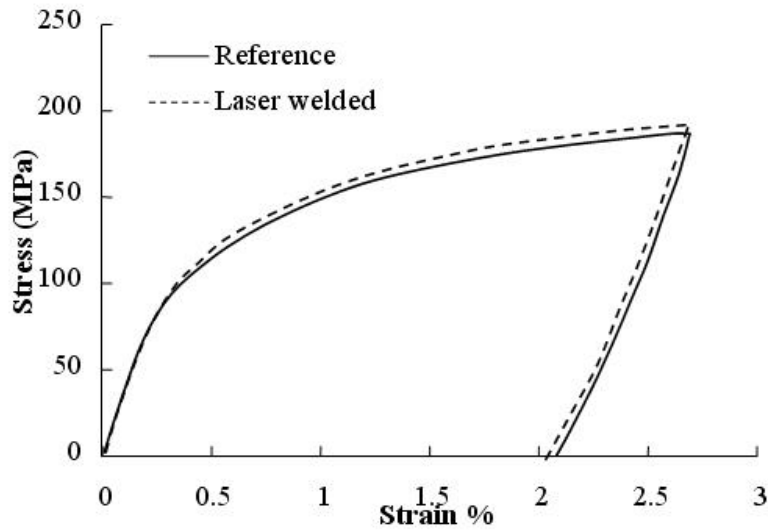
Fig. 17: Stress-Strain curves related to an ε_t=2.7%

However, as reported in Fig. 17, the comparison between the stress-strain curves of both welded and reference material for a total deformation ε_t = 2.7%, shows that the reference and welded material exhibit a similar behaviour; probably in this range of deformation the stresses are not high enough to produce slips in the HAZ so that the prevalent deformation mechanisms is the detwinning. In fact, an heating over the A_f temperature, executed to induce the recovery of the deformation by SME, have shown that no irrecoverable strain appears in both materials, confirming that for lower values of deformation, the SME is preserved in the welded joints. Increasing the total strain ε_t the behaviour of the two materials becomes different, as evident in Fig. 16, and higher irrecoverable strain appears in the welded one. In fact, for a ε_t=6.2%, irrecoverable strain of about 0.3% and 1.7% are observed in the reference and welded specimens, respectively. Although the results show that the material becomes more brittle as a consequence of the welding process, a ductile behaviour of the joint is confirmed by the high value of the elongation to fracture. In fact, the SEM observations of the fracture surface show the coexistence of both brittle and ductile fracture mechanism of the welded joints as shown in Fig 18(a). The Fig. 18(b) shows an example of cleavage fracture zone observed.

3.4 SHAPE MEMORY BEHAVIOUR OF NITI WELDED JOINTS

3.4.1 SPECIMEN PREPARATION AND EXPERIMENTS

Starting from the results obtained in the previous investigation, an optimization of the welding processes was carried out in order to increase the welded joints performance. Furthermore, a different procedure for specimen preparation, in terms of thermal treatment, is used with respect to the studies reported in the previous paragraph.

A better working of the welding equipment is assured by some shrewdness and adjustments; in particular, a better seal of the chamber, a more efficient aspiration of the smoke and a more useful contribution of the positioning system are obtained. The process parameters chosen for the realization of the butt welded sheets have been: spot diameter = 0.6 mm; welding rate = 1.6 m/min; average power = 1000 W.

The material used in this investigation is the same of the previous one but, in this case, the welding processes was carried out on the cold worked sheets before any thermal treatment. Successively, welded materials were thermally treated at 700 °C for 20 min in order to relax the residual stresses generated by the welding process; this procedure permits to investigate the intrinsic material behaviour and to evaluate the response of the welded material to cold working process such that a training procedure executed by induce plastic deformation in the martensitic structure. After the thermal treatment, the nominal M_s temperature of the NiTi alloy is about 60 °C. The experimental characterization of the base material subjected to the same production procedure are reported in the previous chapter.
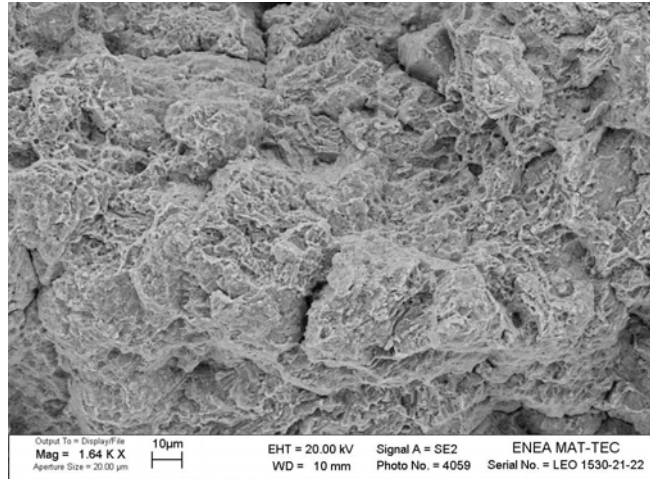
(a)
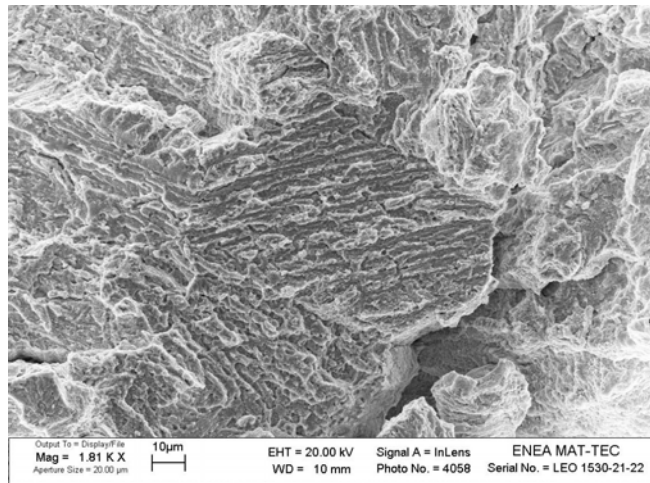
(b)

Fig. 16: SEM micrographs of the fracture surface:

(a) coexistence of ductile and fragile fracture; (b) cleavage fracture

3.4.2 MICRO-HARDNEES TESTS AND MICROSCOPIC INVESTIGATIONS

In Fig. 17 a micrograph of the section of the obtained welded joint is reported. The micrograph clearly shows the same structure observed in the previous observations. In particular, an enlargement of the grain size in the HAZ is also detected together with the columnar structures with large grains of the MZ; however, a significant reduction of the segregation at grain boundaries and dendrites is observed.
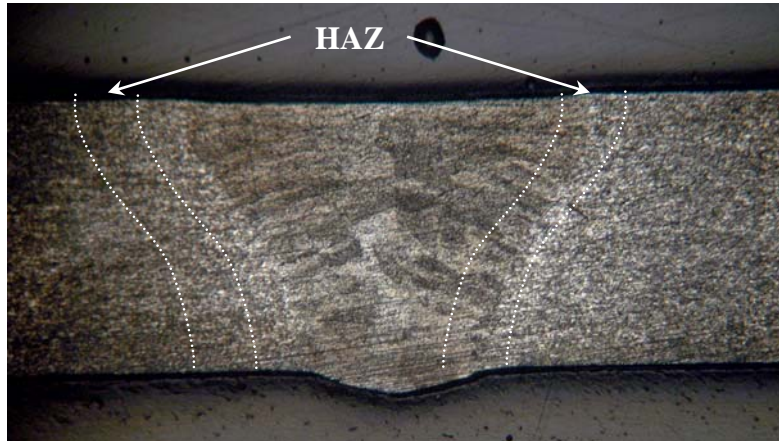
Fig. 17: Micrograph of the welded joint

The microhardness measurements, executed on a transversal section of the joint, have shown a mean value of 270 $HV_{0.2}$ for the base material, 292 $HV_{0.2}$ for the HAZ and 314 $HV_{0.2}$ for the MZ. Differently from the previous investigation, a different extensions of HAZ (1.2 mm) and MZ (0.3 mm) are measured; these results are due to the optimization of the welding procedure. In particular, the lower extension of the HAZ and MZ prove that a better setting of parameters and welding setup is obtained with a consequently lower overheating of the material in these tests. It is important to point out that these observations are relative to the joints before any thermal treatment

3.4.3. EFFECTS OF THERMAL TREATMENT

Both base and welded specimens, which were used for tensile testing and thermo-mechanical training, were produced according to the shape and dimensions shown in Fig. 18, by electro-discharge machining. In this investigation, the welded specimens were made with the weld bead along the load axis; this type of specimen permits to have a better understanding of the influence of the laser welding and to nullify the dependence of the results from the gauge length dimension.
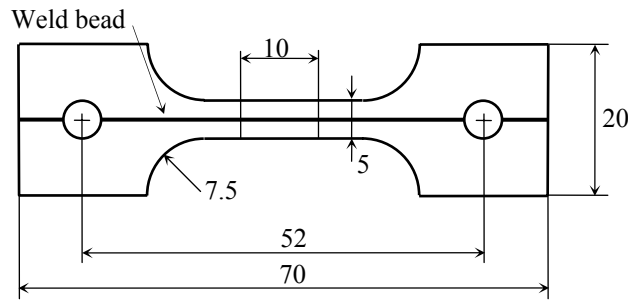
Fig. 18: Specimen for thermomechanical tests

In Fig. 19 the mechanical characterization of both welded and base materials, in terms of isothermal stress–strain tests, carried out in tensile mode at room temperature for a total deformation $\varepsilon_{tot} = 3.5\%$, are reported.

The effects of the thermal treatment (700 ◦C for 20 min) on the stress–strain behaviour are evaluated, through a comparison between treated and untreated materials. In particular, Fig. 19(a) and (b) illustrates the results for the base and welded materials, respectively.

Fig. 19(a) clearly shows, as explained in the previous chapter, that the stress–strain response of the base material is strongly affected by the thermal treatment. Fig. 19(b) illustrates the stress–strain curves of the welded material; the similar behaviour observed between treated and untreated specimens is due to the welding process that nullify the effects of cold working. In particular, both treated and untreated materials exhibit the characteristic reorientation plateau, with a stress for the onset of the detwinning of about 220MPa; however, a small decrease in the slope of the stress plateau, as a consequence of the residual stress relaxation is observed. The increase in the stress for the onset of the detwinning, between base (120 MPa) and welded materials, is probably due to the effects of the thermal treatment on the different microstructure of the base and welded material.
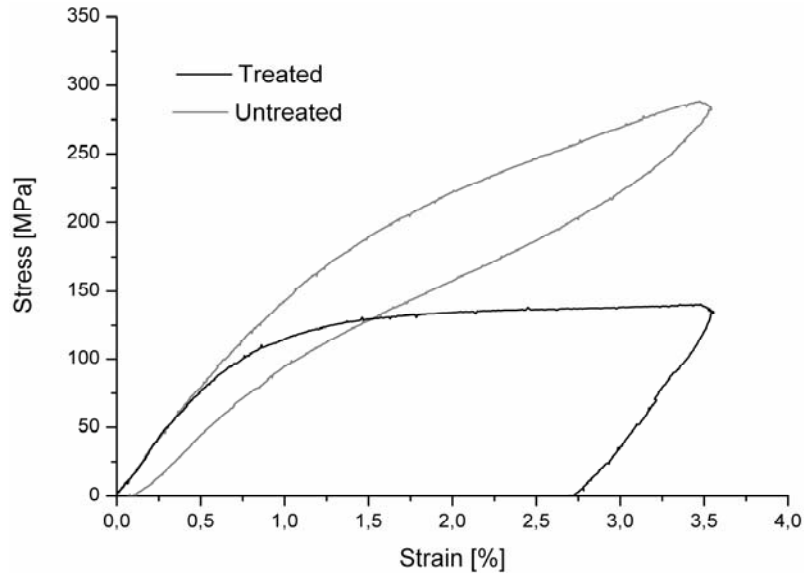
(a)
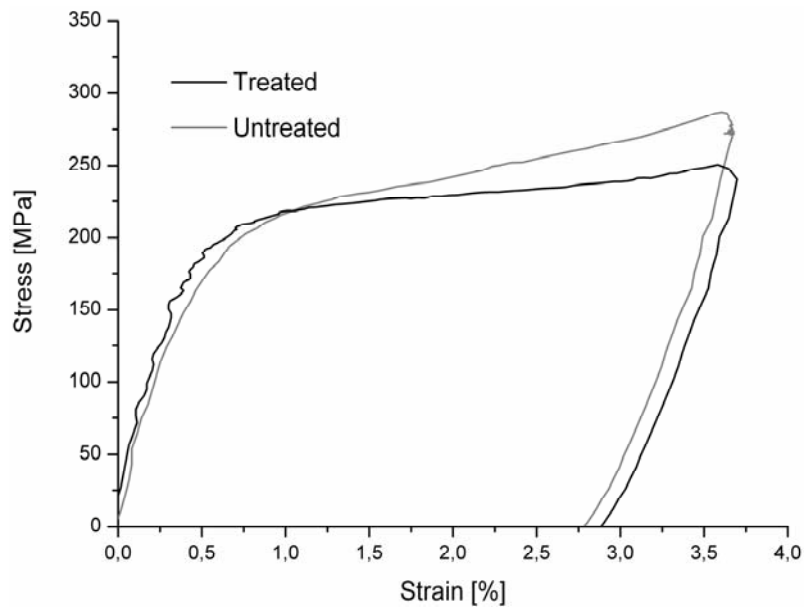
(b)

Fig. 19: Stress–strain response of the thermally treated material and untreated one:
(a) base material; (b) welded material.

3.4.3 TRAINING AND TWO-WAY SHAPE MEMORY BEHAVIOUR

The investigation of the shape memory behaviour of the welded joints was carried out by repeated training cycles executed for a fixed values of training deformation; then the results related to welded and reference material are compared in order to understand the effects of laser welding.

The thermo-mechanical cycles were carried out by a universal testing machine (Instron 8500, USA), equipped with a furnace (MTS 653, USA). The local deformations of the specimen were measured by a resistance extensometer with a gauge length of 10 mm, while the temperature was acquired, in the middle of the gauge length, by a J-type (Fe/Cu–Ni) thermocouple.

The training procedure was carried out through the repetition of several thermo-mechanical cycles composed of four subsequent steps as shown in Fig. 20: (1) strain controlled uniaxial tensile loading at a strain rate of 0.06 min−1 up to a training deformation ε_{tr} = 3.5%; (2) complete unloading at the same rate and recording the residual strain ε_r; (3) heating up to A_f to activate SME and measuring the recovery deformation ε_{re} and plastic strain ε_p; (4) cooling down to Mf and recording the two-way shape memory strain ε_{tw}.

The modification of the stress–strain response of the thermally treated specimens, during thermo-mechanical training, is shown in Fig. 21 for a training deformation ε_{tr} = 3.5%. Eight subsequent training cycles were carried out on the base specimens, while only seven cycles were executed on the welded specimens in order to avoid fracture. Fig. 21(a) shows the stress–strain curves of the base material for the first, an intermediate and the last thermo-mechanical cycle, while Fig. 21(b) illustrates the curves related to the welded material.

Both materials show a similar behaviour: when increasing the number of training cycles an hardening is observed, resulting in large stress level, together with a decrease in the stress for the onset of the detwinning. As shown in Fig. 21(b) this effect is more evident in the welded material, resulting in a very high slope of the reorientation plateau after seven cycles.

A better understanding of these effects can be obtained by evaluating the evolution of the deformation during the cycling.

Fig. 22(a) and (b) shows the measured ε_{tw}, ε_{re} and ε_p, versus the number of training cycles for the thermally treated base and welded materials, respectively.
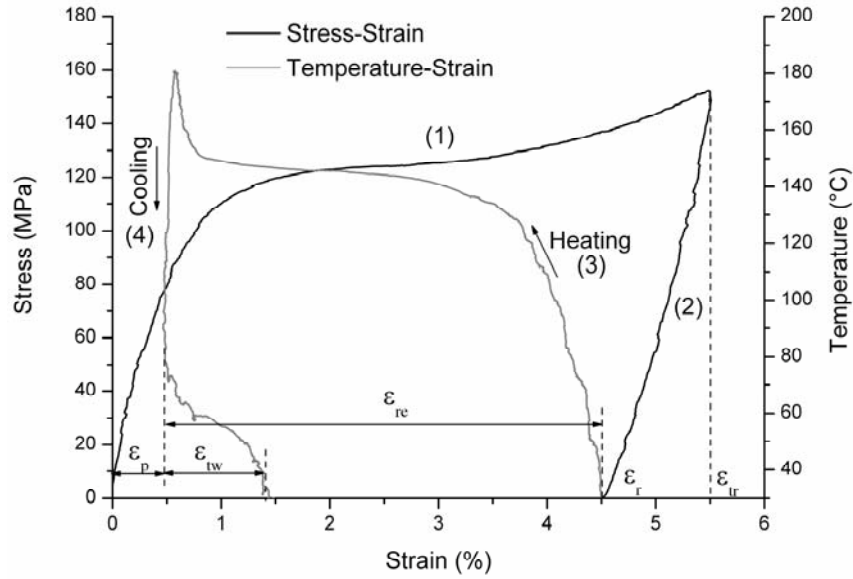
Fig. 20: Thermo-mechanical cycle to induce the two-way shape memory behaviour

Fig. 22(a) clearly shows that in the base material ε_{tw} increases with increasing the number of training cycles and a similar behaviour is observed for ε_{re} and ε_{p}. In particular, ε_{tw} increases from 0.6%, at the first cycle, to 1.7% after eight cycles, while ε_{re} and ε_{p} increase from 2.7% to 3.9% and from 0.6% to 2%, respectively. As shown in Fig. 22(b), the thermally treated welded specimens exhibit a different behaviour; in fact, ε_{tw} and ε_{re} increase in the first five training cycles, from 0.5% to 1.3% and from 2.5% to 3.4% respectively, while they decrease with further increasing the number of cycles, as a consequence of the strong increase in the plastic deformation ε_{p}.

It is important to point out that in this plastic deformation, also known as material amnesia, are computed the deformation due to the stabilization of the martensite variants. The lower resistance of the welded joints to the development of dislocations in the weld bead (Tuissi et al 1999) increase the residual stress field in the material at each cycle with a consequently increase of the martensite stabilization effects. These observations justify the more rapid increase of the plateau slop and the strong decrease of the detwinning stress because, at each cycle, more martensitic variants are first elastically and then plastically deformed in the welded material. The achieving of a maximum value for ε_{re} and ε_{tw}, in the investigated range, confirms these observations as well as the concomitant rapid increase of ε_{p}.
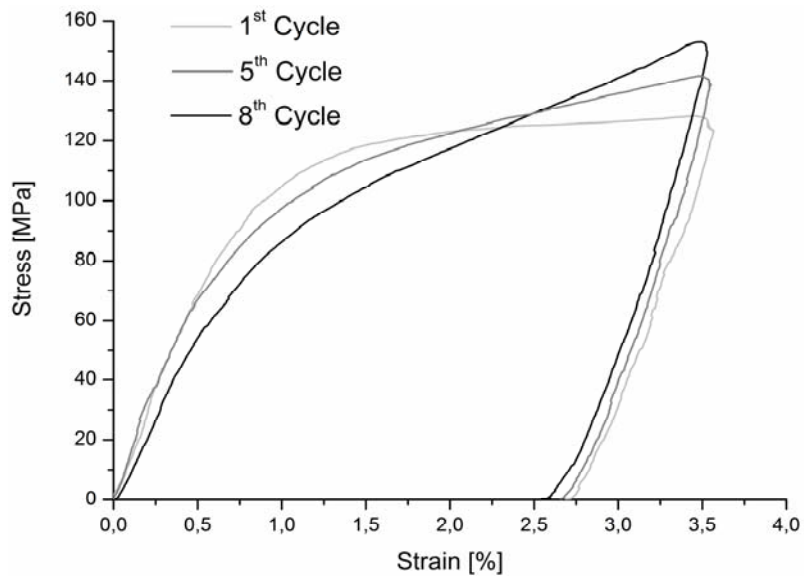
(a)
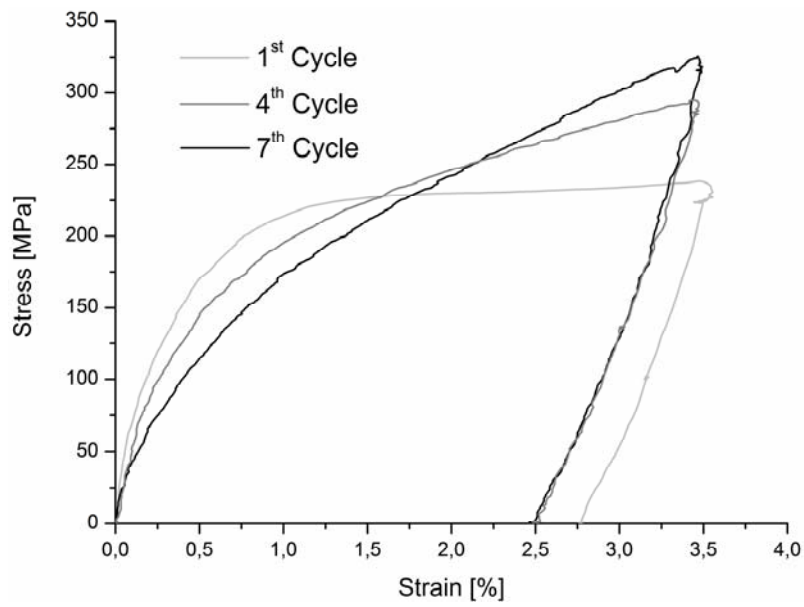
(b)

Fig. 21: Stress–strain curves measured during thermo-mechanical training
(a) base material; (b) welded material.
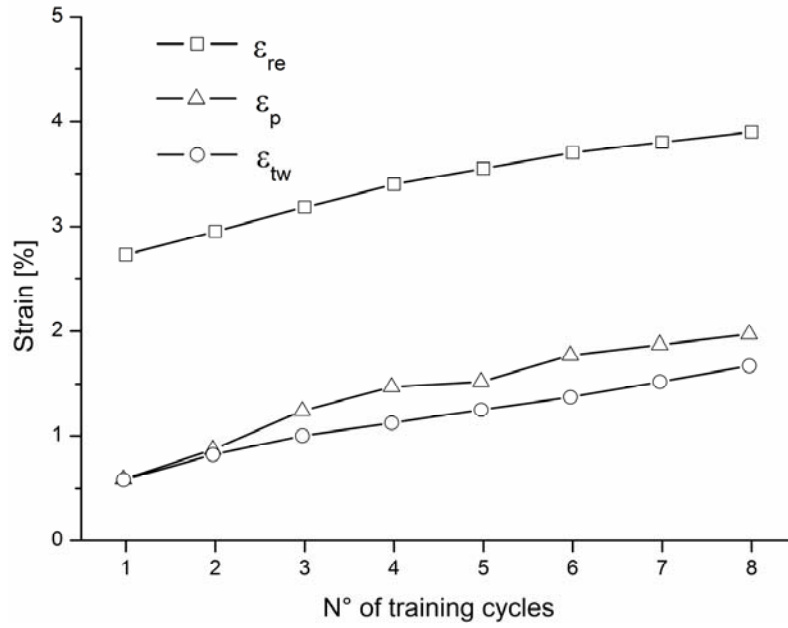
(a)
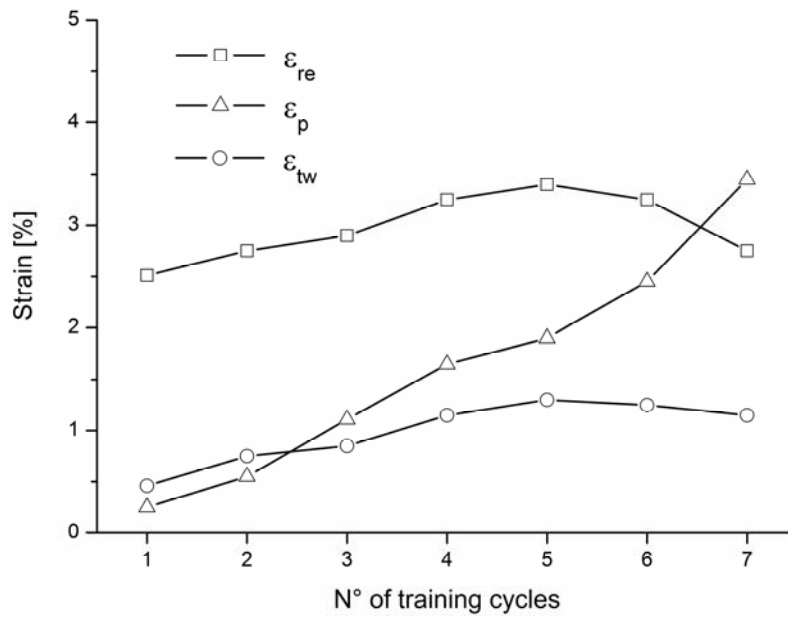
(b)

Fig. 22: Shape memory behaviour and plastic strain of the thermally treated materials vs. the number of training cycles: (a) base material; (b) welded material

The transformation temperatures of the thermally treated base and welded materials were measured, after thermo-mechanical training, from the hysteresis loops using a slope line extension method, as schematically shown in Fig. 23 where the hysteresis loop of the welded specimen after seven training cycles, is illustrated.

In Table 1 the measured transformation temperatures of the two materials are compared and an increase in all transformation temperatures is observed in the welded specimen, with respect to the base one. The major increase in the transformation temperatures observed in the welded material confirms that more stabilized martensitic variants are present in the material.
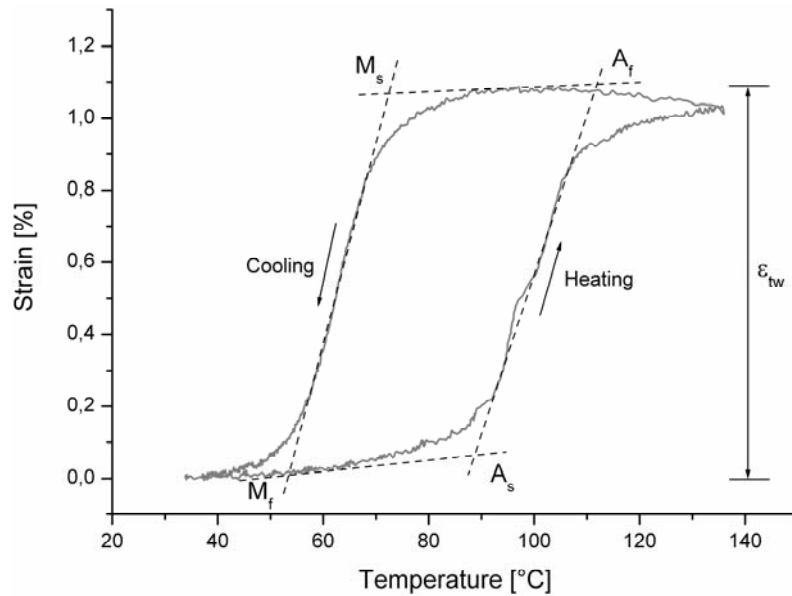
Fig. 23: Hysteresis loop of the thermally treated welded specimen after seven training cycles

Table 1: Temperature di trasformazione [°C]

	M_f	M_s	A_s	A_f
Reference	50	64	80	95
Welded	54	70	90	112

CHAPTER 5

NUMERICAL MODELLING OF TWSME IN NITI ALLOYS

5.1 OVERVIEW

In order to better investigate the potentialities of SMAs, several mathematical model were developed in the last decades, to describe the mechanical and functional behaviour of NiTi alloys (Gall et al. 2000, Pavia et al. 2006). Some of these models are based on microscopic and mesoscopic approaches (Gall et al. 2000, Pavia et al. 2006), where the thermo-mechanical behaviour is modelled starting from molecular level and lattice level, respectively; other models are based on macroscopic approaches, where only phenomenological features of the SMAs are used. The advantage of the microscopic and mesoscopic approaches is their ability to predict the material response using only the crystallographical parameters; however, the high computational resources required to be performed is an important drawback that reduce their application for modelling structural response of SMAs. Instead, phenomenological models do not predict the

behaviour of the material on microscopic level, but the effective behaviour of the polycrystalline SMAs; so that, these models have the advantage of being easily integrated into an existing structural modelling system based, for example, on the finite element method.

The micromechanics-based models start from the crystallographic modelling of a single crystal to obtain the polycrystalline response of the SMA. Such models have been presented in the literature by different researchers. As an example, one of these model based on the analysis of phase transformation in single crystals was presented by Patoor et al. (1988, 1994 and 1996). A micromechanical model for SMAs which is able to simulate the functional behaviour, such as superelasticity and shape memory effect, was presented by Sun et al. (1993 a,b); the model, starting from energy considerations, is able to simulate the material behaviour by considering the evolution of the martensitic volume fraction. One of the recent micromechanical models for SMA has been presented by Gao et al. (2000a,b).

In the field of the model based on a phenomenological approach, some authors proposed one-dimensional models (Falk 1980 and 1983, Boyd et al 1994, Brinson 1993, Liang et al. 1990 and 1992, Tanaka et al. 1982 and 1995). Some of these models are based on an assumed polynomial-free energy potential (Falk 1980 and 1983) which allows SE and OWSME simulation; other models are based on an assumed phase transformation kinetics and consider simple mathematical functions to describe the phase transformation behaviour of the material (Brinson 1993, Liang et al. 1990 and 1992, Tanaka et al. 1982 and 1995). These models probably are the most popular in the literature, due to their phenomenological approaches which allow easy developments without considering the underlying physics of the transformation kinetic. Other models are based on the elastoplasticity theory (Bertran 1982, Souza et al. 1998, Auricchio et al. 1997 a,b,c, Marfia et al. 2003) which are capable to describe the functional behaviour of the material using plasticity concepts.

Most of the constitutive models reported in literature assume a rate-independent behaviour of the material. As explained in the previous chapters, a strong influence of the strain rate on the material behaviour is instead well known. The model developed by Abeyaratne et al. (1993 and 1994a,b) consider this dependence.

Recently, some researchers, based on the experimental observations, have tried to model the behaviour of SMAs under cycling loading. In particular, the accumulation of plastic strain, the evolution of the hysteresis loop with the number of cycles and the incoming of TWSME are taken in account. One-dimensional models for the behaviour of SMA wires under cycling loading have been presented by Lexcellent et al. (1996 and 2000); Tanaka et al. (1995), among others. One of the most recent works on the cyclic behaviour of SMA wires has been presented in a series of papers by Bo et al. (1999 a,b,c,d). In that work most of the issues regarding behaviour of SMA wires under cycling loading, including the development of TWSME, have been addressed and the results compared with the experimental data.

In this chapter, a model to predict TWSME of NiTi alloys is proposed. The model is able to describe the thermal hysteretic behaviour of the material in a phenomenological way, without considering the underlying physics of the phase transformation. In particular, the proposed approach is based on a Preisach-like hysteresis model (Ge et al. 1997), such as the Prandtl-Ishlinskii operators, which were widely used in the last few years to simulate the hysteretic behaviour of magnetostrictive and piezoelectric actuators (Krejci et al. 2001, Kuhnen et al. 2001) while an attempt in using these operators to model the TWSME in NiTi alloys is reported in (Falvo et al. 2007).

Although some of the pre-existing phenomenological models are able to capture several behaviours of NiTi alloys, the main advantages of the proposed approach consist in a very simple implementation as well as a good efficiency and accuracy in predicting the whole strain-temperature hysteretic behaviour under constant stress conditions, *i.e.* describes the response of the material under a generic temperature path with both complete and incomplete phase transformations. Furthermore, the proposed model, unlike most of the literature models, captures the hysteresis modifications with increasing external stress observed in thermal cycling experiments under constant loads, *i.e.* the variation of both two-way shape memory strain and phase transition temperatures. Finally, the model shows also a high computational efficiency, which allows its use in real-time applications. On the other hand the main drawbacks of the model consist in its one dimensional nature, which limits its use in the range of applications where one dimensional assumptions can be made.

Proper numerical procedures were developed to identify the model parameters, which allow the simulation of the complex hysteretic nonlinearities of NiTi alloys, starting from some experimentally measured thermo-mechanical characteristics. The robustness and efficiency of the proposed method was analyzed through a comparison between experimental measurements and numerical predictions. In particular, complete and incomplete martensitic transformations were analyzed as well as the effects of applied stress, and a satisfactory accuracy and efficiency was observed in all cases; therefore the proposed model is particularly suitable for use in real-time applications.

5.2 NUMERICAL MODELLING OF TWSME

Starting from some of the experimental measurements reported in Chapter 2, a numerical model which is able to describe the hysteretic behaviour characteristic of the TWSME was presented. The model was developed in the commercial software package Simulink$^®$ and is also able to simulate the effects of applied stresses on the TWSME as well as partial thermal cycles, which generate incomplete martensitic transformations.

In order to clearly describe the model the measured strain are redefined according to the training cycle reported in Fig. 1: (1) strain controlled uniaxial loading up to a training deformation ε_{tr}; (2) complete unloading and recording the residual strain ε_r; (3) heating up to the temperature austenite finish (A_f), in stress free conditions, to activate SME and measuring the recovery deformation ε_{re} and permanent strain ε_p; (4) cooling down to the temperature martensite finish (M_f), in stress free conditions, and recording the two way shape memory strain ε_{tw}.
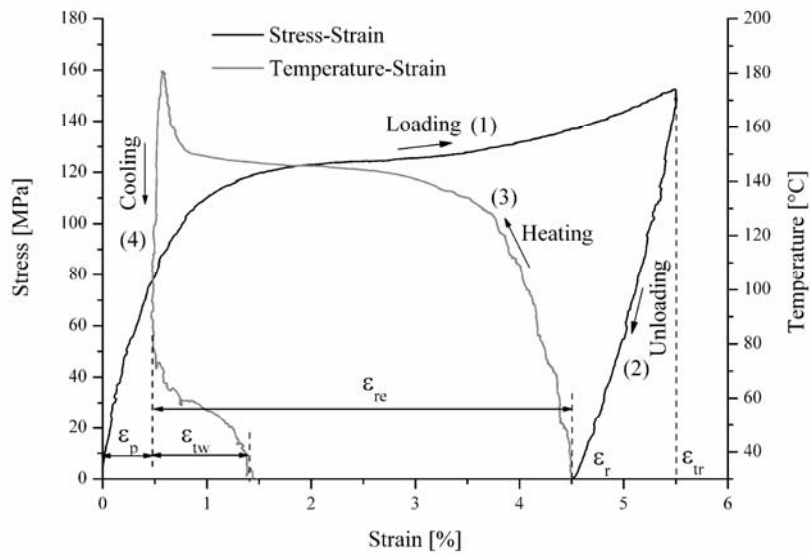
Fig. 1: Training cycles used for the numerical modelling

In Fig. 2 the stress free thermal hysteresis behaviour strain versus temperature, describing the two way shape memory effect of the trained material, is shown. The figure also illustrates the phase transition temperatures, which were identified by using the slope line extension method, drawing two tangential lines along the transforming strain-temperature curves. The subscript 0 in the figure indicates that the measurements were performed in stress free condition.
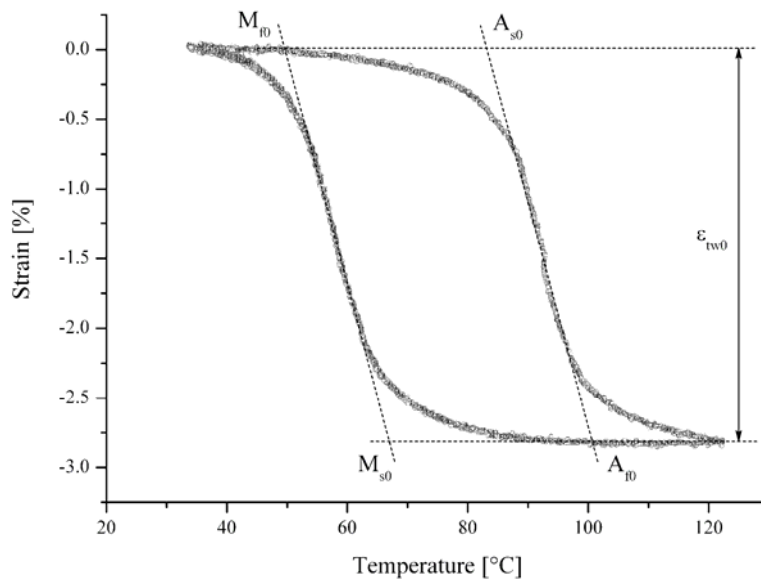
Fig. 2: Stress free thermal hysteresis behaviour of the trained material

In table 1 the measured transformation temperature of the trained material in stress free condition are reported.

Table 1: Measured phase transition temperatures [°C]

M_{s0}	M_{f0}	A_{s0}	A_{f0}
49	66	84	101

The effects of applied stress are shown in Fig. 3 where the thermal hysteresis loops in stress free condition, under 50 and 100 MPa are reported.

Fig. 4 shows the transformation temperatures versus the applied tensile stress; in particular, the points represent the measured characteristic temperatures in the range 0-100 MPa, while the continues lines are obtained by a linear fit of the experimental data. As clearly shown in the figure a linear response stress-versus temperatures can be assumed, in the investigated range of stress.
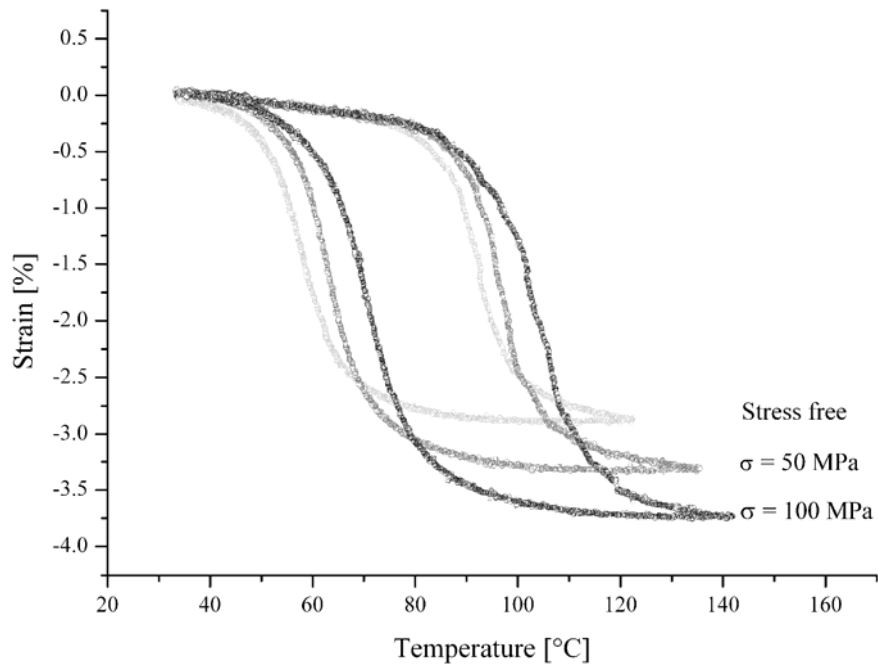
Fig. 3: Thermal hysteresis behaviour under fixed tensile stress
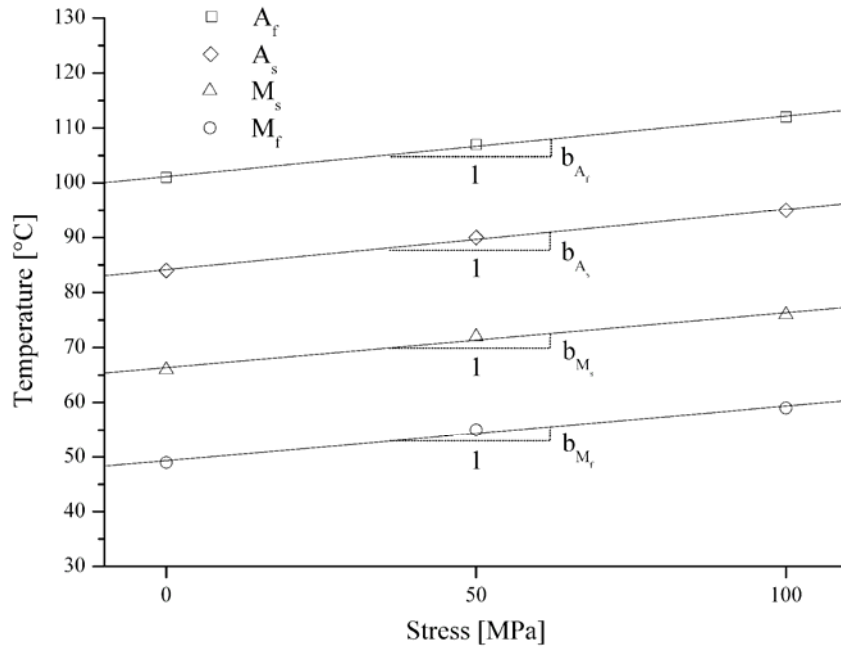
Fig. 4: Phase transition temperatures versus applied stress

The slopes of the lines b_{Ms}, b_{Mf}, b_{As} and b_{Af} are material constants; furthermore, in the Ti rich NiTi alloys the slopes of the martensitic transition temperatures, b_{Ms} and b_{Mf}, can be assumed to be the same, as well as the slopes relative to the austenitic transition temperatures b_{As} and b_{Af} (Hamilton et al. 2004), therefore only two constants, b_M and b_A, can be used and the following values were obtained:

$$b_M = \frac{b_{Ms} + b_{Mf}}{2} = 0.11\,°C\,MPa^{-1}, \quad b_A = \frac{b_{As} + b_{Af}}{2} = 0.12\,°C\,MPa^{-1}. \qquad (2)$$

The transformation temperatures as function of the applied stress can be obtained as follows:

$$M_s = M_{s0} + b_M \sigma, \quad M_f = M_{f0} + b_M \sigma$$
$$A_s = A_{s0} + b_A \sigma, \quad A_f = A_{f0} + b_A \sigma. \qquad (3)$$

Fig. 5 shows the measured values of the two way shape memory strain ε_{tw}, as a function of the applied stress σ, together with a comparison with ε_{tw0}, which represents the measured two way strain in stress free condition. The graph clearly shows that a linear behaviour between ε_{tw} and σ can be assumed in the investigated range of stress.

In a pure phenomenological way the variation in ε_{tw} with respect to the stress free condition, as shown in Eq. (4), can be attributed to two different mechanisms: (1) the variation of the Young's modulus in the thermal hysteresis behaviour between martensite and austenite; (2) the increased volume fraction of favourably oriented martensite variants with increasing external stress (Hamilton et al. 2004),

$$\Delta\varepsilon_{tw} = \varepsilon_{tw} - \varepsilon_{tw0} = \left(\frac{1}{E_M} - \frac{1}{E_A}\right)\sigma + c\sigma \tag{4}$$

where E_M and E_A represent the Young's moduli of martensite and austenite, respectively, while c can be assumed as a material constant, and takes into account of the second mechanism. In Fig. 15 the two terms of the right side of Eq. (4), which are indicated as $\Delta\varepsilon_{mech}$ and $\Delta\varepsilon_{mem}$, respectively, are also shown. In the graph the following values of the aforementioned parameters were used: $E_M = 36 \cdot 10^3$ MPa, $E_A = 67 \cdot 10^3$ MPa and $c = 8.5 \cdot 10^{-5}$ MPa^{-1}. The Young's modulus E_M was measured in the early stage of the unloading path of Fig. 4, while E_A was obtained by a tensile test carried out at the temperature $T = A_f$; finally, the parameter c can be computed by using Eq. (4) starting from the values of $\Delta\varepsilon_{tw}$ and of the Young's moduli, E_M and E_A.
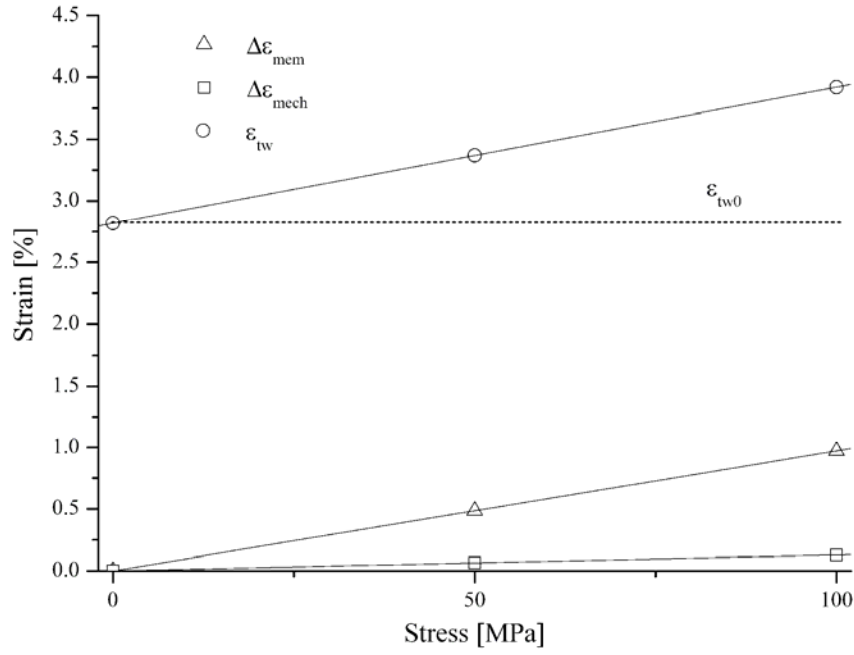
Fig. 5: Two way shape memory strain versus the applied stress: effect of mismatch between Young's modulus of martensite and austenite, $\Delta\varepsilon_{mech}$; effect of increased volume fraction of favourably oriented martensite variants $\Delta\varepsilon_{mem}$

5.2.1 NUMERICAL MODEL

Based on the experimental observations described in the previous section, a one-dimensional phenomenological model was developed, which is based on the so-called Prandtl-Ishlinksii operator (Krejci et al. 2001, Kuhnen et al. 2001). As illustrated in detail in the following the proposed approach has a relatively simple formulation with parameters that can be easily calculated from a set of experimental measurements, without considering the complex mechanism of phase transformation. In addition, the model predicts the whole strain-temperature hysteretic behaviour, *i.e.* describes the response of the material under a generic temperature path, and it captures hysteresis modifications with increasing external stress observed in thermal cycling experiments under constant loads.

The model parameters are calculated starting from two simple mathematical functions, obtained by a numerical fitting of the experimental data, which describe the phase transformation kinetics. In particular, as reported in the model proposed by Tanaka and

Nagaki (1982), the heating and cooling branches of the hysteresis loop can be represented by two exponential curves:

$$\varepsilon = \begin{cases} \varepsilon_{tw} e^{a_A\left(A_f - T + \delta T_M\right)} & M \to A \\ \varepsilon_{tw}\left[1 - e^{a_M\left(M_f - T + \delta T_A\right)}\right] & A \to M \end{cases} \tag{5}$$

where ε_{tw}, M_s and A_s are function of the applied stress as reported in Eqs. (3) and (4); a_M, a_A, δT_M and δT_A, which define the shape of the heating and cooling branches of the loop, are material constants and can be identified by a numerical fitting of the experimental data.

Fig. 6(a) shows a comparison between experimental measurement and exponential curves; in the figure the points P_1 and P_2 represent the range where the numerical fitting is executed to identify the parameters of the heating branch of the loop, while the points P_3 and P_4 are relative to the cooling branch. In Fig. 6(b) a linear fitting, between the points P_1 and P_2, of the experimental data in the $T\text{-}Log_e(\varepsilon)$ plane is shown, where the slope of the line defines the parameter a_A and the intersection with the $Log_e(\varepsilon)$ axis allows to obtain the parameter δT_M.
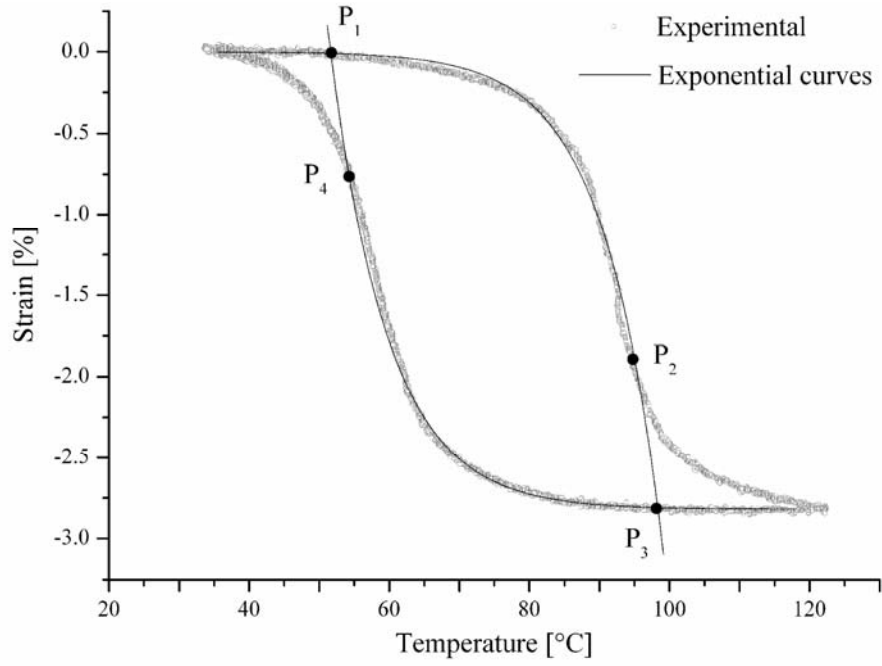
(a)
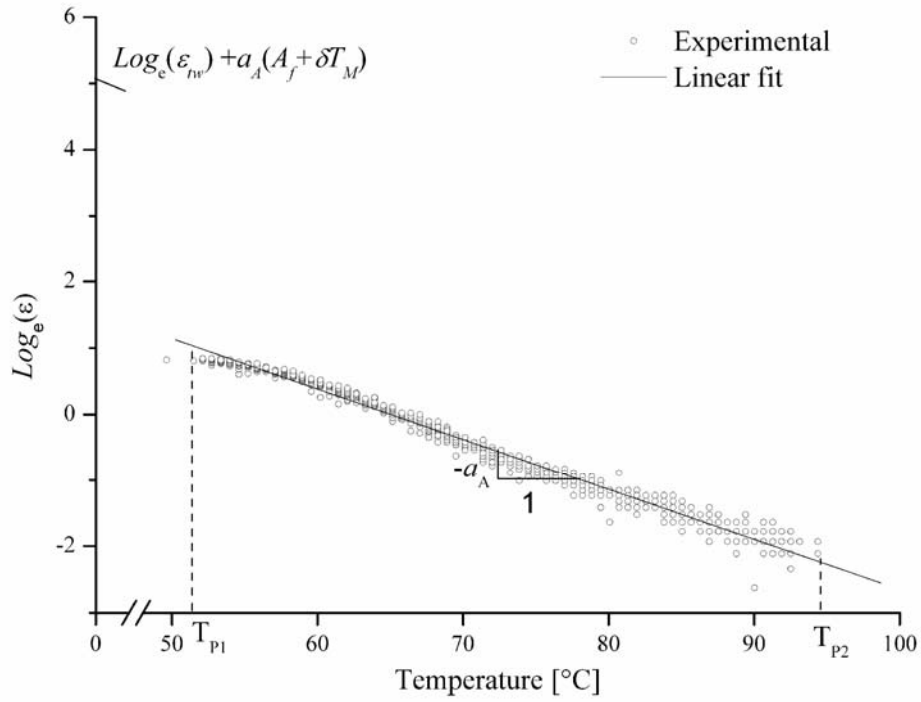
(b)

Fig. 6: Numerical fitting of the experimental data: a) comparison between exponential curves and experimental measurements; b) numerical fitting in the T-Log$_e$(ε_{tw}) plane to identify the parameters of the exponential curve in the heating branch of the hysteresis loop

If the loop is characterized by an odd symmetry with respect to its centre, as it is quite well observed in the investigated material, the same values can be assumed for the constants a_A and a_M and δT_A and δT_M, and the following values were found:

$$a_M = a_A = \frac{Log(7.66)}{A_s - A_f}, \quad \delta T_M = \delta T_A = -2.64 \quad °C \qquad (6)$$

As clearly shown in Fig. 6(a), a good agreement is observed between exponential curves and experimental results in the range P_1-P_2, in the heating stage, and P_3-P_4, in the cooling branch of the loop, while the errors increase significantly when the temperature is above A_f during heating and below M_f in the cooling branch of the loop. However, this drawback will be partially overcome by using a modified Prandtl-Ishlinksii operator, as discussed in the following.

The exponential curves describe the two branches of the hysteresis loop in a parametric way for a generic value of the applied stress, by using the Eqs.(3)-(5). Starting from the curves ε–T, the numerical method based on the Prandtl-Ishlinksii operator, was developed, which is able to predict the output response for a generic temperature signal. The basic idea of this approach consists in modelling the hysteretic behaviour by a weighted superposition of many so called elementary hysteresis operators. These operators have a simple mathematical structure, which are characterized by one or more parameters, and one of the most familiar is the so called backlash operator H_r:

$$y(t) = H_r[x, y_0](t), \qquad (7)$$

where t represents the time, x and y are the input and output variables, respectively, y_0 is the initial value of the output. As shown in Fig. 7(a), the backlash operator is characterized by the control input threshold value r, which is equal to one half of the deadband width dw. A generalized backlash operator is obtained by multiplying the backlash operator H_r by a weight value w:

82

$$y(t) = w H_r[x, y_0](t) , \qquad\qquad (8)$$

where the w defines the gain of the backlash operator and represents the slope of the oblique line in Fig. 7(a). The parameter $2A$ in Fig. 7(a) represents the total amplitude of the input signal.

To obtain a complex hysteretic loop the Prandtl-Ishlinskii hysteresis operator H can be introduced, by a weighted superposition of many elementary operators, with different threshold and weight values (Krejci et al. 2001, Kuhnen et al. 2001):

$$H = \{w\}^T \{H_r\} , \qquad\qquad (9)$$

where $\{H_r\}$ is the vector of backlash operators and $\{w\}$ is the corresponding vector of weights.

As illustrated in Fig. 7(b) the proposed approach consists in modeling the hysteretic loop by a linear piecewise discretization; the accuracy of the model can be improved by increasing the total number of linear pieces, which represent the number of the backlash operators. In Fig. 7(b) three backlash operators are used and they are moved in the origin of the coordinate axis by choosing a proper value of the initial output, $y_0 = dw/2$, and by subtracting a constant value, equal to $dw/2$, to the output signal.

(a)

83

(b)
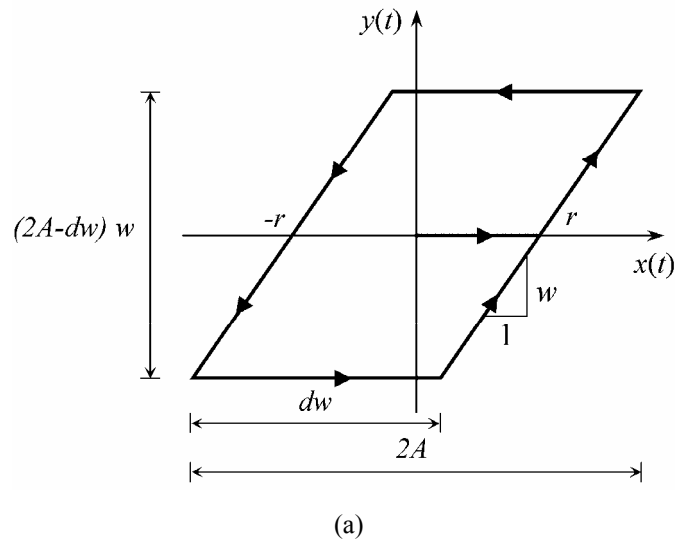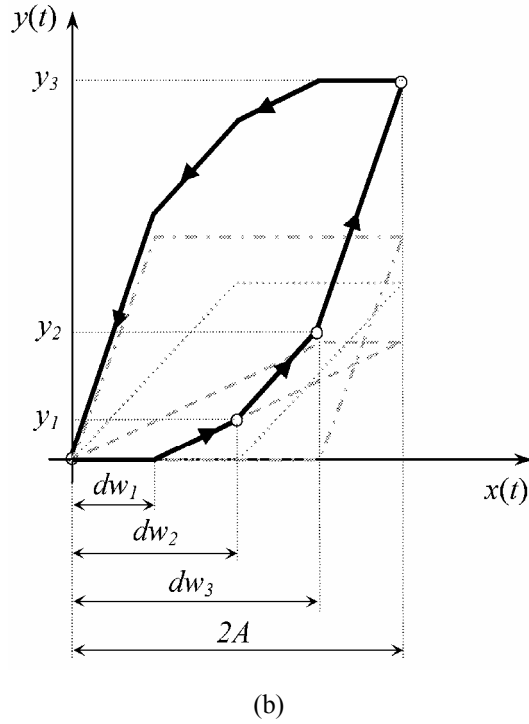
Fig. 7: (a) Generalized backlash operator; (b) Complex hysteretic loop obtained by a weighted superposition of three backlash operators

The problem of modeling the hysterestic behaviour starting from the exponential curves is now reduced to the determination of the deadband width vector $\{dw\}$ of the backlash operators and the associated gain vector $\{w\}$. By some geometrical consideration the following simple relation can be used:

$$y_k = \sum_{i=1}^{k}(dw_{k+1} - dw_i)w_i \qquad (10)$$

where dw_i represents the deadband width of the generic i-th backlash oparator; w_i is the corresponding gain; y_k is the output value of the lower branch of the loop in the generic point of discontinuity k, as shown in Fig. 7(b); the output values y_k are identified by using the exponential functions of Eq. (5). As shown in Fig. 7(b) the vector $\{dw\}$ represents a user defined discretization of the total amplitude of the input signal $2A$. Equation (10) can be rewritten in matrix form as follows:

$$\{y\} = [A]\{w\} \qquad (11)$$

where the matrix [*A*] is constructed, for a given {*dw*} vector, by using Eq. (10); the unknown vector {*w*} can be found by solving a system of *N* linear equations, where *N* is the total number of backlash operators, as follows:

$$\{w\} = [A]^{-1}\{y\} \qquad (12)$$

The numerical method described above was implemented in a Simulink$^{®}$ model, as shown in Fig. 8. In the model, the backlash operators {H_r} are combined in series with gain operators, which represent the weight vector {*w*} reported in Eq. (8). Unfortunately, this simple model is unable to represent dead zones of transformation, therefore it doesn't describe the behaviour of the material when the temperature is above A_f, during heating, and below M_f, in the cooling branch of the hysteresis loop, as it is clearly illustrated in Fig. 6(a). To overcome this drawback the range of the temperature is limited by a saturation operator, as illustrated in Fig. 8; in particular, this operator imposes upper and lower bounds on the temperature, which are A_f and M_f respectively, so that when the temperature is outside these bounds the signal is clipped to the upper or lower bound.
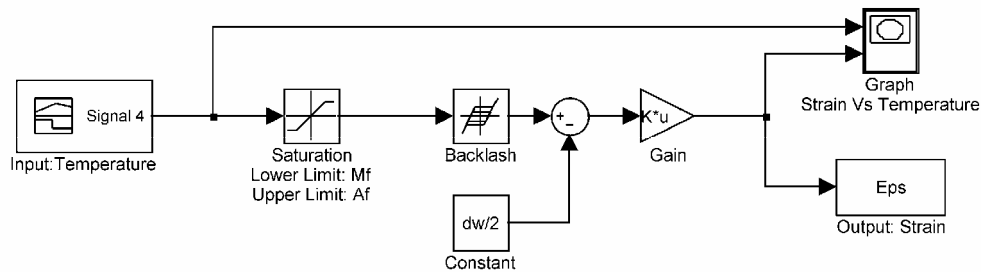
Fig. 8: Simulink model of the Prandtl-Ishlinskii hysteresis operator

In Fig. 9 the response of the numerical model, in terms of strain-temperature loop, is illustrated, for a thermal cycle between the temperatures $T_0 < M_f$ and $T_1 > A_f$; the figure clearly shows that the hysteretic behaviour of the material is properly described in the range of temperature between M_f and A_f, and the dead zone of transformation, when the temperature exceeds A_f or falls below M_f, are also simulated.
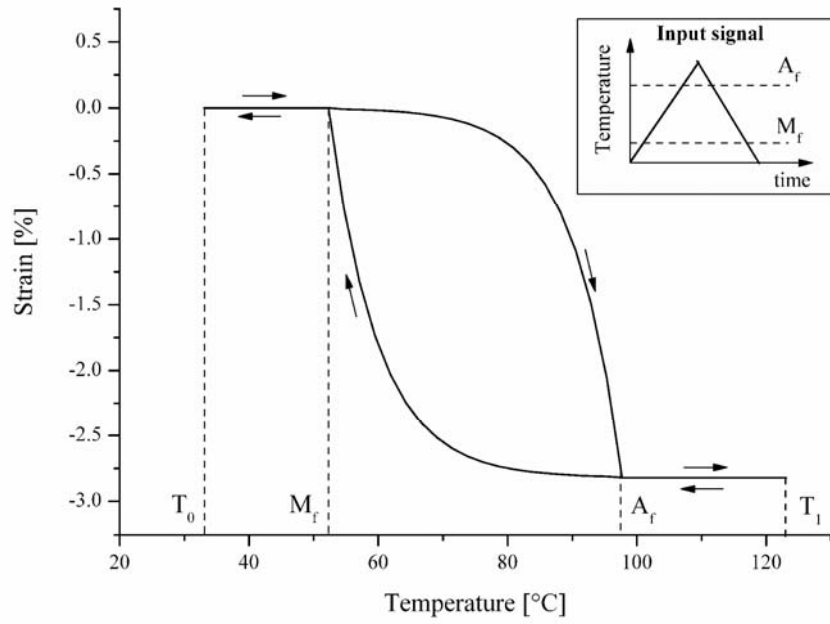
Fig. 9: Numerically simulated loop for a thermal cycle between the temperatures $T_0 < M_f$

Unfortunately, when comparing the experimental results with the numerically simulated loops high errors are observed in the extremity of the hysteretic region, or better when the temperatures is below M_f, during cooling and above A_f, during heating. To overcome this limitation the modified Simulink model, illustrated in Fig. 20, was developed.
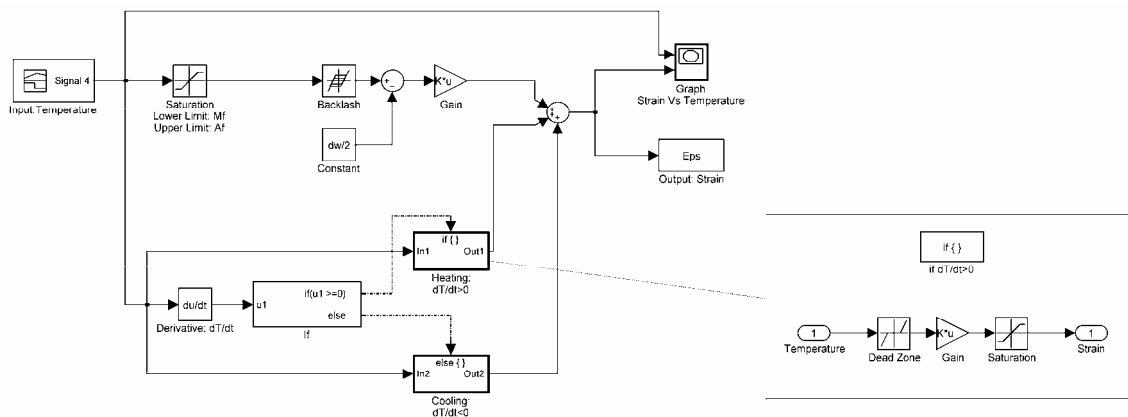
Fig. 10: Simulink model of the modified Prandtl-Ishlinskii hysteresis operator

The model uses two subsystems, for the heating and cooling branches of the loop, which modifies the output response of the system when the temperature is near M_f and A_f. In particular, each subsystem implements a weighted superposition of several dead band operators, which is executed by the series of a dead band block and a gain block,

while the saturation block assure that the correction is carried out only in a limited range of temperatures near M_f and A_f. Fig. 11 shows a simulated hysteresis loop, obtained by the modified model, between the temperatures $T_0<M_f$ and $T_1>A_f$; the figure clearly shows that the model allows a better simulation of the extremity of the hysteretic region with respect to Fig. 9.
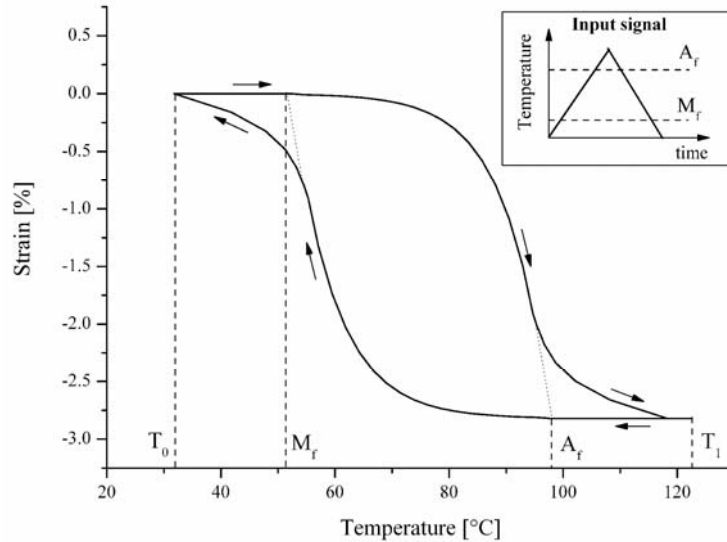
Fig. 11: Numerically simulated loop for a thermal cycle between the temperatures $T_0<M_f$ and $T_1>A_f$ obtained by the modified Prandtl-Ishlinskii model

5.2.2 *VALIDATION OF THE PROPOSED MODEL*

In this section the accuracy and efficiency of the proposed numerical method is illustrated by comparing some experimentally measured hysteresis loops with the corresponding numerical predictions. The simulations were carried out by using a model with 20 backlash operators and 5 dead zone operators to modify the loops in the extremity of the hysteretic region.

Fig. 12 shows a comparison between experimentally measured hysteresis loop for a stress free martensitic transformation, between the temperatures $T_0<M_f$ and $T_1>A_f$, and the numerically simulated loop; the figure clearly shows a good accuracy of the numerical model with very small errors.

87
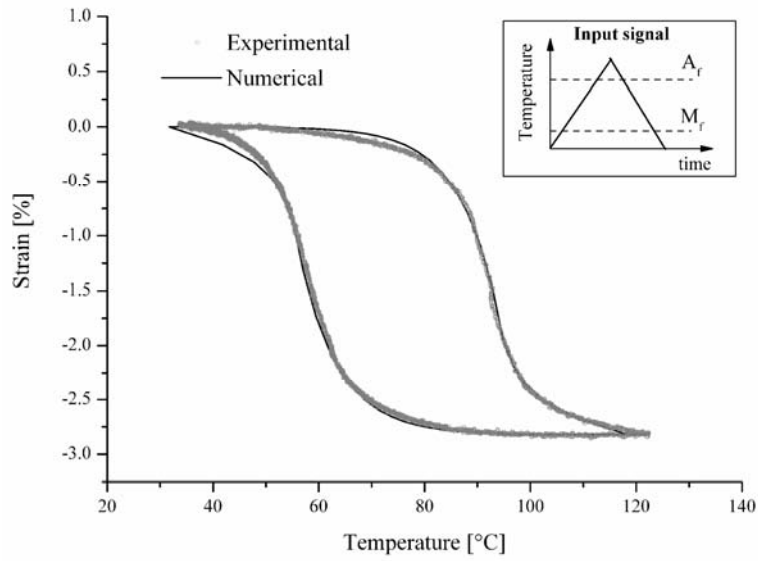
Fig. 12: Comparison between experimental measurements and numerical predictions for a stress free thermal cycle between the temperatures $T_0 < M_f$ and $T_1 > A_f$

In Fig. 13 a comparison between numerical predictions and experimental results when the material is subjected to a tensile stress of 50 MPa, Fig. 13(a), and 100 MPa, Fig. 13(b), is shown. Also in this case a satisfactory agreement is observed but the errors increase when increasing the applied stress as shown in Fig. 13(b). However, its important to point out that the model parameters were identified by using the hysteresis loop of the previous example, which was obtained in stress free condition, and by applying Eqs. (2)-(4) to modify both the transformation temperature and ε_{tw}.
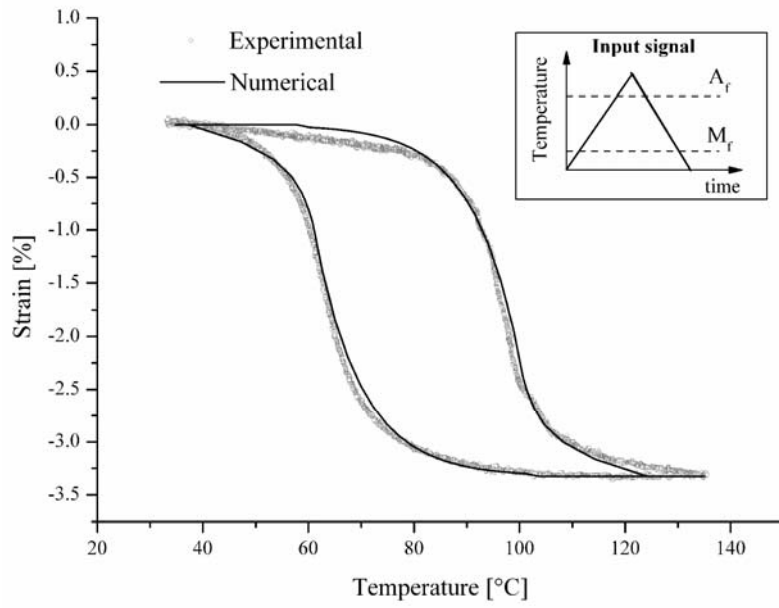
(a)
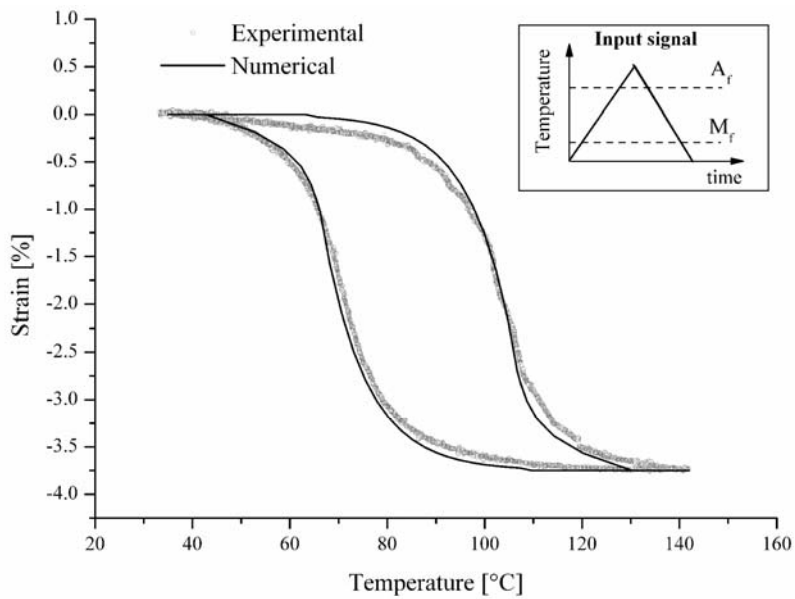
(b)

Fig. 13: Comparison between experimental measurements and numerical predictions for a thermal cycle between the temperatures $T_0 < M_f$ and $T_1 > A_f$ under a fixed tensile stress: a) 50 MPa; b) 100 MPa.

The accuracy of proposed model was also analyzed when the material is subjected to partial thermal cycles, or better to incomplete martensitic transformations. Figures 14(a) and (b) show the hysteretic behaviour of the material for two different temperature-time paths in stress free condition; in particular Fig. 14(a) shows incomplete A→M

transformations, while Fig. 14(b) illustrates incomplete M→A transformations. As shown in the figures the comparison between experimental measurements and numerical predictions show a good accordance in both cases. It is worth noting that the same model parameters of the first example were used in these numerical simulations.
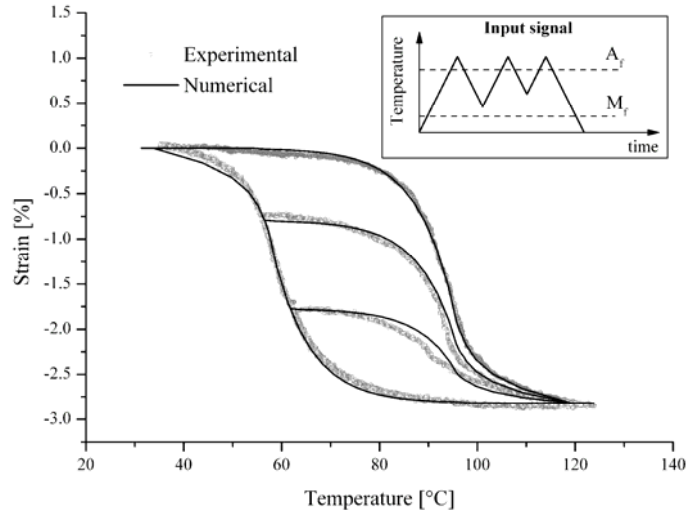
(a)
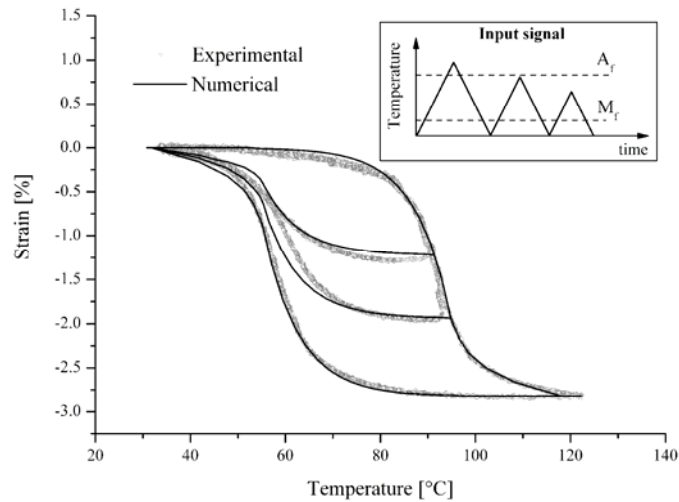
(b)

Fig. 14: Comparison between experimental measurements and numerical predictions for two different temperature-time paths: a) incomplete A→M transformations; b) incomplete M→A transformations.

In addition to the comparisons between numerical predictions and experimental measurements illustrated above, further numerical simulations were carried out in order

to assess the response of the numerical model under different temperature paths. As an example, Figs. 15 report the strain-temperature hysteretic behaviour of the material for a temperature path which involves both incomplete A→M and M→A phase transformations; in particular, Fig. 15(a) shows the simulated strain-temperature hysteretic behaviour of the material in stress free conditions while Fig. 15(b) reports the numerical results of the model under a constant applied stress of 100 MPa. Based on the experimental validations reported above the results are likely to be accurate and illustrate the capability of the model in predicting outer and inner hysteretic loops in stress free conditions as well as under fixed values of applied stress.

Finally, Fig. 16 illustrates the numerical predictions of several subsequent thermal cycles between the temperatures $T_0 < M_f$ and $T_1 > A_f$, carried out for different values of fixed applied stress in the range between 0 and 100 MPa. The figure clearly shows that the numerical model is able to capture the hysteresis modifications, due to the applied stress, in terms of both two-way strain and phase transition temperatures.

As a final remark, it is worth noting that the all numerical simulations were executed by identifying the model parameters from the measured hysteresis loop in stress free condition and by using Eqs. (2)-(4) to describe hysteresis modification under fixed applied stress.
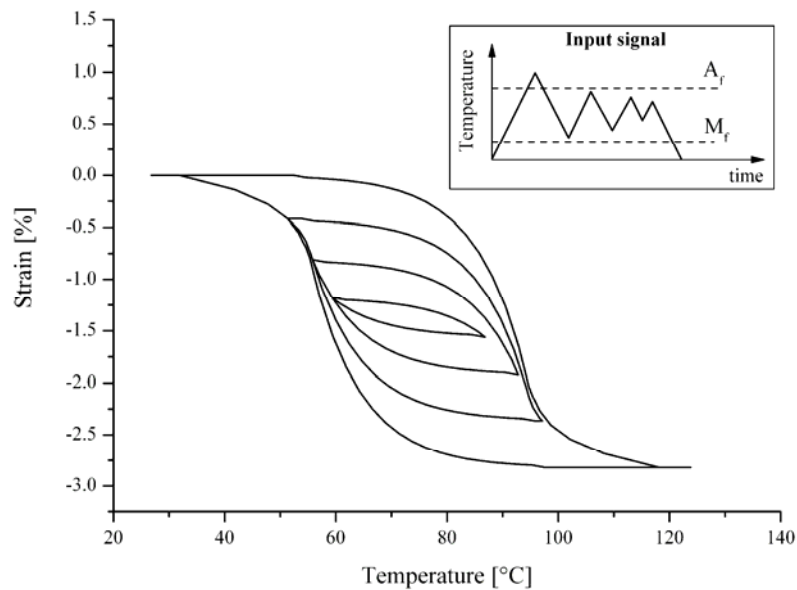
(a)
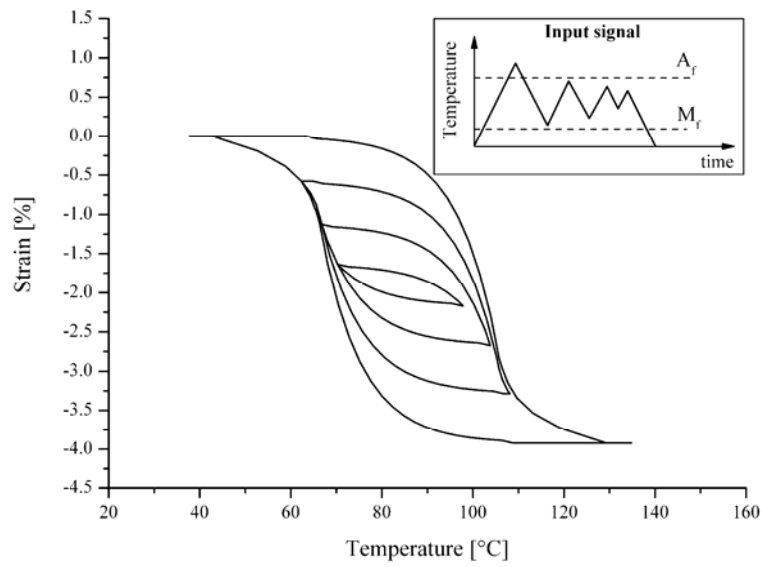
(b)

Fig. 15: Numerical predictions for a temperature-time path which involves both incomplete A→M and M→A phase transformations: a) Stress free condition; b) under a fixed tensile stress of 100 MPa.
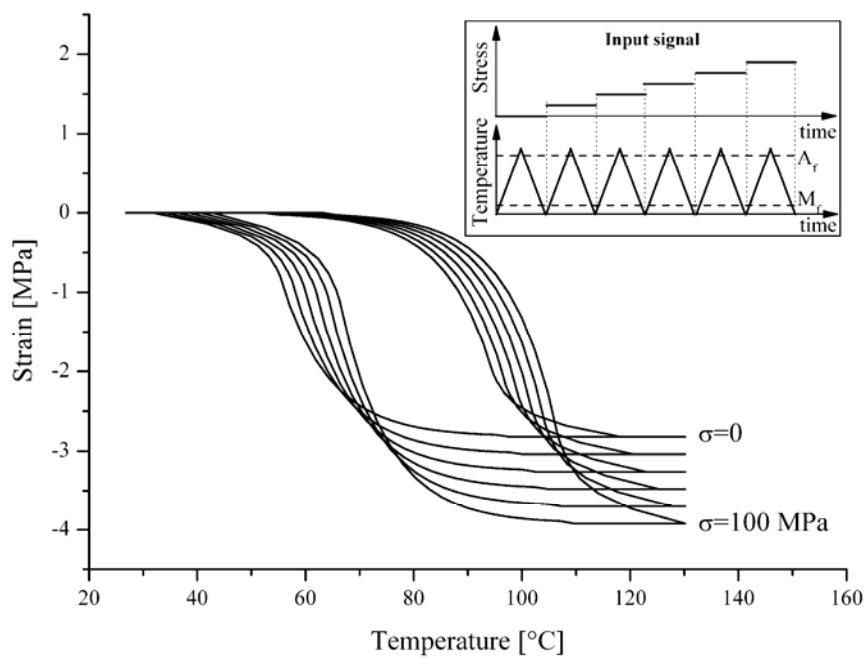
Fig. 16: Numerical predictions for subsequent complete transformations under different fixed values of applied stress

CHAPTER 5

BIOMIMETIC COATING OF NITI ALLOYS

5.1 OVERVIEW

NiTi alloys has been increasingly applied to medical and dental appliances due to its high damping capacity, high corrosion resistance and shape recovery (Castleman et al 1981; Dai, 1996). These properties could be very useful for the realization of orthopaedic and dental implants. However, despite the satisfactory clinical use of NiTi in some applications, the high Ni content in the alloy is of great concern with regards to its biocompatibility (Castleman et al. 1981, Putters et al. 1992, Assad et al. 1994, Shabalovskaya et al. 1995).

Original NiTi surface has revealed a tendency towards preferential oxidation of titanium. This behaviour is in agreement with the fact that the free enthalpy of formation of titanium oxides is negative and exceeds, in absolute value, the enthalpy of formation of nickel oxides by at least two-three times (Gu et al, 2005). As a result, Ni is

mostly present in elemental state on the NiTi surfaces; furthermore, due to corrosion phenomena, it is possible that Ni dissolves from the inside material (Gu et al, 2005) reducing the implant safety. In fact, Ni has been reported to be responsible for the clinic toxic and allergic responses (Gu et al, 2005; Van Hunbeeck et al, 1998); so that, in order to restraining Ni release, improving the NiTi biocompatibility, its necessary to modify the material surface properties (Gu et al, 2005).

On the other hand, the use of the NiTi functional properties in the realization of orthopaedic and dental implants is strongly related to their osteoconductivity. In fact, biomaterial osteointegration is one of the most important aspects involved in the design and realization of implants useful for the regeneration or substitution, as a results of traumas or some pathologies, of bone in the human body (Fini et al. 2004). Osteointegration depends not only on the characteristics and regenerative capability of the host bone, but also on the properties of the implanted material (Fini et al. 2004). The biological response to implant materials is directly related to their surface properties in terms of morphological and chemical properties. In fact, the optimization of the bone ingrowth strongly depends on the improvement of mechanical and biological conditions at bone-implant interface; in particular, the surface treatments on the materials, usually used in many orthopaedic and dental applications, have a fundamental role for increasing the bone ingrowth rate and the mechanical properties of the bio integrated joint (Nanci et al. 1999).

In the last few years, various approaches are currently under development to prevent undesirable Ni release, ensuring NiTi implants safety and to improve the material osteoconductivity (Gu et al. 2005, Firstov et al. 2002, Shabalovskaya et al. 1995, Chan et al. 1990). Some researchers have persecuted this objective modifying the material surface properties by different thermal and chemical treatments; however, the use of coatings with high biological performance is probably more promising in terms of long period safety shielding the substrate by the biological environment (Oliverira et al. 2003).

In this field, Hydroxyapatite (HA), and related Calcium-Phosphates (Ca-Ps), could be very useful. These materials have been used in medicine because of their biocompatibility and osteoconductive properties (Oliverira et al, 2003); however, their low mechanical performance limit the application as structural materials. Their use as

coating is probably the most useful way for their applicability permitting to obtain implants with excellent strength, biocompatibility and bioactivity. In fact, these coatings favour the take and the proliferation of the cells and, consequently, the vascularization of the new tissue (Oliverira et al. 2003). In fact, it is already known that the essential requirement for an artificial material to bond to living bone is the capability to form a bone-like apatite layer on its surface in the body environment (Oliverira et al. 2003). These effects assure lower risks of implant mobilization and a reduction of the hospitalization period. Nevertheless, the applicability of this type of biocompatible coatings needs a further improvement of their chemical, biological and mechanical properties.

A large number of processes for coating metals, such as stainless steel and titanium alloys, with Ca-Ps have been proposed for obtaining tough bioactive materials usable as bone substitutes even under highly loaded conditions such as hip joints (Pham et al. 2000). Among them, titanium alloys coated with hydroxyapatite by plasma spray method is already clinically used (Gan et al, 2004, De Groot et al. 1987). However, this techniques is characterised by many drawbacks in terms of control of Ca-P phases, adhesion, and the long term stability of the implant; furthermore, the high process temperatures would reduce the mechanical properties of the substrate (Oliverira et al. 2003). As well known and reported in the previous chapters, the NiTi properties are strongly influenced by the production conditions, and, in particular, by the thermal effects due to the working process that modify the thermomechanical condition of the alloys. For these reasons, the use of many of the common coating technologies are not applicable for NiTi alloys especially in the case of low thickness components.

In the recent years, a new approach to coating materials, called biomimetic, has attracted many interest because it allows to obtain Ca-P coatings bypassing many drawbacks related to the other coating processes. This method consists on getting the nucleation of the Ca-P on the substrate by precipitation, at physiological pH and temperature values, from supersaturated solutions simulating the body fluids (Simulated Boby Fluid, SBF) (Kim et al, 1997, Barrere et al. 2004, Gu et al. 2005). The process strongly depends on the conditions of the substrate surface, then a control of its chemistry and morphology is necessary in order to obtain a fast and uniform deposition and a good adhesion of the coating (Kim et al. 1997, Gu et al 2005). For these reasons,

surface pre-treatments, like thermal and chemical pre-treatment, can be carried out in order to assure a better chemical bond between the coating and the substrate (Kim et al, 1997).

In this chapter, the effects of different surface conditions of a NiTi alloy on the properties of the Ca-P coatings obtained by a biomimetic procedure are presented.

In order to understand the evolution of the nucleation process, the analysis were carried out after different immersion times. The effects of chemical and thermal treatments were investigated by Scanning Electron Microscopy (SEM), Energy Dispersive X-Ray (EDX) and X-Ray Diffraction (XRD), in order to evaluate the chemistry and the morphology of the material modified surfaces and the coatings. Finally, a comparison of the results were carried out.

5.2 EXPERIMENTAL

5.2.1 PREPARATION OF SUBSTRATES

The material used in the experiment is a Ni-51 at.% Ti sheets produced by cold rolling with a successive thermal treatment at 400°C for 45 min. Samples were cut from the sheets to a size of 10 x 10 x 1 mm^3; before any surface treatments, the specimens were mechanically polished progressively using grits SiC emery papers (from 400 to 1200), in order to remove macro-level surface defects and contaminations, then ultrasonically cleaned for 10 min with pure acetone and distilled water separately, and, finally, dried in air.

Two types of NiTi surface were analyzed in this investigation; the type 1 was obtained by chemical etching using an HNO$_3$ solution, while the type 2 was obtained, after the chemical etching, by thermal treatment carried out at 600 °C in air. Finally each samples were thoroughly washed with distilled water and dried overnight at room temperature. Successively, the two types of substrate were subjected to the coating process carried out by dipping in a proper SBF (Simulated Body Fluid) solution.

5.2.2 BIOMIMETIC COATING PROCEDURE

In order to study the in vitro behaviour, every samples were incubated in a proper simulated body fluid solution. A five times concentrated SBF was prepared, according to Barrere et al. 2004, by dissolving reagent grade mixture of NaCl, $CaCl_2 * 2H_2O$, $MgCl_2 * 2H_2O$, $NaHCO_3$, Na_2HPO_4 in distilled water. The use of supersaturated SBF rise to the need of accelerate the deposition process. The solution was prepared at 37°C under constant bubbling of carbon dioxide gas (CO_2) in order to decrease the pH and to obtain, consequently, the complete dissolution of the salts. In fact, it is well known that low solution pH is required to increase ionic solubility if the accelerated techniques, that is necessary for the supersaturated SBFs, were applied (Chou et al. 2004).

The SBF have a pH $\sim$ 8 and the supply of CO_2 lead to pH $\sim$ 6 allowing the complete dissolution of the salts and so a clear solution. At this point, the supply of CO_2 was stopped and each specimen was immersed separately in a plastic vessel filled with about 100 ml of SBF and put in an incubator at 37°C under continuous stirring. The pH of the SBF progressively increase inducing the precipitation of the Ca-Ps that nucleate on the substrate. In order to evaluate the evolution of the Ca-Ps deposition the specimens was treated for 5 and 30 h and then taken out, rinsed with demineralised water and dried at 50°C in air.

5.3 RESULTS

5.3.1 ANALYSIS OF THE TREATED SURFACES

Before any treatments, the material presents a smooth surface, showed in Fig. 1 (a), with many sketches, due to the mechanical polishing; this confirms the presence of a very thin oxide layer made up during the production of the material and, in particular, as consequence of the low temperature of the thermal treatment. The related XRD, in Fig. 1 (b), shows the characteristic peaks of a NiTi alloy together with a low peck related to Ti_2Ni compound that is present in the alloy as precipitates; furthermore, no evidence of titanium oxides is observed as consequence of the low thickness of the layer.

In Fig 2 (a) the type 1 surface is shown; the chemical etching, carried out using an HNO$_3$ aqueous solution, creates a microporous surface with many pores of few microns in diameter. Probably, this type of surface morphology is able to increase not only the nucleation points for the apatite globs, but also the adherence between the coating and the substrate.

Furthermore, the related XRD, Fig. 2 (b), shows the presence of a low crystalline titanium oxides (TIO$_2$) layer, as result of the oxidation occurred during the chemical etching, together with an increase of the Ti$_2$Ni peck probably due to the erosion made by the etching that reveal the material internal state.

In Fig 3 (a) the type 2 surface is shown; as expected, the thermal treatment, carried out after the chemical etching, creates an high oxidation of the material surface that seems very roughly and made by very small crystals. The XRD pattern, shown in Fig. 3 (b), confirms not only the high crystallinity of the surface, but also the low presence of Nickel; in particular, the high NiTi peak is visible together with titanium oxides peaks and very low Ni compounds peaks.

According to these results, the type 2 surface could be more biocompatible than the others due to the very low Ni presence; however, further studies is necessary to understand their long term chemical stability. Furthermore, both surface morphologies are, probably, more useful for promoting the CaPs nucleation and adhesion, with respect to the reference surface that is too much smooth for assure a good adhesion of the coating.

5.3.2 ANALYSIS OF COATED SURFACES

After the surface pretreatments, the specimens were subjected to the biomimetic coating. In order to evaluate the deposition process the specimens were immersed in the SBF solution for 5 and 30 hours and then analyzed.

In Fig. 4 the SEM micrographs and the XRD pattern related to the type 1 surface after 5 hours of immersion in the SBF are reported. After only 5 hours of immersion, the surface of the type 1 specimen appears to be randomly covered by many spherical particles with dimension of few microns. As confirmed by the XRD analysis, these

particles are hydroxyapatite (HA) globules that nucleate on the material in early stage of the immersion time.

Increasing the immersion time, an increase in the apatite formation is observed as confirmed by the broadness of the HA peaks observed in the XRD pattern shown in Fig. 5 (b). In particular, after 30 hours many agglomerates hydroxyapatite cover, in a non uniform way, the surface of the material as can be seen in Fig. 5 (a).

In Fig. 6 an high magnification of the hydroxyapatite agglomerates is reported. The figure shows that, during the deposition time, the hydroxyapatite globules increase in number and in dimension, linking together to form large agglomerates. These agglomerate are linked to the substrate by an glassy interface composed, probably, by hydroxyapatite globules with nanometre dimensions (Barrere et al. 2004).

In Fig. 7 the results related to the type 2 specimen after 5 hours of immersion in the SBF are reported. In particular, the type 2 surface seems to be no so able to induce the deposition of the CaPs coating as the type 1. In fact, after 5 hours, very few HA particles is observed on the material surface, as can be seen in Fig. 7 (a). The very low HA peaks measured, visible in Fig. 7 (b), confirms that the nucleation process in the type 2 specimen is more slow than in the type 1.

Furthermore, after 30 hours, the specimen surface appears to be randomly covered by HA agglomerates and, as can be seen in Fig. 8 (a), many voids are present on the coated surface. These observation are confirmed by the XRD pattern shown in Fig. 8 (b) in which only one HA peak is observed. Furthermore, the HA agglomerate observed in type 2 specimen have a very different morphology with respect to the type 1 case; in particular, as reported in Fig. 9, the HA globules appears to be no linked together probably as consequence of a different interaction with the substrate.

In order to evaluate the chemical composition of the coating, the EDX analysis of the two coated specimens is carried out. As reported in Fig. 10, the EDX spectrums reveal a different Ca/P ratio for the two types of surface. In particular, the Ca/P ratio for the type 1 is measured to 1.67 that is the characteristic value of the hydroxyapatite. For the type 2 specimen, a value of 1.31 have been measured; it can be speculated that the surface layer does not only contain HA but also other apatites.
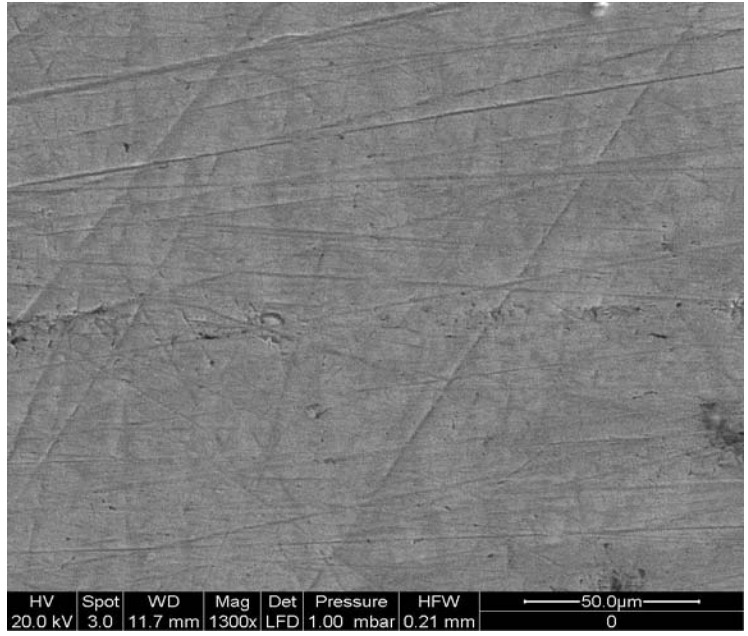
(a)
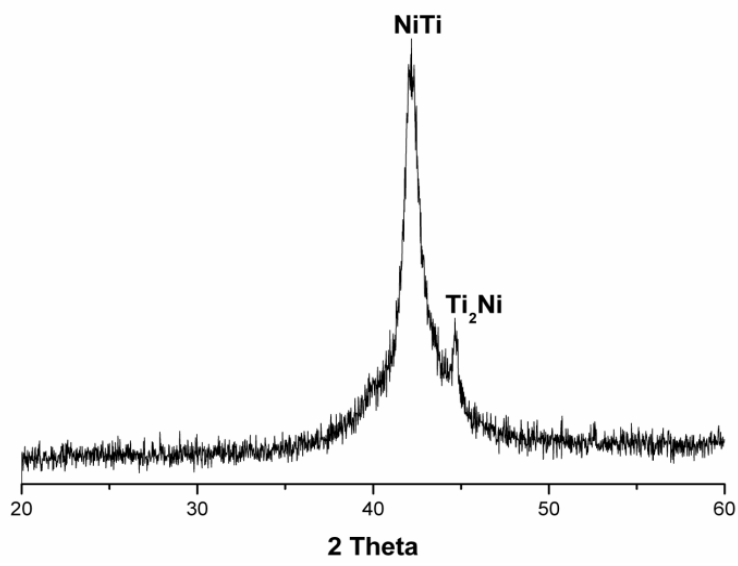
(b)

Fig.1: Morphology of untreated NiTi surface (a) and related XRD patterns (b)
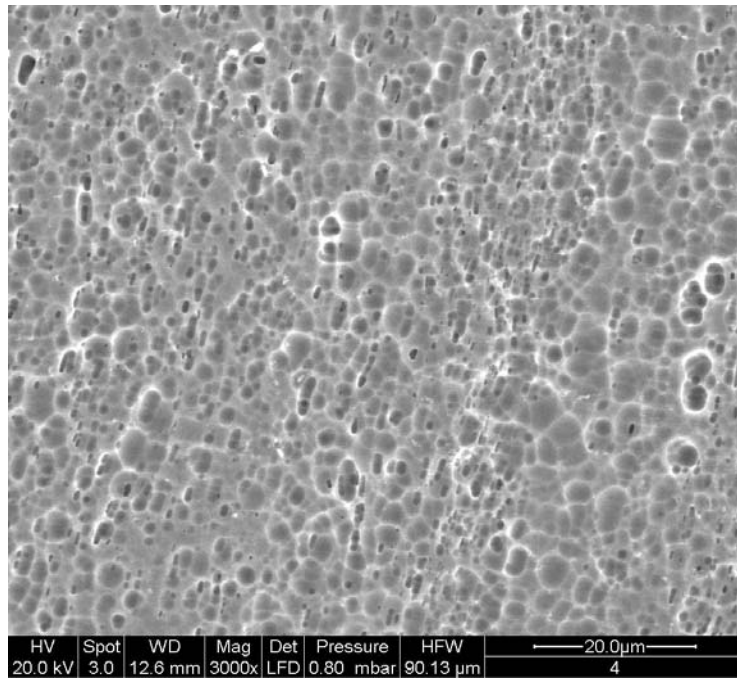
(a)
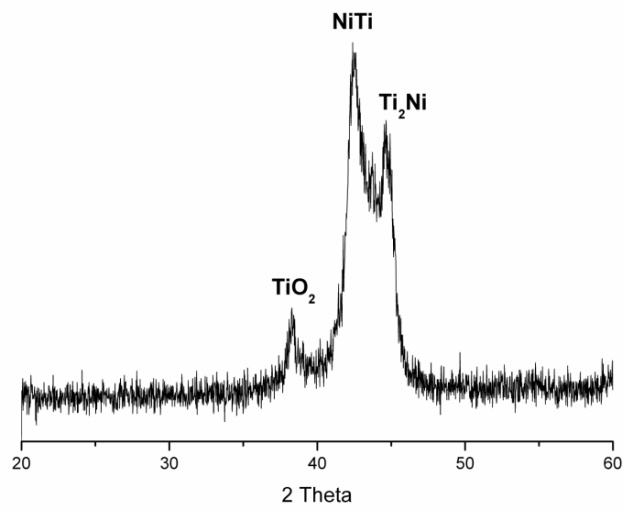
(b)

Fig 2: Morphology of type 1 surface (a) and related XRD patterns
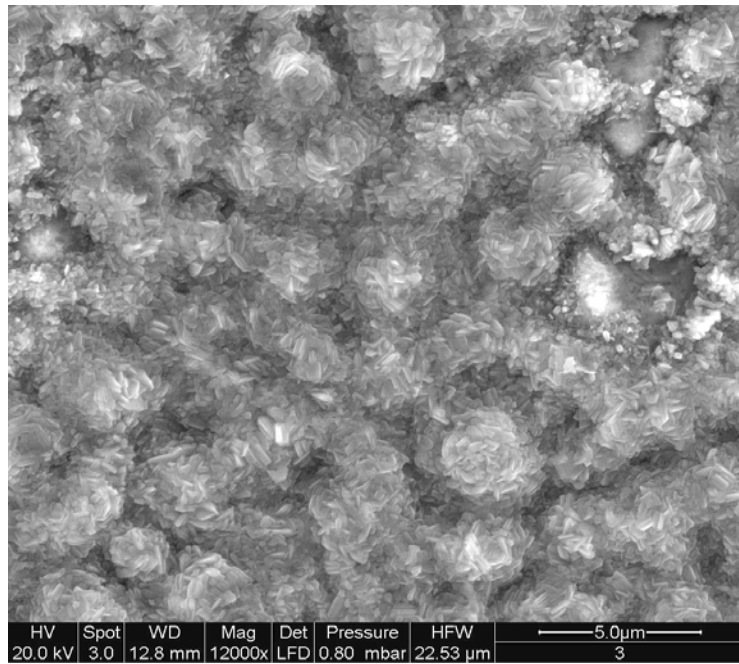
(a)
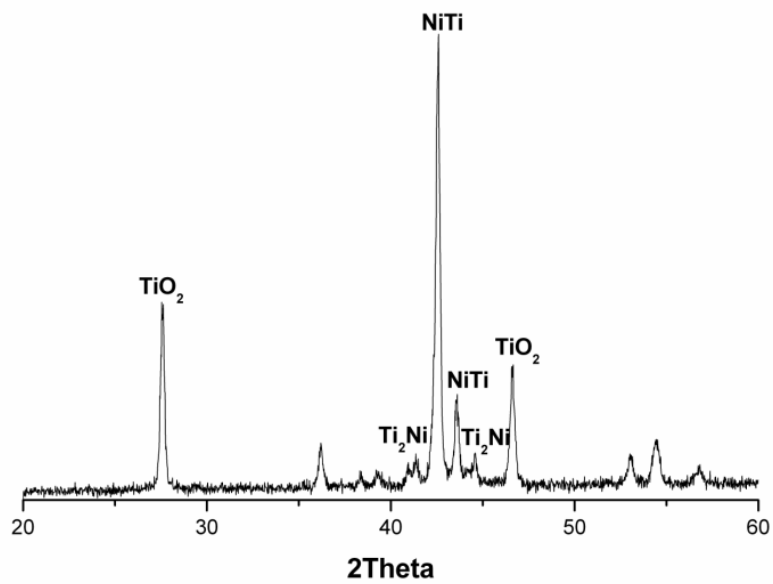
(b)

Fig 3: Morphology of type 1 surface (a) and related XRD pattern (b)
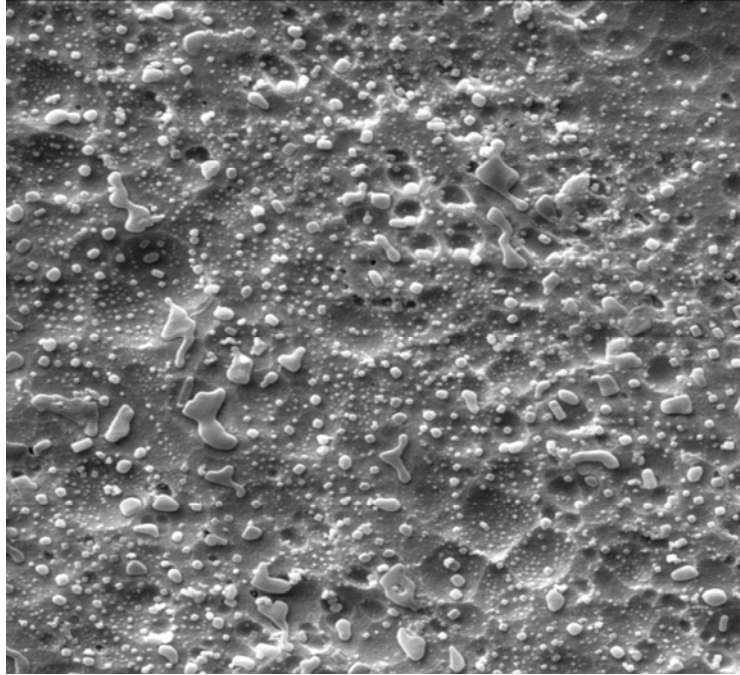
(a)
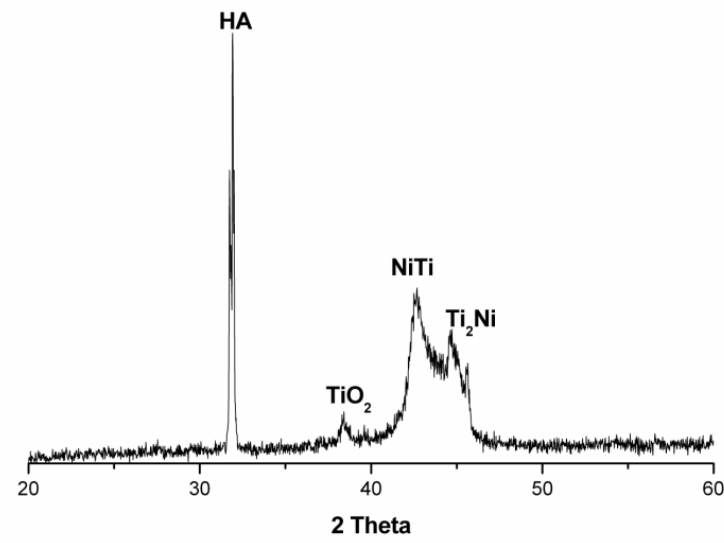
(b)

Fig 4: Morphology of type 1 surface (a) and related XRD pattern (b) after 5 hours of immersion in SBF
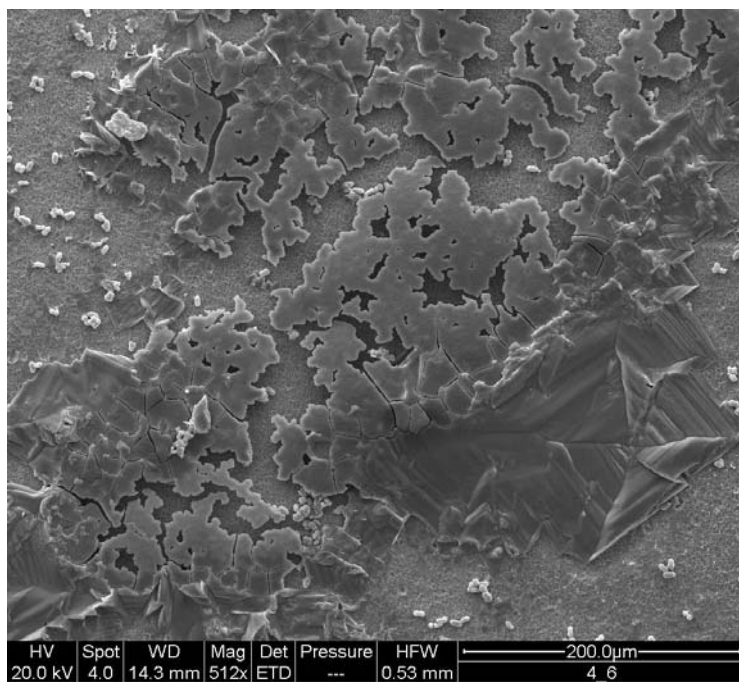
(a)
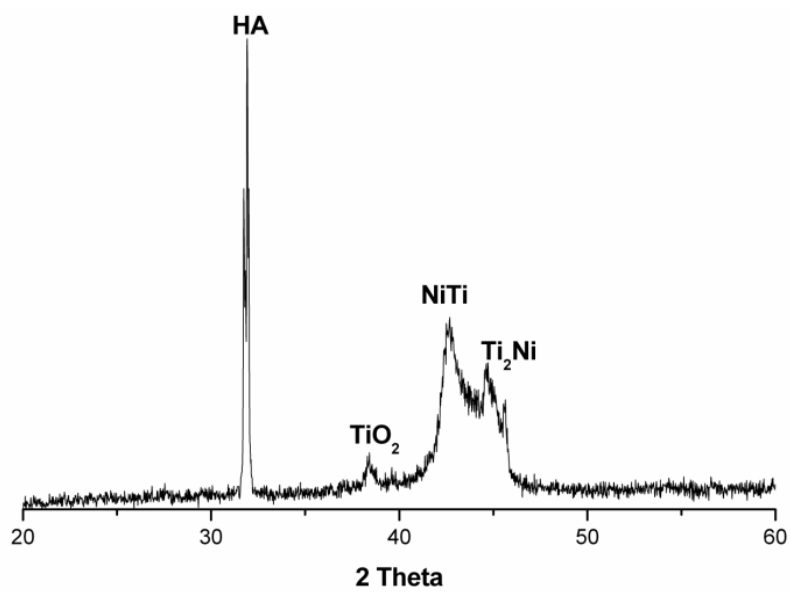
(b)

Fig 5: Morphology of type 1 surface (a) related XRD pattern (b) after 30 hours of immersion in SBF
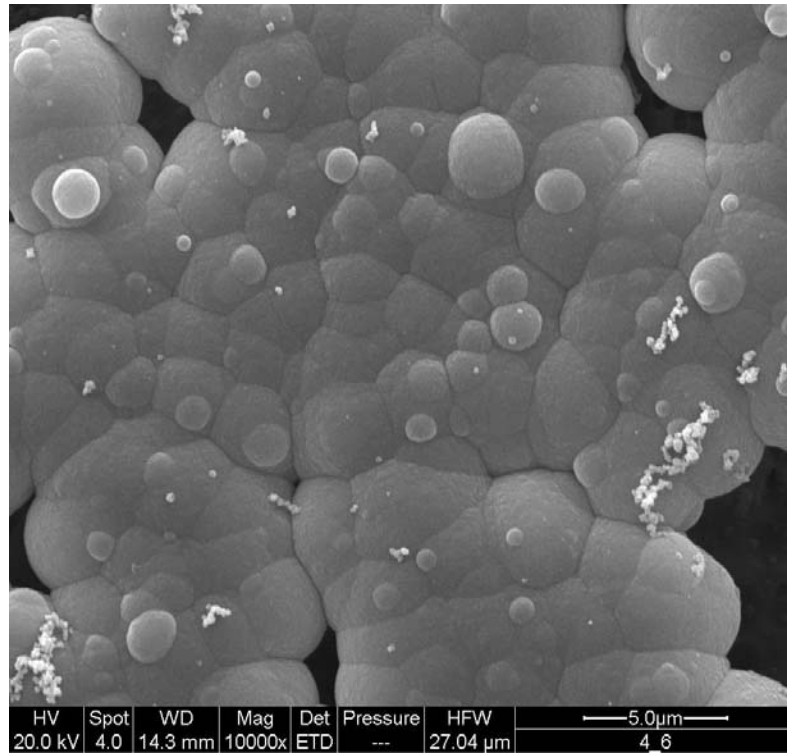
Fig 6: Morphology of the hydroxyapatite agglomerate
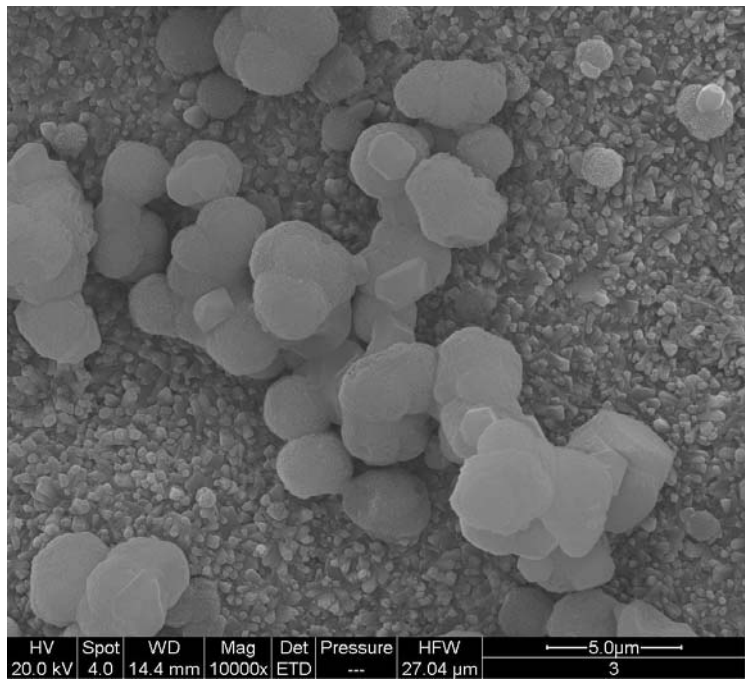
(a)
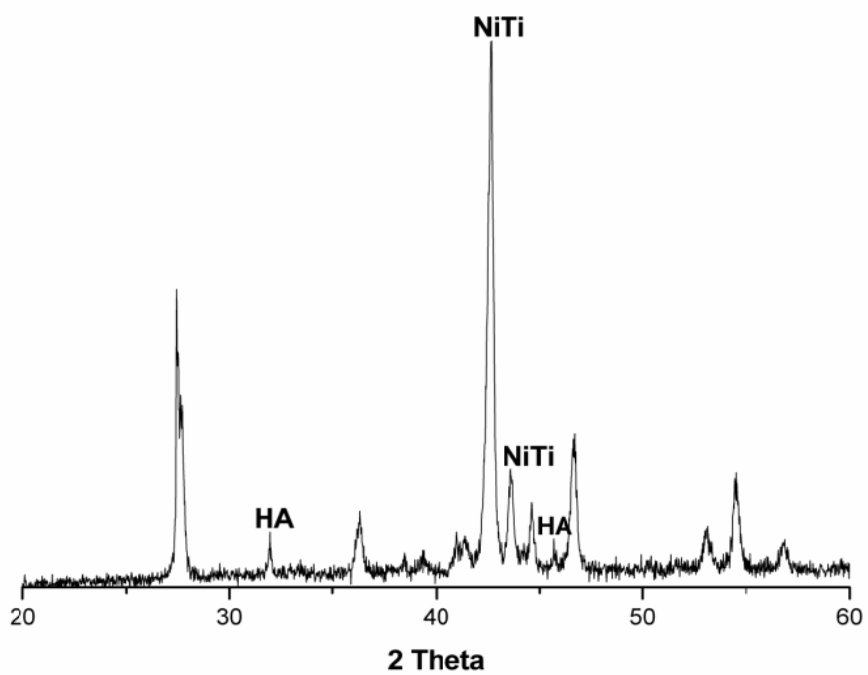
(b)

Fig 7: Morphology of type 2 surface (a) related XRD pattern (b) after 5 hours of immersion in the SBF
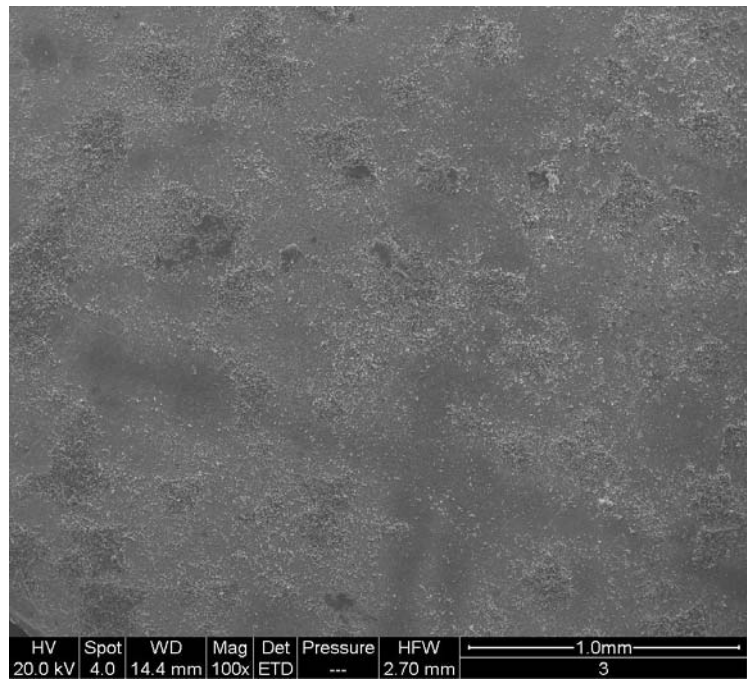
(a)
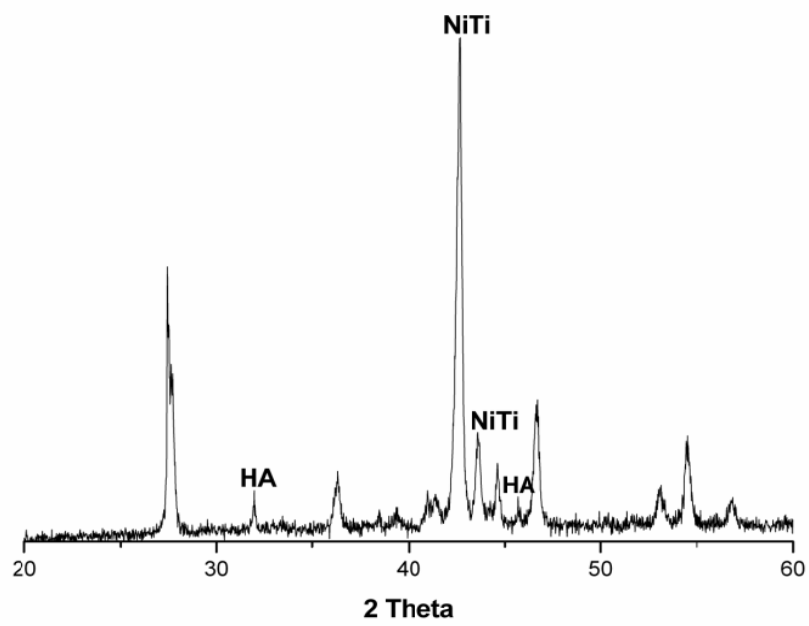
(b)

Fig 8: Morphology of type 2 surface (a) related XRD pattern (b) after 30 hours of immersion in the SBF
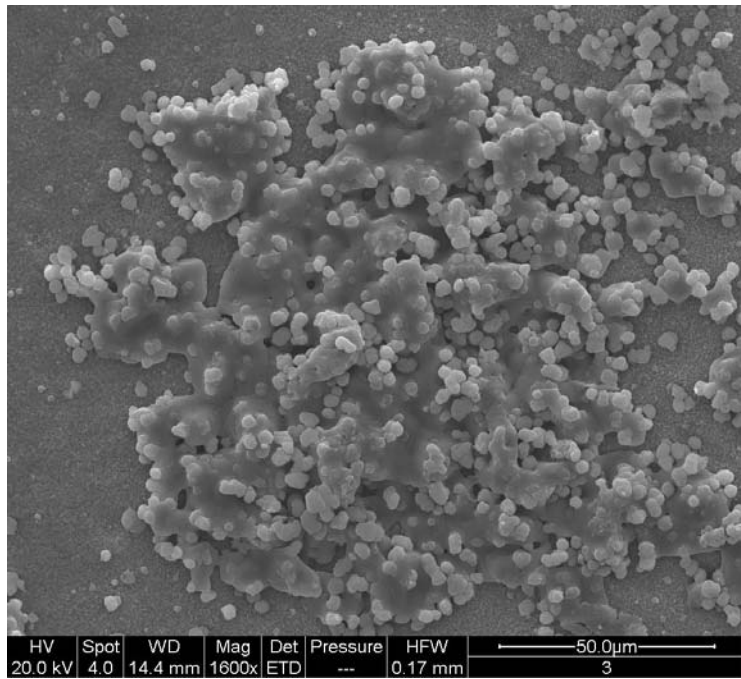
Fig 9: Morphology of the hydroxyapatite agglomerate
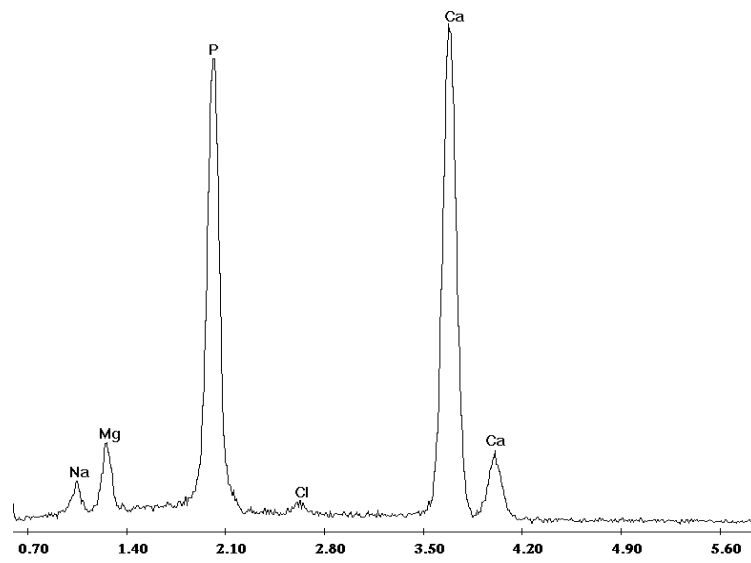
(a)
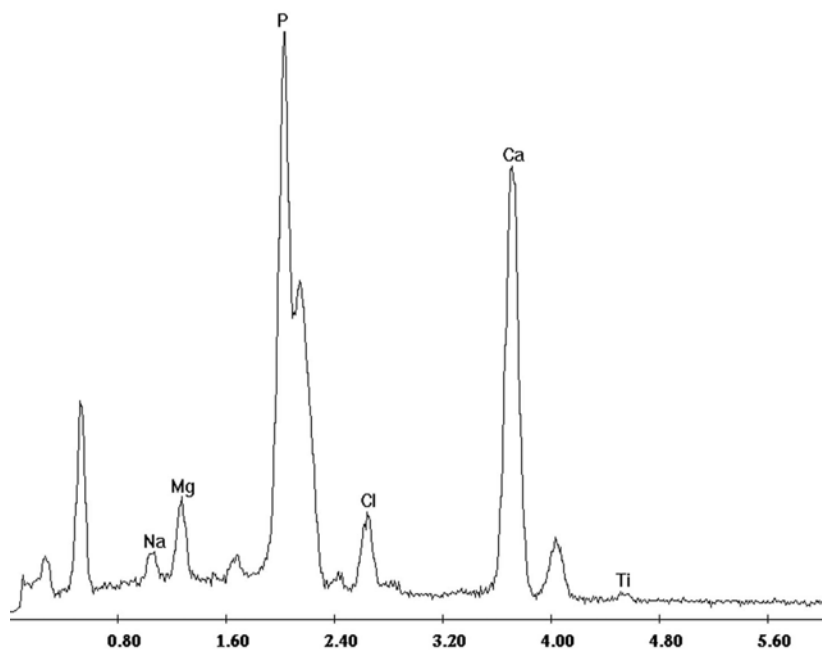
(b)

Fig. 10: EDX pattern of type 1 (a) and type 2 (b) specimens after 30 hours of immersion in SBF

CHAPTER 6

CONCLUSIONS & FUTURE WORK

6.1 SUMMARY AND CONCLUSIONS

In the present dissertation, the research activities carried out during my Doctoral Course in Mechanical Engineering at the University of Calabria is reported. The research regarded different aspects concerning Nickel-Titanium Shape Memory Alloys.

An experimental study about mechanical and functional properties of a Ni- 51 at.% Ti alloy was executed evaluating also the effects due to Nd:YAG laser welding. In particular, the deformation mechanisms involved in the material stress-strain behaviour during thermomechanical cycling (training) was investigated; the incoming of the Two Way Shape Memory Effect (TWSME) was studied together with the variation in the its characteristic hysteretic behaviour under different applied stress. Furthermore, the effects of a thermal treatment on the material behaviour are evaluated in terms of stress-strain curve. Many of the experimental investigations summarized above, are executed

on both base and welded materials and the results was compared in order to evaluate their mechanical and functional performance.

The results confirms that the deformation mechanism involved in the shape memory behaviour are related to the development of plastic strain and stabilized martensite in the material structure during repeated training cycles. In the observed range of deformation, a constant increase in the shape memory performance of the material was observed confirming that the chosen thermal treatment favour the detwinning deformation mechanism. During cycling, due to the development of plastic strain, an internal stress field was created; this stress field interact with the phase transformation during the thermal step of the training cycle, allowing the formation of a preferentially oriented martensitic structures during cooling. This effects benefit the formation of the TWSME in the material that, guided by the internal stresses remember a low temperature shape. Increasing the number of training cycles, these structure was stabilized by the residual stress field and do not participate to the transformation. The increase in the phase transformation temperatures and in the slop of the stress plateau together with a reduction in the stress for detwinning are the consequence of these effects. Furthermore, when the material was subjected to an applied stress and thermally cycled between the transformation temperatures, a proportional increase in the deformation recovered for TWSME was observed as a consequence of the increase in the internal stress field. According with the Clausius-Clapeyron rule, a further increase in the transformation temperatures was measured. Finally, the thermal stability of the TWME was analyzed subjecting the material at successive thermal treatments; the results show a degradation in the deformation recovered for TWSME characterized by an high cycles stabilization. These effect are probably due to the relaxation of the stress field described before as consequence of a further stabilization of the martensitic structures.

The observed welded joints show the same behaviour of the base material but a lower resistance to plastic deformation. The thermal treatment carried out on the welded material seems to relax the residual stress due to welding, as confirmed by the reduction in the stress plateau slop. However, the welded joints show higher deformation with respect to the base material when they are subjected to the same training cycles. This is probably due to the different effects that the thermal treatment have on the

microstructure of the welded material. In fact, the measurements show that a maximum was reached for both one way and two way deformation, with a successive decrease for higher number of cycles. These maximum values are observed together with an exponential like increase of the plastic deformation that strongly damage the martensitic structures avoiding the shape recovery. However, the welded joints seem to have good shape memory performance but at lower deformation values compared to the base material.

Future works could be oriented to the optimization of the welding processes in order to improve the welded joints performance; the obtaining of a welded joint with high functional performance is a interesting topic in order to realize innovative applications. In particular, the realization and the characterization of a functionally graded NiTi component obtaining by joining alloys with different properties could permit the realization of "modular" actuators. These actuator could be useful for the production of composites materials for shape and vibration control opening new perspective in many industrial applications.

The experimental data acquired during the material testing was used to develop a robust numerical method which is capable to simulate the two TWSME in Nickel-Titanium alloys. The method is based on a phenomenological approach and uses the Prandtl-Ishlinskii hysteresis operator to model the thermal hysteresis behaviour of the material associated with the TWSME. Simple numerical procedures were developed to identify the model parameters starting from the results of some experimental tests. It is worth noting that a single set of experimental data, such as the hysteresis loop in the stress free martensitic transformation and some well known thermo-mechanical parameters, is required to model the whole strain-temperature hysteretic behaviour of the material under constant applied stress.

The results show a good accuracy of the method in simulating the TWSME under different values of fixed applied stresses and even in simulating incomplete martensitic transformations. Furthermore, the model shows very small computational time, therefore it is suitable for use in real time applications. The aforementioned characteristics represent the main advantages of the proposed approach, with respect to the other phenomenological models, while the most relevant drawback consists in its one dimensional nature.

Future works should be carried to analyze the capabilities of the proposed approach in predicting the hysteretic behaviour of the material under more complex loading conditions, such as simultaneous variation of both stress and temperature, through specific experimental tests. Furthermore, to increase the practical usefulness of the proposed method in controlling NiTi actuators, which are usually driven by an electric current, further studies should be carried out to improve the model with the relationship current versus temperature.

In this dissertation the results concerning the biomimetic coating of a surface modified NiTi alloy is also reported. The results regard the first start up of a research activities regarding the use of the NiTi alloy for the realization of osteoconductive implants; in fact, their good damping properties, corrosion resistance and functional properties are of great interest in this field.

In this research, the effects of two different surface treatments, executed on a NiTi alloy, on the CaPs coating obtained by a biomimetic procedure are evaluated. The biomimetic coating procedure are very interesting for NiTi alloys because of it is conducted at low temperature, so that no degradation in the properties of the substrate are induced during the process. However the technique are strongly influenced by the surface morphology and chemical composition of the substrate, so that their preliminary modification is often necessary.

The results show that both treatments are able to induce the nucleation of the CaPs on the substrates, but different morphology and chemical properties of the coating are observed in the two types of surfaces conditions analyzed. In particular, the chemical treated surface seems to induce a more fast deposition of the apatite than the thermal treated one, even if, after 30 hours both types of substrate appears to be covered by the CaP coating. Furthermore, the coating deposited on the chemical treated substrates is composed by hydroxyapatite, as confirmed by the Ca/P ratio measured using EDX analysis, while the Ca/P ratio measured in the thermally treated coated samples demonstrate that the coating is composed by various types of apatite compounds.

Future works must be oriented to optimize the coating procedure in order to obtain an uniform coating of the material. A better control of the processes parameter are necessary due to the low stability that permits the nucleation of the CaPs on the material surface. Furthermore, a systematic study on the effects of different surface preparation

procedure are certainly necessary. The coated substrate could be also investigated in terms of shape memory behaviour in order to understand the adhesion when the material is subjected to high deformation recovery.

REFERENCES

(complete but in draft)

Abeyaratne, R., Knowles, J. K., 1993. Continuum model of a thermoelastic solid capable of undergoing phase transformation. J. Mech. Phys. Solids 41, 541–571.

Abeyaratne, R., Knowles, J. K., 1994a. Dynamics of propagating phase boundaries: adiabatic theory for thermoelastic solids. Physica D 79, 269–288.

Abeyaratne, R., Knowles, J. K., 1994b. Dynamics of propagating phase boundaries: Thermoelastic solids with heat conduction. Arch. Ration. Mech. Anal. 126 (3), 203–230.
Angst DR, Thoma PE, Kao MY. J Phys IV (ICOMAT-95) 1995;C8:747.

Assad M, Lombardi S, Berneche S, Desrosiers EA, Yahia LH & Rivard CH (1994) Essais de cytotoxicite sur l"alliage a memoire de forme Nickel-Titane. Ann.Chir. 48: 731-736.

Auricchio, F., and Lubliner, J., 1997, "A uniaxial model for shape memory alloys", International Journal of Solids and Structures, 34(27), pp. 3601–3618.

Auricchio, F., and Sacco, E., 1997, "A one-dimensional model for superelastic shape memory alloys with different elastic properties between austenite and martensite," International Journal of Non-Linear Mechanics, 32(6), pp. 1101–1114.

Auricchio, F., Reali, A., 2007, "A phenomenological one-dimensional model describing stress-induced solid phase transformation with permanent inelasticity", Mechanics of Advanced Materials and Structures, 14, pp. 43-55.

Auricchio, F., Taylor, R. L., and Lubliner, J., 1997, "Shape-memory alloys: Macromodelling and numerical simulations of the superelastic behaviour," Computer Methods in Applied Mechanics and Engineering 146 (3-4), pp. 281–312.

Barrere F., M.M.E. Snel, C. A. Van Blitterswijk, K. De Groot, P. Layrolle, Biomaterials, 25 (2004), pp. 2901-2910.

Basavaraj S Balapgol, Kamal M Bajoria, Sudhakar A Kulkarni ,Natural frequencies of a multilayer SMA laminated composite cantilever plate, Smart Materials and Structures, 15 (4) (2006) 1021-1032.

Bertran, A., 1982, "Thermo-mechanical constitutive equations for the description of shape memory effects in alloys," Nuclear Engineering and Design, 74(2), 173–182.

Beyer J., E.J.M. Hiensch, P.A. Besselink, in: E. Hombogen, N. Jost (Eds.), The Martensitic Transformation in Science and Technology, DGM, Oberursel, Germany, 1989, p. 199.

Beyer J., P.A. Besselink, J.H. Lindenhovius, in: Y. Chu, T.Y. Hsu, T. Ko (Eds.), Proceedings of International Symposium on Shape Memory Alloys, China Academic Publishers, Guilin, China, 1986, p. 492.

Bo, Z., Lagoudas, D. C., 1999a. Thermomechanical modeling of polycrystalline SMAs under cyclic loading, Part III: Evolution of plastic strains and two-way memory effect. Int. J. Eng. Sci. 37, 1141–1173.

Bo, Z., Lagoudas, D. C., 1999b. Thermomechanical modeling of polycrystalline SMAs under cyclic loading, Part I: Theoretical derivations. Int. J. Eng. Sci. 37, 1089–1140.

Bo, Z., Lagoudas, D. C., 1999c. Thermomechanical modeling of polycrystalline SMAs under cyclic loading, Part IV: Modeling of minor hysteresis loops. Int. J. Eng. Sci. 37, 1174–1204.

Bo, Z., Lagoudas, D. C., Miller, D., 1999. Material characterization of SMA actuators under nonproportional thermomechanical loading. Journal of Engineering Materials and Technology 121, 75–85.

Boyd, J. G., Lagoudas, D. C., 1994. Thermomechanical response of shape memory composites. J. Intell. Mater. Systems Struct. 5, 333–346.

Brinson L. C., Schmidt I., Lammering R. J Mechanics and Physics of solids 52 (2004) 1549-1571.

Brinson, L. C., 1993, "One dimensional constitutive behaviour of shape memory alloys: themomechanical derivation with non-constant material functions and redefined martensite internal variable," Journal of Intelligent Material Systems and Structures, 4, pp. 229–242.

Buehler WJ & Wang FE (1967) A summary of recent recearch on the Nitinol alloys and their potential application in ocean engineering. Ocean Eng. 1: 105-120.

Cary, Howard B. and Scott C. Helzer (2005). Modern Welding Technology. Upper Saddle River, New Jersey: Pearson Education. ISBN 0-13-113029-3.

Castleman LS & Motzkin SM (1981) The biocompatibility of Nitinol. In: Williams DF (ed.) Biocompatibility of clinical implant materials, Volume 1. CRC Press, Inc., Boca Raton, Florida, p 129-154.

Castleman, L. S., Motzkin, S. M., in Biocompatibility of Clinical Implant Materials, ed. D. F. Williams Vol. 1, CRC Press, 1981, p. 129.

Chan C.M., Trigwell S, Duerig T. Oxidation of a NiTi alloy. Surf Interface Anal 1990; 15:349-54.

Chang LC & Read TA (1951) Plastic deformation and diffusionless phase changes in metals - The gold-cadmium beta phase. Trans.AIME 189: 47-52.

Chang-jun Q., M. Pei-sun, Y. Qin, Sens. Actuators A-Phys. 113 (1) (2004) 94.

Chen M.F., Yang X.J., Liu Y., Zhu S.L., Cui Z. D., Man H.C., Study on the formation of an apatite layer on NiTi shape Memory alloy using a chemical treatment method. Surf. Coat. Technol 2003; 173:229 34.

Chen Y.B. Laser welding technique in modern time. Beijing: Science Press; 2005

Chou Yu-Fen, Wen-An Chiou, Yuhuan Xu, J.C. Y. Dunn, B. M. Wu, Biomaterials, 25 (2004), pp. 5323-5331.

Dai K., Bio-Med Materials Engineering,6 (1996), p.233.

de Groot K., Geesink R., Klein C.P., Serekian P., Plasma sprayed coatings of hydroxyapatite. J Biomed Mater Res 1987; 21:1375 81.

Des Roches R. and Delemont M., (2002) "Seismic retrofit of simply supported bridges using shape memory alloys", Engineering Structures, Vol. 24, pp. 325 332.

Dolce M., Cardone D., (2001) "Mechanical behavior of shape memory alloys for seismic applications, 2. Austenite NiTi wires subjected to tension", International Journal of Mechanical Sciences, Vol. 43, pp. 2657-2677.

Dolce M., Cardone D., and Marnetto R., (2000) "Implementation and testing of passive control devices based on shape memory alloys", Earthquake Engineering and Structural Dynamics, Vol. 29, pp. 945-968.

Donkersloot HC, Van Vucht JHN. J Less-Comm Met 1970;20:83.

Duerig, T.W., K.N. Melton, D. Stokel, and C.M. Wayman (1990), "Engineering aspects of shape memory alloys", Butterworth-Heinemann pub.

Eckelmeyer KH. Scripta Metall 1976;10:667.

Falk , F., 1983, "One-dimensional model of shape memory alloys," Archives of Mechanics, 35(1), pp. 63–84.

Falk, F., 1980, "Model free-energy, mechanics and thermodynamics of shape memory alloys," ACTA Metallurgica, 28(12), pp. 1773–1780.

Falvo, A., Furgiuele, F., and Maletta, C., 2007, "Two-way shape memory effect of a Ti rich NiTi alloy: experimental measurements and numerical simulations", Smart Materials and Structures, 16, pp. 771-778.

Falvo, A., Maletta, C., and Furgiuele, F. M., 2005, "Laser welding of a NiTi alloy: Mechanical and shape memory behaviour," Material Science and Engineering A, 412, pp. 235–240.

Falvo, A., Maletta, C., and Furgiuele, F. M., 2006, "Functional behaviour of a NiTi welded joint: Two-way shape memory effect," Material Science and Engineering A, doi:10.1016/j.msea.2006.11.178.

Fini M., G. Giavaresi, P. Torricelli, V. Borsari, R. Giardino, A. Nicolini, A. Carpi, Biomedicine & Pharmacotherapy, 58 (2004) p. 487.

Firstov G.S., Vitchev R.G., Kumar H., Blanpain B., Van Humbeeck. J. Surface Oxidation of NiTi shape Memory alloys. Biomaterials 2002; 23:4863 71.

Fischer H., B. Vogel, W. Pfleging, H. Besser, Mater. Sci. Eng. A 273–275 (1999) 780.

Gall K., Sehitoglu H, Anderson R., Karaman I., Chumlyakov Y.I., Material Science and Engineering A317 (2001) 85-92.

Gall, K. A., Seitoglu H., Chumlyakov, Y., 2000, "NiTi experiments versus modeling: where do we stand?," Proc. of SPIE, Smart Structures and Materials: Active Materials: Behaviour and Mechanics, Christopher S. Lynch, eds., 3992, pp. 536-547.

Gan Lu, Jian Wang, A. Tache, N. Valiquette, D. Deporter, R. Pilliar, Biomaterials, 25 (2004), p. 5313.

Gao, X., Huang, M., Brinson, L. C., 2000a. A multivariant micromechanical model for SMAs. Part 1. Crystallographic issues for single crystal model. Int. J. Plasticity 16, 1345–1369.

Gao, X., Huang, M., Brinson, L. C., 2000b. A multivariant micromechanical model for SMAs. Part 2. Polycrystal model. Int. J. Plasticity 16, 1371–1390.

Ge, P., and Jouaneh, M., 1997, "Generalized Preisach model for hysteresis nonlinearity of piezoceramic actuators," Precision Engineering, 20, pp. 99-111.

Geusic, J.E., Marcos, H.M, and Van Uitert, L.G.: "Laser oscillations in Nd-doped yttrium aluminum, yttrium gallium and gadolinium garnets". Applied Physics Letters 4 10, 182-184 (1964).

Graesser E.J. and Cozzarelli F.A., (1991) "Shape-memory alloys as new materials for aseimic isolation", Journal of Engineering Mechanics, Vol. 117, No. 11, pp. 2590-2608.

Greninger AB, Mooradian VG (1938) Strain transformation in metastable beta copper-zinc and beta copper-tin alloys. Trans.AIME 128: 337-368.

Gu Y.W., B. Y. Tay, C.S. Lim, M.S. Yong, Applied Surface Science, 252 (2005), pp. 2038-2049.

Gu Y.W.,B.Y. Tay, C.S. Lim, M.S. Yong, Biomaterials, 26 (2005), pp. 6916-6923

Haas T., A. Schuessler, in: W. van Moorleghem, P. Besselink, D. Aslanidis (Eds.), Proceedings of the European Conference on Shape Memory and Superelasticity Technologies, SMST, Antwerp, Belgium, 1999, 103.

Hamilton, R.F., Sehitoglu, H., Chumlyakov, 2004, Y., Maier, H.J., "Stress dependence of the hysteresis in single crystal NiTi alloys, Acta Materialia, 52, pp. 3383-3402.

Hesse T., M. Ghorashi, D.J. Inman, J. Intel. Mater. Syst. Struct. 15 (2004) 577.

Ho K. H. and S. T. Newman State of the art electrical discharge machining (EDM) International Journal of Machine Tools and Manufacture Volume 43, Issue 13, October 2003, Pages 1287-1300.

Homa T. In: Funakubo H, editor. Shape memory materials. New York: Gordon and Breach Scientific Publishers; 1987. p. 83.

Hurlbut, Cornelius S.; Klein, Cornelis, 1985, Manual of Mineralogy, 20th ed., ISBN 0-471-80580-7.

Hurlebaus, S., Gaul, L. , Smart structure dynamics, Mech. Syst. Sign. Proc., 20 (2) (2006) 255-281.

Ikai, K. Kimura, H. Tobush, J. Intel. Mater. Syst. Struct. 7 (1996) 646.

Inaudi, J., and Kelly, J. ~1994!. ''Experiments on tuned mass dampers using viscoelastic, frictional and shape-memory alloy materials.'' Proc., 1st World Conf. on Structural Control, Los Angeles, 127–136.

Johansen K., H. Voggenreiter, G. Eggeler, Mater. Sci. Eng. 273–275 (1999) 410–414.

Kim H. M., F. Miyaji, T. Kokubo, T. Nakamura, J. of Materials Science: Mterials in Medicine, 8 (1997), pp. 341-347.

Krejci, P., and Kuhnen, K., 2001, "Inverse Control of Systems with hysteresis and Creep," IEE Proceedings: Control Theory and Applications, 148(3), pp. 185-192.

Kuhnen, K., and Janocha, H., 2001, "Inverse feedforward controller for complex hysteretic nonlinearities in smart material systems," Control and Intelligent System, 29(3), pp. 74-83.

Kurdjumov GV & Khandros LG (1949) Dokl.Akad.Nauk.SSSR 66: 211-213.

Lexcellent, C., Bourbon, G., 1996. Thermodynamical model for cyclic behaviour of Ti-Ni and Cu-Zn-Al shape memory alloys under isothermal undulated tensile tests. Mech. Mater. 24, 59–73.

Lexcellent, C., Leclerq, S., Gabry, B., Bourbon, G., 2000. The two way shape memory effect of shape memory alloys: an experimental study and a phenomenological model. Int. J. Plasticity 16, 1155–1168.

Liang, C., and Rogers, C. A., 1990, "One-dimensional thermomechanical constitutive relations for shape memory materials," Journal of Intelligent Material Systems and Structures, 1, pp. 207–234.

Liang, C., Rogers, C. A., 1992. A multi-dimensional constitutive model for shape memory alloys. Journal of Engineering Mathematics 26, 429–443.

Lin H.C., K.M. Lin and I.S. Cheng, J. Materials Science, Vol. 36, No. 2 (2001), p.399.

Lindquist PG, Wayman CM. Proc MRS Int Mtg Adv Mater 1989;9:123.

Marfia, S., Sacco, E., and Reddy, J.N., 2003, "Superelastic and shape memory effects in laminated shape-memory-alloy beams," AIAA Journal, 41, pp. 100-109.

Meijer J., J Mat Proc Tech, 149 (2004) 2-17.

Miller D.A., D.C. Lagoudas, Smart Mater. Struct. 9 (2000) 640.

Miyazaki S., Y. Igo, K. Otsuka, Acta metall., 34, 2045-2051 (1986).

Miyazaki S., Y. Ohmi, K. Otsuka, Y. Suzuki, J. Phys. Colloq., 43,C4-255 (1982).

Nagai Hideki, Ryutaro Oishi, Shape memory alloys as strain sensors in composites, Smart Mater Struct., 15 (2) (2006) 493-498.

Nagasawa A, Enami K, Ishino Y, Abe Y, Nenno S. Scripta Metall 1974;8:1055.
Nanci A., D.A. Puleo, Biomaterials, 20 (1999), p. 2311.

Nishida M, Honma T. Bull Res Inst Mineral Dressing and Metallurgy, Tohoku University 1981;37:79 [in Japanese].

Ogisu Toshimichi, Masakazu Shimanuki, Satoshi Kiyoshima, Junji Takaki, Ichiro Taketa, Nobuo Takeda, Damage behavior analysis of smart composites with embedded pre-strained SMA foils, Smart Mater. Struct, 15 (1) (2006) 41-50.

Oliverira A.L., J.F. Mano, R.L. Reis, Current Opinion in Solid State and Material Science, 7 (2003) p. 309.

Oshima R, Naya E. J Jpn Inst Met 1975;39:175. [in Japanase].

Otsuka K, Wayman CM. In: Feltham P, editor. Deformation behaviour of materials, vol. II. Israel: Freund Publishing House; 1977. p. 122.

Otsuka K. and Wayman C.M., (1998) "Shape Memory Materials", Cambridge University Press.

Otsuka, K., and Ren, X., 2005, "Physical metallurgy of Ti-Ni-based shape memory alloys," Progress in Materials Science, 50, pp. 511–678.

Paiva, A., and Savi, M. A., 2006, "An overview of constitutive models for shape memory alloys," Mathematical Problems in Engineering, art. no. 56876, pp. 1-30.

Patoor, E., Eberhard, A., Berveiller, M., 1988. Thermomechanical behaviour of shape memory alloys. Arch. of Mech. 40 (5-6), 775–794.

Patoor, E., Eberhardt, A., Berveiller, M., 1994. Micromechanical modelling of the shape memory behavior. In: Brinson, L. C., Moran, B. (Eds.), Proc. ASME WAM'94: Mechanics of Phase Transformation and Shape Memory Alloys. Vol. AMD189/PVD292. ASME.

Patoor, E., Eberhardt, A., Berveiller, M., 1996. Micromechanical modelling of superelasticity in shape memory alloys. Journal de Physique IV 6, C1–277–292.

Perkins J., Metall. Trans. 4, 2709-2721 (1973).

Putters JL, Kaulesar SD, de ZG, Bijma A & Besselink PA (1992) Comparative cell culture effects of shape memory metal (Nitinol), nickel and titanium: a biocompatibility estimation. Eur.Surg.Res. 24: 378-382.

Saburi T, Nenno S. Scripta Metall 1974;8:1363.

Scherngell H., A.C. Kneissl, Scripta Mat. 39, 205-212 (1998).

Schlossmacher P., T. Haas, A. Shussler, J. Phys. IV Coll. C 5 (1997) 251–256.

Schlossmacher, P., Haas, T., and Shussler, A., 1997, "Laser-welding of a Ni-rich TiNi shape memory alloy: Mechanical behaviour," Journal De Physique. IV : JP, 7(5), pp. 251-256.

Schroeder TA, Wayman CM. Scripta Metall 1977;11:225.

Schuster, H.F. Voggenreiter, D.C. Dunand, G. Eggeler, J. Phys. IV 112 (2003) 1177–1180.

Serneels A., (1999) "Shape Memory Alloy Characterisation and Optimisation", SMST-99: Proceedings of the First European Conference on Shape Memory and Superelasticity, 1999, pp. 6-23.

Shabalovskaya S.A. Biological aspects of TiNi alloy surfaces. J Phys IV 1995; 5: C8-1199-204.

Shabalovskaya S.A., Anderegg JW. Surface spectroscopic characterization of TiNi equiatomic shape memory alloys for implants. J Vac Sci Technol 1995; A13: 2624-32.

Shaw J.A., (2002) "A Thermomechanical Model for a 1-D Shape Memory Alloy Wire with Propagating Instabilities", International Journal of Solids and Structures, Vol. 39, pp. 1275-1305.

Souza, A. C., Mamiya, E., and Zouain, N., 1998, "Three-dimensional model for solids undergoing stressinduced phase transformations," European Journal of Mechanics - A Solids, 17(5), pp. 789–806.

Sun, Q. P., Hwang, K. C., 1993a. Micromechanics modeling for the constitutive behaviour of polycrystalline shape memory alloys — I. Derivation of general relations. J. Mech. Phys. Solids 41 (1), 1–17.

Sun, Q. P., Hwang, K. C., 1993b. Micromechanics modelling for the constitutive behavior of polycrystalline shape memory alloys — II. Study of the individual phenomena. J. Mech. Phys. Solids 41 (1), 19–33.

Suzuki Y., Fabrication of Shape Memory Alloys (Shape Memory Materials, ed., K. Otsuka and C.M. Wayman, Cambridge University Press 1998).

Takezawa T, Sato S. Proc 1st JIM Int Symp on New Aspects of Martensitic Transformations, Suppl. Trans JIM 1976;17:233.

Tanaka, K., and Nagaki, S., 1982, "Thermomechanical description of materials with internal variables in the process of phase transitions", Ingenieur Archive, 51, pp. 287–299.

Tanaka, K., Nishimura, F., Hayashi, T., Tobushi, H., Lexcellent, C., 1995 Phenomenological analysis on subloops and cyclic behavior in shape memory alloys under mechanical and/or thermal loads. Mechanics of Materials 19, 281 292.

Theisen, W., and Schuermann, A., 2004, "Electro discharge machining of nickel-titanium shape memory alloys," Material Science and Engineering A, 378, pp. 200-204.

Tuissi, A., Besseghini, S., Ranucci, T., Squatrito, F., and Pozzi, M., 1999, "Effect of Nd-YAG laser welding on the functional properties of the Ni-49.6at.%Ti," Material Science and Engineering A, 273-275, pp. 813-817.

Van Hunbeeck J., R. Stalmans, P.A. Besselink, in: J. A. Helsen, H.J. Breme (Eds.), Metals as Biomaterials,Wiley, Chichester, 1998, pp. 73-100.

Wada K., Liu Y., J. Alloys Compd. 400 (2005) 163–170.

Wang, Welding of Nitinol to Stainless Steel. Proceedings of SMST-97, 1997, 131-136.

Weman, Klas (2003). Welding processes handbook. New York: CRC Press LLC. ISBN 0-8493-1773-8.

Wu Ming H., in: Y.Y. Chu, L.C. Zhao (Eds.), Shape Memory Materials and Their Applications, Trans Tech Publ. Inc., Kunming, China, 2001, p. 285.

Wu Ming, H., 2002, "Frabication of Nitilon Materials and Components," Materials Science Forum, 394-395, pp. 285-292.

Yong L., in: A.R. Wilson, H. Asanuma (Eds.), Proceedings of the Conference on Smart Structures and Materials - 4234, SPIE, Newport Beach, CA, 2001, p. 92.

Yuse Kaori, Yoshihiro Kikushima, Development and experimental consideration of SMA/CFRP actuator for vibration control, Sensors and Actuators A 122 (2005) 99–107.

Zhang Zhonghua, Jan Frenzel, Klaus Neuking and Gunther Eggeler. On the reaction between NiTi melts and crucible graphite during vacuum induction melting of NiTi shape memory alloys, Acta Materialia Volume 53, Issue 14, August 2005, Pages 3971-3985